Concordia
UNIVERSITY

TN-EMC-95-01
March 31, 1995
Final Report

CHARACTERISTICS OF ELECTROMAGNETIC FIELDS PRODUCED BY PORTABLE HANDHELD TRANSCEIVERS

Dr. C.W. Trueman
Dr. S.J. Kubina

FACULTY OF ENGINEERING AND COMPUTER SCIENCE

EMC LABORATORY
DEPARTMENT OF ELECTRICAL AND COMPUTER ENGINEERING
7141 Sherbrooke St. West, L-AD-532
Montreal, Quebec, Canada H4B 1R6

Releasable
CRC-CR-95-005

TN-EMC-95-01
March 31, 1995
Final Report

CHARACTERISTICS OF ELECTROMAGNETIC FIELDS PRODUCED BY PORTABLE HANDHELD TRANSCEIVERS

Dr. C.W. Trueman
Dr. S.J. Kubina

Scientific Authority Lauber, W.

Communications Research Centre

Prepared For:

Public Works and Government Services Canada
Communications Research Centre

PWGSC/CRC 36001-4-0395/01-ST

Table of Contents

Characteristics of Electromagnetic Fields Produced by Portable Handheld Transceivers

CHAPTER 1

Introduction

This is the Final Report in Contract Number PWGSC/CRC 36001-4-0395/01-ST for the Communications Research Centre of Public Works and Government Services Canada. It covers the period July, 1994 to March, 1995. This is a continuation of the work carried on during the first year of this project, reported in "Computational Studies for Prediction of Energy Deposition in Humans Exposed to RF Fields from Cellular Phones"[1]. North American cellular telephones transmit signals on frequencies from 824 to 850 MHz, and receive between 870 and 890 Mhz. Cellular phones often radiate 600 milliwatts of power. The broad objective of the project is to calculate the field strengths of a cellular phone or other portable radio, and to assess how these fields are affected by the presence of the human operator. The "far fields" or radiated fields are of interest to assess the coverage of the antenna in both polarizations of the electric field, and how that coverage changes when a human operator is holding the handset, at various orientations to the head. The "near fields" are of interest to assess the field strengths generated around the human operator, and how these fields change as the orientation of the handset to the operator's head is changed. The field strengths induced inside the head are of interest to assess the effect of various antenna designs and handset configurations on these fields.

This report investigates the far fields and near fields of a typical cellular phone handset operating at 850 MHz. Initially, "wire-grid modelling" is used to find the fields of a perfectly-conducting handset, with no human operator. In Chapter 3, the near and far fields of three different antenna types are compared.

The Finite-Difference Time-Domain method(FDTD)[2,3] allows the modelling of dielectrics of various permittivies and conductivities, as well as perfectlly-conducting objects, and so is suitable for investigating a handset held by a human operator. This report summarizes the FDTD method in Chapter 4. In this method space is subdivided into cubical cells. The head is modelled by designating cells as having the material properties of the various tissues inside the head: skin, muscle, brain, bone, and so forth. Information from an atlas of anatomical cross-sections[4] is used to derive a cell model of the head in Chapter 2. Software was developed for this project allowing each cross-section to be represented on a computer, and then to assemble the digitized cross-sections into a complete head model.

The telephone set is modelled by designating the cells that lie inside the handset as "perfectly-conducting", to model a handset with a metal case. Chapter 3 studies the radiation patterns and near fields of a handset with three different types of antennas, using the "wire-grid modelling" method[5]. Chapter 4 studies the handset's fields computed by FDTD in comparison to those computed by wire-grid modelling. To carry out this study, an FDTD computer program or "code" called FDTDC[6] that was intended to compute the scattered field from objects exposed to an incoming a plane wave was developed into a code capable of computing the radiated fields from a portable radio excited by a voltage generator at the base of a wire antenna. The revised code is presented in Chapter 4 and is called FDTDANT. Chapter 4 identifies many improvements that can be made to the FDTDANT code to make it faster and more efficient.

Chapter 5 makes extensive recommendations to carry on this work. Substantial improvements to the FDTDANT code are recommended. A series of measurements of the near and far field of a telephone handset are suggested to establish good agreement of the calculations with measurements. Then simplified "heads" near the handset should be studied by measurement and calculation to establish good correspondence between the measurements and calculations when

lossy dielectrics are included in the problem. With this extensive validation of the computations against measured data, we will be ready to proceed with calculations using the full head model developed in Chapter 2.

1.1 Summary of Previous Work

The work carried out in the first year of the project, 1993-94, was presented in Ref. [1]. That report assembled a collection of papers on portable radios and the human body, which formed the starting point for the bibliography presented here. The literature was searched for information on the finite-difference time-domain method on various topics. The use of FDTD to model radiating antennas was investigated. This report implements a wire antenna in an FDTD program. The electrical parameters of human tissue were researched, and tissue was found to be dispersive, that is, the permittivity and the conductivity vary significantly with frequency. Modifications to the FDTD method to account for the dispersive dielectric materials were investigated. Other numerical techniques suitable for investigating portable radios and humans were identified. Thus the "moment-method" can be used to study problems involving perfect conductors such as the handset and its antenna, and regions of uniform dielectric material, such as a model of the head or the whole body[7]. The "multiple multipole method"(MMP) can be used to model an antenna on a handset near a uniform or non-uniform dielectric head[8].

The results of the above investigations carried out in the first year of this project were consolidated in the first two months of the 1994-1995 project. Many additional papers were added to the bibliography. Considerable effort was expended in tabulating the electrical parameters of tissue from various sources. Methods of dealing with dispersive dielectrics were carefully examined. The techniques in the literature for constructing an FDTD model of the human head from anatomical cross-sections were studied. These results were summarized in a paper presented to the 1994 Symposium on Antenna Technology and Applied Electromagnetics(ANTEM) in Ottawa in August, 1994[9]. That paper is reproduced in this report as Appendix 1.

1.2 Objectives for 1994-1995

The objectives of this contract year were as follows. First, to develop a discretized model of the human head. This has been completed and is presented in Chapter 2 of this report. Second, the planning of a concurrent measurement project. Chapter 5 of this report recommends an extensive series of measurements with portable radio handsets, with simplified heads, and with a full head phantom. The objective of these measurements is to fully validate the calculations for configurations starting with the handset alone. Then a spherical "head" with uniform electrical parameters can be introduced near the handset and the fields measured to provide validation data for the calculations for a case of moderate complexity, which can be modelled precisely by computation. Finally, measurements can be made in the very complex case of a handset near a head phantom which accurately represents the electrical properties of the layers of tissue in a human head.

The third objective of the project was to search for other head models and data. An extensive bibliography of papers that have been published relating to modelling of antennas near humans has been assembled and is included in this report in two parts. The "References" are papers that are specifically cited in the text relating to the various topics discussed. The "Bibliography" contains an extensive list of papers not included in the "References".

The final objective of the present project was to carry out some initial calculations for a cellular phone handset. This work is presented in Chapters 3 and 4 of this report. The near fields and far fields of cellular phone handsets are explored in Chapter 3 using a wire-grid model of a telephone handset. It was found that three types of antennas are commonly used: the quarter-wave monopole with the generator at the connection point to the case; the half-wave monopole, "end fed" with the generator at the connection point to the case; and the half-wave monopole "centre fed", with the generator half-way along its length. These three antennas are modelled in Chapter 3 and the far and near fields are compared. Chapter 4 presents computations for a telephone handset made using the FDTD method. The FDTDC scattering code was modified to become the FDTDANT code for radiating antennas, and the chapter serves to validate this modification by comparing the results with the near fields and far fields of the same telephone handset computed by wire-grid modelling. Excellent agreement is achieved.

1.3 Tracking of the Literature

The "References" and the "Bibliography" sections of this report contain an extensive list of papers that have been assembled and studied. The References are papers that are specifically cited to support work reported in the text of this report. The Bibliography contains additional papers not cited in the main body of the report.

The textbook by Gandhi[10] presents a thorough summary of the state of development of computer modelling of humans as of its publication date in 1993. The book summarizes the extensive work done by Gandhi and others, presented in Refs. [11], [12], [13], [14], [15], [16], and [17].

The paper presented at ANTEM in August, 1994[9], reproduced as Appendix 1, discussed the state of the art in numerical modelling of the human head at that time. Since then several significant papers have been published, which are summarized in the following.

The paper by Schmidt[18] at the JINA conference in November used measurements to determine the amount of power absorbed by the head when operating a cellular telephone. The power input to the handset was carefully monitored, and compared with the power radiated by integration of the power density on a radiation sphere, using measured patterns. It was found that there can be significant absorption of power. It was interesting to note that one antenna used on the handset was a monopole of length one-half wavelength, which was fed at the connection point of the antenna to the handset case. Such an antenna is studied in Chapter 3 of this report.

Hirose and Miyake[19], working at 1.9 GHz, studied the radiation patterns of a quarter-wave monopole on a metallic handset. The handset is hinged approximately at its midpoint, as are many cellular telephone handsets. The hinge is plastic and non-conducting; it is bridged with a passive load. By controlling the value of the load, a significant increase in gain in the azimuth plane was achieved. Note that at this frequency a quarter-wave monopole is only about 4 cm in length and the case of the cellular telephone is more than a full wavelength tall. The paper was not concerned with the effect of the human head adjacent to the handset.

Bahr and Wolff[20] investigated the near field and the input impedance of a hand-held portable telephone, with and without a human head model, using FDTD. The telephone set was represented as a perfectly-conducting box. The antenna was either a quarter-wave monopole or a half-wave monopole. The head and hand of the operator were simulated with material having the electrical parameters of muscle, at 914 MHz. The head was a sphere of diameter 18 cm, as in Ref. [21]. The hand was represented as a dielectric layer surrounding the telephone set on three sides. The input impedance of the quarter-wave monopole was found to be much more dependent on the presence of the head than the impedance of the half-wave monopole. Maps of the field strength surrounding the telephone set, and inside the spherical head were presented in two planes. The authors identified wave propagation along the upper side of the head.

Martens[22] used FDTD to model the fields inside the head at 900 MHz. The head was represented with six different tissue types: grey brain, white brain, muscle, fat, bone, and cerebral spinal fluid. Anatomical data was obtained from nuclear magnetic resonance(NMR) images of a human head. The head model is about 45 cells in diameter. The far field patterns of a portable radio were studied without and with the head present. It was found that the head can absorb more than fifty percent of the power radiated.

Wang and Chen[23] model the human head with 57,263 cells. The cellular telephone set was modelled as a dipole antenna at 835 MHz. For a radiated power of 600 milliwatts, the specific absorption rate(SAR) inside the head was found to be in the range 1.2 to 2.5 W/kg for distances separating the dipole from the head of 1 to 2.5 cm. To keep the SAR within the IEEE limit of 1.6 W/kg, a separation of more than 2 cm was required.

Jensen and Rahmat-Samii[24] study the radiation patterns, reflection coefficient at the antenna connector, and input impedance of antennas on a portable radio similar to a cellular telephone, up to about 3 GHz. The handset is modelled by FDTD, including the plastic case of the handset. Three antenna types are studied: a quarter-wave monopole, a planar inverted-F antenna, and a loop antenna. The case, 3.28 mm thick with relative permittivity equal to 2, has little effect on the reflection coefficient for the monopole antenna below 2 GHz. But for the inverted-F, which is mounted directly on the plastic case, the plastic lowers the resonant frequency significantly. The loop antenna is highly inductive and difficult to match below 2 GHz, but may be a practical antenna above that frequency. The plastic case affects the loop's resonant behavior very significantly.

Jensen and Rahmat-Samii[25] extend their study to include the fields and SAR inside the head using a portable radio with various designs of antenna. The model of the head is based on an atlas of cross-sections of the head and body[4] that is used in Chapter 2 of this report to develop a cell model of the head. Ref. [25] uses a 6.56 mm grid size, and supplements the data of Ref. [4] with NMR images. The resulting head uses 24 by 33 by 31 cells, for a total of 24,552 cells. Seven tissue types were included: bone, skin, muscle, brain, humour, lens, and cornea using the electrical parameters for these tissues at 915 MHz. The user normally holds a cellular telephone so that the antenna is at an angle of about 45 to 60 degrees to the vertical. The head model in Ref. [25] was rotated in three-dimensional space so that the portable radio's antenna, oriented parallel to the z-axis, lies at a realistic angle to the main axis of the head. The study models the hand surrounding the portable radio. The paper presents radiation patterns for the handset alone, for the handset and the hand, and the handset, hand and head. Maps of the field strength surrounding the handset and inside the head are presented. The SAR for various antennas is compared. Peak values of 2 to 3.8 mW/kg are found for 1 watt of power delivered to the antenna. The tissues are found to absorb between 53 and 68% of the power for a head to handset separation of 2 cm.

Gutschling and Weiland[26] use NMR images consisting of 109 slices of the head form the basis of a head model using cells of dimension 2.5 by 2.5 by 3.3 millimeters. Brain, bone, and muscle are included as tissue types. The head is illuminated by a dipole at 915 MHz and the field strength throughout the head is calculated using the software package called MAFIA[27], using a time-stepping solution to achieve steady state with a sinusoidal oscillator. About 3000 time steps were needed. For a radiated power of 1 watt, the SAR is evaluated on cross-sectional planes throughout the head. The area of highest absorption is in the skin. Reflection from the bone appears to produce large peaks in the skin and muscle. Significant differences are found between a homogeneous model of the head and the more realistic model including several tissue types. SARs for the homogeneous model are found to be significantly lower.

Meier, Egger, Schmid and Kuster[28] describe a method for measuring the field strength in a "phantom" of the head and shoulders of a person. A thin-walled, full-size fibre-glass shell of the head and shoulders is constructed. The shell is positioned to "lie" on its left side, with the telephone set located below the left side of the face. The right side of the head is cut away. The shell is filled with liquid prepared to have the electrical properties of tissue. A probe is inserted into the liquid and measures the strength of the electric field in two or three orthogonal direc-

tions. A robot moves the probe in the liquid to measure the field on planar grids of points. There is concern that this homogeneous model of the head may not lead to field strengths inside the head that are representative of those found inside the actual head, with its highly non-uniform composition.

The following chapter presents the computer software and methods used to construct a cell model of the head from anatomical cross-sections. Subsequent chapters present an initial study of the field strengths due to a portable radio, and then make extensive recommendations for further work.

CHAPTER 2

Modelling the Head with Cubical Cells

In this chapter a cell model of the head is developed based on the anatomical cross-sections in Ref. [4]. This chapter summarizes the work done by research assistant Mina Danesh in the summer of 1994. Ms. Danesh developed software to assist in "digitizing" each anatomical cross-section according to the tissue type in each cell. Then the set of digitized cross-sections are assembled into a complete cell model. Her work was reported in a report entitled "Absorption of RF Energy by the Human Head"[29], which is reproduced in its entirety in Appendix 2. This chapter summarizes the work presented in Appendix 2 and some of that in Appendix A[9]. Throughout this chapter will refer to figures in Appendix 2.

2.1 Biological Cross-Sections

The atlas entitled "A Cross-Section Anatomy" by Eycleshymer and Schoemaker[4], published in 1911, has been the basis for most cell models of humans and of the human head[10,11,14,25,30]. The atlas deals with a "standard man"[11] of height 1.75 m and weight 70 kg. Fig. 3 in Appendix 2 shows the locations of the cross-sections of the head presented by Eycleshymer and Schoemaker. There are 20 cross-sections in the top part of the head, labelled 1, 1', 2, 2', and so forth separated by about 0.25 inch or 6.35 mm. There are a further eight cross-sections, numbered 11 to 18, for the lower part of the head, separated by about one-half an inch or 12.5 mm. It is important to note in the figure that the cross-sectional planes are not parallel, which complicates the use of this anatomical data in constructing a cell model made up of parallel planes of cubical cells.

The methods used to construct the cell model are summarized in Sections 2.3 and 2.4 below.

2.2 Electrical Parameters of Biological Materials

The permittivity and conductivity of biological tissues can be found in the literature[10,14,21,30,31,32,33,34,35]. Particularly useful is the extensive table in Ref. [33]. Tables 1 and 2[9] give the permittivity and conductivity, respectively, of brain or nerve tissue, bone or fat, muscle, skin, eye, and blood at 10, 27.12, 100, 350, 400, 500, 750, 900, 1000 and 1500 MHz, drawn from the above references. Note that the permittivity of some types of tissue is quite high, and that both permittivity and conductivity change very significantly in the frequency range covered by the tables.

Tables 1 and 2 illustrate that tissue is quite "dispersive", that is, the permittivity and conductivity of tissue varies quite rapidly with frequency. But in Yee's FDTD the relative permittivity ε_r and conductivity σ are constant with frequency. To obtain the fields inside a model of a head or body over a wide frequency band, a Yee FDTD code must be run with a sine wave excitation at many individual frequencies, with the appropriate permittivity and conductivity at each frequency. In doing so we lose the inherent advantage of a time domain method, in which the

response to a pulse input function obtains wideband information in a single run. To regain this capability, the FDTD algorithm must be modified to directly incorporate the dispersive nature of biological materials.

The frequency range over which cellular phones transmit in North America is quite narrow, 824 to 850 MHz. Over this small range the electrical parameters of tissue can be considered to be constant with frequency, and then a Yee FDTD code can be used with a suitable excitation to compute the fields strengths in the head over the band in a single run of the code. Ref. [25] uses a Gaussian pulse modulated with a sine wave to construct an excitation containing energy primarily in the desired narrow frequency band.

If wider band information is required, over a bandwidth in which the permittivity and conductivity of tissue changes significantly with frequency, then the FDTD algorithm itself must be modified to account for the frequency dependence of the tissue. The simplest model of materials with frequency-dependent permittivity and conductivity is given by the Debye equation[10]. Inherently, when the material is polarized, the polarization cannot be removed instantaneously by removing the field that caused it. Instead, the polarization decreases exponentially with time, and the time constant is called the "relaxation time". In the frequency domain a single time constant corresponds to a simple "Debye pole". Ref. [36] describes a frequency-dependent finite-difference time-domain or $(FD)^2TD$ method, suitable for modelling materials with one relaxation time. Some materials with parameters having a more complex frequency dependence can be modelled in terms of two or more relaxation times, as in Ref. [37], while some materials require multiple "Lorentz poles" in complex conjugate pairs, as in Ref. [38].

Ref. [39] offers an alternate formulation to that of Refs. [36], [37] and [38] for $(FD)^2TD$ for materials with two relaxation times, that is, two simple Debye poles. Ref. [40] gives the permittivity of muscle in terms of five relaxation times, valid over a wide frequency range. In Ref. [39] the representation is simplified to use only two time constants, to obtain a reasonable representation of frequency variation of muscle's permittivity from 20 MHz to 20 GHz. The $(FD)^2TD$ method is applied to the parts of a whole-body model composed of muscle to calculate induced currents in the body at 40, 150 and 350 MHz.

Ref. [30] provides estimates of the parameters required to represent 12 types of biological tissue with the two relaxation time model, valid up to 3 GHz. Each tissue has its individual values of the two "static" permittivities, and the "high frequency" permittivity required for the dispersion model. But all the tissue types are modelled as having the same relaxation times τ_1 and τ_2. This permits the actual permittivity of each cell of the FDTD model to be chosen by volume averaging according to the fraction of the cell occupied by each type of tissue. This improves the resolution of models having a somewhat coarse cell size. Then a single run of the $(FD)^2TD$ code obtains the field strengths in each cell up to 915 MHz, which would require many runs of the Yee FDTD code with a single-frequency sine wave excitation.

Table 1
The permittivity of biological materials at various frequencies.

Tissue	Ref	Frequency (MHz)									
		10	27.12	100	350	400	500	750	900	1000	1500
Brain,	10	163-352		57-90						37-55	
nerve	10		155	52	60						
	31							49			46
	32			63		50.3			41.2		
	14				74						
Bone,	10	37		23							
Fat	10		29	7.5	5.7						
	31							5.6			5.6
	32			12.2		9.2			7.3		
	14				5.7						
Muscle	10	162-204		64-90						57-59	
	10		106	74	53						
	31							52			49
	32			70.5		62.5			54.7		
	33			71-76			52-54			49-52	
	34			63		52.6	52.4		52		
	21								50.5		
	14				54						
Skin	10		106	25	17.6						
	31							52			49
	33			57			46.5			43-46	
	14					17.4					
Eye	10		155	85	80						
	31							80			80
Blood	10		102	74	65						
	33			69-81			67-70			60.5	
	14				65						

Table 2
The conductivity of biological materials at various frequencies.

Tissue	Ref	Frequency (MHz)									
		10	27.12	100	350	400	500	750	900	1000	1500
Brain,	10	0.21-0.63		0.48-0.95						0.81-1.2	
nerve	10		0.45	0.53	0.65						
	31							1.2			1.4
	32			4.7		7.5			12.2		
	14				0.62						
Bone,	10	0.024		0.057							
Fat	10		0.04	0.07	0.072						
	31							0.09			0.12
	32			0.215		0.88			1.4		
	14				0.07						
Muscle	10	0.69-0.96		0.75-1.05						1.38-1.45	
	10		0.74	1.0	1.33						
	31							1.54			1.77
	32			6.8		9			13.8		
	34			0.62		0.68	0.72		0.92		
	21								1.2		
	14				1.3						
Skin	10		0.74	0.55	0.44						
	31							1.54			1.77
	32				0.42						
Eye	10		0.45	1.9	1.9						
	31							1.9			1.9
Blood	10		0.28	1.1	1.2						
	14				1.22						

2.3 Software for Digitizing Head Cross-Sections

The anatomical cross-sections of Ref. [4] were digitized by superimposing over each cross-section a grid measuring 18 by 20 cm of 2.5 mm cells, on a transparent piece of plastic. Because the cross-sections in Ref. [4] are three-quarters of actual size, the cell size corresponds to 3.3 mm cells full-scale. The centreline at the back of the head in each cross-section was taken as a reference point. Then Fig. 3 in Appendix 2 was used to derive the geometrical relationship of each cross-section to the full head in a global coordinate system.

A FORTRAN program was written which allows the operator to use a mouse to designate which type of tissue occupies the most area in each cell. With tissue type #1 as free-space, tissue types from #2 to #30 were identified as listed on the right-hand edge of Fig. 6 in Appendix 3. These include ligament, nerve, nucleus, grey brain, white brain, eye, skin, bone or fat, muscle, and other types of tissue. Each of the 28 head cross-sections in Ref. [4] was then digitized cell-by-cell, a lengthy and tedious task. Every cell in each cross-section was required to be assigned a tissue type. For example, cross-section number 8' is shown in Fig. 4 of Appendix 2, and the resulting digitization in Fig. 5. It is interesting to note that there are some voids or empty space cells inside the head. In this way a data base of 28 head cross-sections was assembled.

2.4 Cell Model of the Head

The data base of 28 anatomical cross-sections was used to assemble a cell model of the head as follows. A global coordinate system is defined, with z oriented vertically, x as back-to-front coordinate, and y for side-to-side. The location of the reference point for each cross-section, in global coordinates, is read from Fig. 3 in Appendix 2, taken from Ref. [4]. Also, from the same drawing, the unit vector perpendicular to the cross-section is read. This information is sufficient to permit local coordinates on a digitized cross-section to be translated to global x, y, z coordinates in three dimensional space.

A FORTRAN program was then written to assign a tissue type to every cell in an FDTD cell space of 64 by 72 by 76 cells or 350,208 cells in total. For each cell, the program determines which of the 28 cross-sectional planes is closest, by finding the perpendicular distance from the cell centre point to each of the cross-sections, accounting for the fact that they are not parallel to one another. The tissue type for that cell is then assigned by determining the tissue type of the nearest point on the nearest anatomical cross-section. The resulting cell model was then examined in xy cuts or horizontal-plane cuts, and in xz cuts or vertical plane cuts. Minor adjustments were made in reference to the anatomical data to ensure that the cell model is consistent and reasonable. Fig. 6 in Appendix 2 shows a yz cross-section along the centreline of the head, with the location of anatomical cross-sections from Ref. [4] shown as thin red lines.

Chapter 5 makes recommendations for further work in this project. The 350,208 cell head model is too detailed for many purposes, as analyzing it with FDTD will require much memory and CPU time on the available computers. It will be useful to derive a coarser model by replacing every 8 cells with one cell, for a total of 43,776 cells. Each cell's material properties are to be the average of the underlying eight cells. Initial calculations can be made with the coarse model relatively quickly with modest computer resources. The more detailed model can be used when information with a fine resolution is required.

CHAPTER 3

Modelling the Handset and Antenna

3.1 Typical Handset and Antennas

This chapter investigates the radiation patterns and near fields of a cellular telephone of the dimensions shown in Fig. 3.1. The handset is about 16.8 cm tall, 5.6 cm wide and 2.0 cm thick. The antenna is located on the top of the handset, near the front edge, offset 0.75 cm from the nearby edges. This chapter compares the radiation patterns and near fields for three antenna designs. The first is a monopole of length equal to a quarter of the wavelength at the operating frequency of 850 MHz. The monopole is fed coaxially at its base. The second antenna is a monopole a half-wavelength long, which is also fed coaxially at its base. The third antenna is a half-wavelength long, but is fed at its centre point.

This chapter investigates the far field radiation patterns and the near field near the handset for the three types of antennas. Fig. 3.2 is a flow chart of the programs and processing steps used to obtain the results presented here. Each program and processing step in the flow chart is described briefly below.

In this chapter the handset is modelled as a solid metal box, which is represented by a "wire-grid model", as shown in Fig. 3.3. The interconnection of wires is designed to be electrically equivalent to the solid box, using the "wire-grid" modelling guidelines summarized in Refs. [5] and [41]. The radii of the wires of the grid is chosen according to the "equal-area rule"[42,43,44] and is calculated as described in Ref. [41] using programs MESHES and FNDRAD, which are described in Ref. [45]. The wire-grid model is analyzed using the well-known "Numerical Electromagnetics Code"(NEC)[46,47,48]. NEC determines the current flowing on the wires of the grid and on the antenna. The currents are used to find the far-field radiation patterns, and the near fields at points designated by the user. To be accurately analyzed by the NEC program the wire grid model must conform to restrictions called "wire-grid modelling guidelines" imposed by the methods upon which NEC is based[5,41,47,48], which are discussed extensively in Refs. [41] and [49]. Program CHECK[49] examines the wire-grid for conformance to the wire-grid modelling guidelines, and reports any violations. The wire-grid model presented below has been verified with CHECK.

The following describes the set of processing steps used to generate a wire-grid model, to analyze it with NEC, and then to examine the far fields and near fields. Then the far fields of the handset with each of the three types of antennas will be examined. Finally the near fields will be investigated.

3.2 Wire-Grid Model of the Handset

Fig. 3.2 shows the set of programs(rectangles) and data files(ellipses) that are used to calculate and investigate the radiation patterns and near fields of a cellular telephone by wire-grid modelling. The first step is the creation of the wire-grid model of the handset, using program MKPHONE.

3.2.1 Wire-Grid Model Design

Figures 3.3 and 3.4 show the wire grid model of the handset. Fig. 3.3 shows that the broad faces of the handset have been gridded with nearly square mesh cells, using a grid of 17 by 6 wire segments. The narrow sides use 17 by 2 segments, and the ends 2 by 6 segments. The length of the segments is about 0.93 cm. The NEC program is expected to solve the grid very accurately at frequencies where the length of the wire segments is shorter than one-tenth of the wavelength, that is, at frequencies less than 3,230 MHz, much larger than our operating frequency of 850 MHz. The connection point of the monopole to the handset has been gridded with eight radial wires, clearly seen in the isometric view of the wire-grid in Fig. 3.3. Fig. 3.4 shows three views of the handset grid, with the wires expanded to show their radii. The radii of the wires in the grid were calculated according to the equal-area rule using programs MESHES and FNDRAD, as described in the following. The wire radii are proportional to the areas of the adjacent cells in the grid. Thus where the cells are small, such as near the feed point of the monopole, the wire radius is also small.

Fig. 3.5 shows the orientation of the coordinate system that will be used to study the telephone handset. The handset is oriented so that the operator faces in the positive x direction. The handset is held in the left hand so that the operator's head would be located in the negative y halfspace. The standard spherical angles are shown in Fig. 3.5. If $\overline{R}$ points towards the observer located at a distant point in the far field, then angle θ is measured from the z axis to $\overline{R}$, and angle ϕ is measured from the x axis to the projection of $\overline{R}$ onto the xy plane.

3.2.2 Program MKPHONE

The first step is to use the program called MKPHONE(MaKePHONE) to create the wire-grid model of the antenna and telephone set, coded as "GW cards" for input to the NEC program. The FORTRAN source code for program MKPHONE is edited to supply the dimensions of the telephone handset and the length and location of the antenna, and the operating frequency. The program is compiled and run to obtain an input file for the NEC program, called PHONE1.GW. The "GW" extension is used here to describe a geometry file in the format of an input file for the NEC program. The MKPHONE program also produces a geometry file called OUTLINE.GW, which contains wires along the edges of the handset box, and along the antenna. This file is used later by program MAKEMAP to superimpose the image of the handset on a contour map of the field strength.

The handset grid, or indeed any file with the "GW card" format, can be displayed on computer graphics using program MODEL. MODEL draws isometric views of wire-grids, and can draw the wires showing the wire radius as in Fig. 3.4, to allow the user to inspect the fatness of the wires compared to their spacing to their neighbors. MODEL works in conjunction with other programs such as MESHES and CHECK to locate errors in a wire-grid model and display those errors on computer graphics. However, MODEL depicts wire-grids as see-through cages, which can sometimes be quite confusing. Program HIDNMOD was developed to draw the wires as if they are mounted on the surface of an opaque solid such as a styrofoam block, and was used to draw the telephone handset in Fig. 3.3. Wires on the sides of the handset facing away from the observer are not drawn.

Program MKPHONE includes a standard set of "control cards" in the input file for the NEC code, PHONE1.GW. These command lines specify the frequency as 850 MHz, and set the location of the voltage generator, at the base of the quarter-wave monopole antenna. The control cards then command execution of the program to compute the currents flowing on the monopole and on the wires of the grid representing the handset. The control cards specify which far-field

radiation patterns are to be computed. Here we will compute the standard set of conical cut radiation patterns shown in Fig. 3.6. The conical cuts cover the radiation sphere uniformly in equal steps of $\cos\theta$. The conical angles are: θ =0, θ =0, 25, 37, 45, 53, 60, 66, 72, 78, 84, 90, 96, 102, 108, 114, 120, 127, 135, 143, 155, and 180 degrees; and the elevation cuts at ϕ =0 and 90 degrees. With this comprehensive set of far-field patterns the power density over the radiation sphere can be integrated to find the radiated power.

In order to command NEC to calculate the near field of the handset over planes where the operator's head would be located, we must include "NE" control cards in the input file. These cards are assembled by program NEDIS and added to the input file as described below.

3.2.3 Computing the Wire Radii

MKPHONE creates the set of GW cards that describe the handset geometry, and assigns an arbitrary, "thin" wire radius to each wire in the grid. To obtain the best performance from a wire-grid model the wires must be assigned radii according to the "equal-area rule"[42,43]. For a regular grid such as that on the broad face of the handset in Fig.3.3, the total surface area of the wires in one orthogonal direction must be made equal to the area of the surface. Each wire segment subtends two mesh cells and must represent half the area of each mesh cell. If the segment is of length Δ and radius a, and the mesh cells have areas A_1 and A_2, then the radius must be chosen as

$$a = \frac{A_1}{4\pi\Delta} + \frac{A_2}{4\pi\Delta}$$

If the mesh cells are square of area $A_1 = A_2 = \Delta^2$, then the radius is $a = \Delta/(2\pi)$. Ref. [45] discusses the problem of choosing the wire radius in grids that do not contain regular, square mesh cells, such as the region at the base of the wire antenna. Then the equal-area rule is modified to obtain[41,45]

$$a = \frac{A_1}{4\pi\Delta}\frac{4\Delta}{L_1} + \frac{A_2}{4\pi\Delta}\frac{4\Delta}{L_2}$$

where L_1 is the distance around the periphery of the mesh cell of area A_1, and L_2 is the periphery of A_2. The formula simplifies to

$$a = \frac{A_1}{\pi L_1} + \frac{A_2}{\pi L_2}$$

Computing the equal-area radius for each wire thus requires the areas of the mesh cells and the lengths of their peripheries. Fig. 3.4 shows that where mesh cells are large and nearly square, the equal-area radius is $\Delta/(2\pi)$ or about 1/6 of the segment length. Where mesh cells are small, near the feed point of the monopole, the wire radius is also small.

LEV determines the radiated power and rewrites the PHONE1.1 file including the radiated power, for reference by other programs.

3.2.6 Displaying the Far Field Patterns

Program PATCMP (PATtern CoMParison) is used to display the radiated fields and gain patterns of wire grid models of antennas. PATCMP uses the power level found by ISOLEV and written into the PHONE1.1 data file as the basis of rescaling the far field patterns to any desired power level.

The "isotropic level field strength" or simply the "isotropic level" is the field strength which, radiated uniformly in one polarization over the whole radiation sphere, radiates the same power as the actual antenna. Thus, if E_{iso} is the isotropic level, the power radiated is

$$P_r = \int_0^{2\pi}\int_0^{\pi} \frac{E_{iso}^2}{2\eta} \sin\theta d\theta d\phi = \frac{4\pi}{2\eta} E_{iso}^2$$

then

$$E_{iso} = \sqrt{\frac{\eta P_r}{2\pi}} = \sqrt{60 P_r}$$

where $\eta = 120\pi$. In this report we will choose to rescale the far fields to an isotropic field strength of 1 volt/meter over the radiation sphere, and we will plot field strengths in decibels relative to 1 volt/metre isotropic.

PATCMP is oriented toward comparing the radiation patterns of two different antenna configurations, on the basis of equal radiated power. Thus PATCMP opens two different input files, for example for the cell phone with the quarter-wave monopole radiating P_1 watts, and for the cell phone with the half-wave monopole, radiating P_2 watts. The field strengths in the first file are multiplied by a scale factor of $1/\sqrt{60P_1}$ and in the second file by $1/\sqrt{60P_2}$ so that the isotropic level for both antenna configurations is 1 volt/metre.

It is often of considerable interest to examine the field strength radiated by a cellular phone handset as a function of θ and ϕ over the whole radiation sphere. PATCMP uses the standard set of conical cut radiation patterns to write a "table file" of either E_θ or E_ϕ scaled to an isotropic level of 1 volt/metre. The table file can be displayed as contours of constant field strength over the (θ, ϕ) plane with CPLOT; or as a surface above the (θ, ϕ) plane with SPLOT, or as a contour map in a polar format, with θ on the radial axis and ϕ as the angle axis, as presented below.

The following examines the far fields of the cellular phone handset of Fig. 3.1 with the three antenna types. Then the construction of near field maps will be described, and finally the near fields of the handset will be examined.

3.3 Far Field Patterns for Three Antenna Types

This section examines current distributions and the far field radiation patterns for three antennas on the handset shown in Fig. 3.1, namely: the quarter-wave, end-fed monopole; the half-wave, end-fed monopole; and the half-wave centre-fed monopole.

Fig. 3.7 shows the current distribution on the antenna in the three cases, each excited by a one volt generator. Fig. 3.7(a) shows that the quarter-wave monopole fed at its base has the expected standing-wave of current, strong at the base and tapering to zero at the top. The centre case carries about 1/10 the current at the antenna base. The top of the case carries a substantial horizontally-oriented current flow. The impedance calculated by the NEC program is $(56.5 - 44.0j)$ ohms, or 56.5 ohms resistance and 44.0 ohms capacitive reactance. If the length of the antenna is increased to half a wavelength, we might expect to see a current distribution similar to that on a half-wave dipole, with a null at the connection point to the case, and a low impedance at the feed point at the centre of the antenna. However, Fig. 3.7(b) shows that the current flow when the half-wave antenna is centre fed is quite different from what is expected. We see a maximum current at the point where the antenna is connected to the case, tapering to about one third of the maximum at the feed point at the centre of the antenna, then dropping to zero at the tip of the antenna. The impedance is high: 1076 ohms resistance, plus 356 ohms inductive reactance. There is considerable coupling to the case. In fact, the current on the case is about the same relative to the maximum current on the antenna in parts (a) and (b) of Fig. 3.7.

When the half-wave monopole is excited at the point where the antenna connects to the case, we obtain the current distribution in Fig. 3.7(c). The current is similar to that expected of an isolated, centre-fed half-wave dipole: the current is a standing wave with a maximum in the middle of the antenna, a null at the tip, and a minimum at the connection point to the case, which is the feed point. Hence the impedance is high, equal to 861 ohms resistance and 813 ohms capacitive reactance. The current on the case is less in Fig. 3.7(c) relative to the largest current on the antenna. This suggests that the near fields surrounding the case will be smaller for the end-fed, half-wave antenna than for the other two antennas. This is investigated further later in this chapter.

3.3.1 Principal Plane Patterns

This section examines the principal plane patterns of the three antenna types.

3.3.1.1 End-Fed Quarter-Wave Monopole

Fig. 3.8 shows the principal plane patterns for the handset with the end-fed, quarter-wave monopole. Fig. 3.8(a) shows the azimuth or $\theta = 90$ pattern. The scale is decibels relative to 1 volt/metre; the isotropic field strength is set to 1 V/m or zero dB. Fig. 3.8(a) shows that the principal polarization, E_θ, has a quasi-circular radiation patten, with a field strength about 8 dB below isotopic in the "forward" or $+x$ direction at $\phi = 0$ degrees, and about 1 dB above isotropic in the "backward" or $\phi = 180$ direction. The cross-polarized field shows a figure-of-eight pattern with a maximum value about 10 dB below isotropic.

Fig. 3.8(b) and (c) show the elevation patterns for the quarter-wave, end-fed monopole. In the $\phi = 0$ plane, the E_θ pattern shows minima at about $\theta = 80$, 185 and 300 degrees, where the field strength is about -18, -12 and -17 dB, respectively. The cross-polarized component has a circular pattern about 29 dB below the isotropic level. The $\phi = 90$ pattern shows an inverted "butterfly" shape, with deep minima above and below the handset, and minima at θ =70 and 290 degrees, where the field is about 19 dB below isotropic.

3.3.1.2 Centre-Fed, Half-Wave Monopole

The half-wave monopole can be centre-fed by making its lower half a coaxial cable, with the upper half an extension of the inner conductor. This puts the feed point at the centre. The configuration is like a sleeve monopole. Fig. 3.9 shows the radiation patterns when the feed point is at the centre of the half-wave monopole. The azimuth pattern in part (a) shows that the E_θ component differs considerably from circular, having a field strength in the $\phi = 0$ direction which is about 16 dB below the isotropic level, whereas the field strength in the $\phi = 180$ direction is equal to the isotropic level. The cross-polarized component is a figure-eight with maxima down about 12 dB from the isotropic level. The elevation pattern for $\phi = 0$ shows a deep minimum in E_θ at about 85 degrees where the field strength is about 23 dB below isotropic, and again at 290 degrees where the field is 20 dB down. The cross-polarized pattern is circular, about 30 dB below isotropic. The $\phi = 90$ elevation pattern in part (c) shows a butterfly in E_θ, with minima at $\theta = 80$ and 285 degrees about 30 dB below the isotropic level, with the cross-polarized component having a circular pattern about 22 dB below isotropic.

Comparing Figs. 3.8 and 3.9 shows that the radiation patterns of the quarter-wave monopole and the half-wave monopole fed at its centre are very similar. The azimuth pattern has less field strength in the forward or $+x$ direction than in the backward direction. The half-wave monopole's field is about 6 dB less than the quarter-wave monopole in the forward direction. The $\phi = 0$ elevation patterns in part (b) of the figures are remarkably similar, with somewhat deeper minima for the half-wave case. The $\phi = 90$ patterns are also remarkably similar. **It was not expected that these two antennas would radiate such similar fields.**

3.3.1.3 End-Fed, Half-Wave Monopole

Fig. 3.10 shows the principal plane patterns of a half-wave monopole fed coaxially at one end. In part (a) the azimuth pattern in E_θ is nearly circular, at a level equal to or slightly exceeding the isotropic level. The cross-polarization, E_ϕ, is a figure-eight with a maximum value about 23 dB below the isotropic level. The elevation pattern for $\phi = 0$ in part (b) in E_θ is a figure-eight with minima above and below the handset, about 23 dB down from the isotropic level. The E_ϕ component is nearly circular at about 45 dB below isotropic. Part (c) shows the elevation pattern for $\phi = 90$ degrees, showing that E_θ has deep minima above and below the handset, with the field about 45 dB below isotropic. The E_ϕ component is circular about 23 dB below the isotropic level.

The end-fed half-wave monopole patterns are very similar to the radiation patterns of a dipole in free space, and quite different from those of the other two antenna configurations.

3.3.2 Field Strength Over the Radiation Sphere

Figs. 3.11, 3.12 and 3.13 show the field strengths in E_θ and E_ϕ over the radiation sphere for the three types of antennas. The graphs show field strength on a false-color "hot scale", using blue for the lowest or "coldest" field strengths, through cyan, green and yellow to red for the "hottest" or strongest field strengths. The field strengths are plotted in decibels relative to an isotropic field strength of 0 dB. The minimum and maximum limits of the scale are the same in all three figures. The axis format is polar. The angle axis is azimuth angle ϕ in the reference coordinates of Fig. 3.5, with the operator facing in the $\phi = 0$ direction, and with $\phi = 90$ on the operator's left and $\phi = 180$ on the operator's right. The radial axis is angle θ in Fig. 3.5, with $\theta = 0$ at the center of the graph being above the operator's head, the $\theta = 90$ circle corresponding to the azimuth plane, and $\theta = 180$ on the outer circle, below the user's feet. Thus the azimuth plane, $0 \le \phi \le 360$ at $\theta = 90$ degrees, corresponds to the black circle in Fig. 3.11(a) at a radius of half the outer radius of the polar plot.

Figs. 3.11(a) and (b) show the field strengths in E_θ and E_ϕ, respectively, for the quarter-wave monopole. Comparing Fig. 3.11 with the azimuth pattern in Fig. 3.8(a), we see that E_θ is substantially a circle, but that the largest field strengths in E_θ fall at θ angles between about 100 and 150 degrees. Hence the "donut" pattern of the monopole antenna is angled downward in elevation, as indeed is seen in the elevation patterns of Fig. 3.8(b) and (c). Also, there is a minimum in the field strength at approximately 80 degrees which appears as a green circle in Fig. 3.11(a), at a field strength of about -20 dB. Fig. 3.11(b) shows that the cross-polarized field component, E_ϕ, has a figure-eight pattern minima near $\phi = 0$ and 180 degrees for all θ angles. The field strength in E_ϕ has a maximum level in the green-yellow color range, at about -10 dB, relative to a maximum field in E_θ of about 4 dB.

Figs. 3.12 and 3.13 show the field strengths for the centre-fed half-wave monopole and the end-fed half-wave monopole, respectively. The field strength for the quarter-wave monopole in Fig. 3.11 is remarkably similar to that for the centre-fed half-wave monopole in Fig. 3.12, in both E_θ and E_ϕ. There are some slight differences. For example, for the centre-fed case there are minima at about -30 dB at $\phi = 130$ and 240 degrees, which appear as cyan spots in Fig. 3.12(a) at $\theta \approx 75$, which are not seen for the quarter-wave monopole.

The end-fed half-wave monopole's patterns in Fig. 3.13 are quite different from the other two cases. There is no green circle in E_θ at $\theta = 80$ degrees as in Fig. 3.11(a). Instead, as shown in the elevation patterns of Fig. 3.10(b) and (c), the field has a broad lobe with maxima at about $\theta = 60$ and 120 degrees, which is modestly flattened at $\theta = 90$ degrees. Thus Fig. 3.13(a) shows a broad, red band roughly centered at θ=90 degrees, with a yellowish, broad minimum at $\theta = 90$ between $\phi = -150$ (that is +210) degrees and + 140 degrees. The cross-polarized component in Fig. 3.13(b) is much smaller than in Figs. 3.11(b) or 3.12(b); the largest field strength is green, more than 20 dB below isotropic, whereas in Fig. 3.11(b) the largest field is about 10 dB below isotropic. The white areas in Fig. 3.13(b) correspond to fields that are "off scale", lower than the fields which plot dark blue. (These regions should be filled in black; however a bug exists in the software preventing plotting black as a color.)

3.3.3 Comparison of the Three Cases

Of three antenna types, the quarter-wave monopole and the centre-fed half-wave monopole have remarkably similar radiation patterns as shown in Fig. 3.11 and 3.12. For both these antennas there is a minimum in the field strength at about $\theta = 80$ degrees, and the cross-polarized field is high, about 10 dB below isotropic. The end-fed, half-wave monopole's patterns in Fig. 3.13 show a broad band of large field strengths around the $\theta = 90$ azimuth plane. The cross-polarized component is more than 20 dB below isotropic. Thus the centre-fed monopole appears to be more suitable as an antenna for a portable radio.

3.4 Software Setup for Constructing Maps of the Near Field

The purpose of this report is to investigate the near field structure of handheld radios at 850 MHz, and so this section explains how the software system of Fig. 3.2 is used to construct maps of the near field. The first step is to specify the coordinates of points close to the handset where the near field is to be evaluated. Then NEC is used to calculate the field strength at these points. Then we must scale the field strength to the desired radiated power of 700 milliwatts. Finally we construct a contour map of the near field.

3.4.1 Specifying a Plane of Near-Field Points

Suppose we wish to calculate the near field in an xz plane in the coordinates of Fig. 3.5, located at $y = -1$ cm, which is 1 cm from the case of the cellular phone, approximately at the location of the side of the operator's head. Fig. 3.14 shows a plane of 51 by 51 points in the near field, centered on the base of the antenna and located one cm to the side of the cellular phone. To calculate the near field at each point in the plane we must supply an "NE" card for each point, giving the xyz coordinates of that point in three dimensional space, a total of 2601 NE cards. This is most easily done using a program to generate the desired point coordinates and write the NE cards as an ASCII file.

Program NEDIS at the top of Fig. 3.2 is set up to prepare groups of NE cards for this type of problem. A short input data file "XZPLANE.DAT" is prepared which describes the plane of points by specifying the following data. First, specify the coordinates of the centre point of the plane, at y=-1 cm, and at x and z corresponding to the base of the antenna. The spacing of the points in the near field plane must be specified, and the number of points in the x and z directions. NEDIS prepares an NE card and also an NH card for each point in the plane, a list of 5202 cards in file NENH.GW. The NH cards are included so that the magnetic field can be examined if desired. A file editor is used to incorporate the NE and NH cards into the NEC input file called PHONE1.I1. To be sure that no mistake has been made, that is, that the desired set of points has been specified relative to the telephone handset, NEDIS prepares file GRID.GW, which can be displayed with program MODEL to show the points in relation to the handset as in Fig. 3.14. Program NEDIS prepares three files that are used later to display the fields in three dimensional space. NORMALS.NOR contains the unit normal to the plane at each near field point. AXIALS.TAN and CIRCUM.TAN contain the unit tangential vectors to the plane in two directions at each point. For a plane of points these normals and tangentials are very simple. NEDIS also permits near fields to be examined over more complex surfaces, for which the normal and tangential vectors are very convenient to have.

3.4.2 Calculating the Near Field

The NEC program is run to calculate the currents on the monopole and handset, and from the currents the far fields on the standard set of conical cut radiation patterns, as described above, and also the electric field at each point on the plane of near field points. The power is determined by program ISOLEV and written into the data file PHONE1.1 in Fig. 3.2, which now contains currents, far fields, and near fields.

Program NEDIS displays the near fields in three dimensional space schematically as in Fig. 3.15. The wire-grid model is drawn, and then the field at each near field point. NEDIS reads the coordinates of each near field point and the components of the electric field, E_x, E_y, and E_z, from the PHONE1.1 data file. One component of the electric field is then drawn as a line segment in the direction of that field component, of length proportional to the strength of the electric field. Thus Fig. 3.15 shows E_z at each near field point in the xz plane of Fig. 3.14. Fig. 3.15 suggests that strong fields are found near the tip of the antenna, near the feed point at the base of the antenna, and near the bottom of the case.

3.4.3 Preparing a Contour Map

For this project it is useful to prepare contour maps of the electric field strength, such as that shown in Fig. 3.16. NEDIS is set up to rescale the input data to our desired power level of 700 milliwatts, and write the scaled data to a "table file" FIELD.TBL for display with program CPLOT as a contour map, or with program SPLOT as a surface above the xz plane. CPLOT is used to compose the contour map, select the decibel scale, specify the interval between contours as 3 dB, and label the contours with their field strengths. An image of the contour map is then written to the graphics file CPLOT.LAB. The image file uses an arbitrary scale on each distance axis. Program MAKEMAP rescales the image so that the distance scale is the same for both the x and the z directions, and also superimposes the outline of the handset on the near field map, to obtain file MAP.LAB containing a map such as that of Fig. 3.16. Seeing the handset and antenna on the field map makes easy the association of hot spots with their corresponding sources. Near field maps can be constructed by this system for both xz planes and also for yz planes. Also, field maps can be prepared in the format of color contour maps, using a color scale similar to that used for the far fields given above.

3.4.4 Making Hard Copies

To prepare reports such as this one, it is necessary to have hardcopies of graphs, made on a laser printer. Any line drawing that can be created with any of the graphics programs in Fig. 3.2 can be written as a graphics file with the extension "LAB", such as CPLOT.LAB. These programs are: MODEL, HIDNMOD, PATCMP, IDIS, NEDIS, CPLOT, SPLOT and PPLOT. These graphics image files can be manipulated with the mini-CAD program called LABLNG, to make customized drawings for inclusion as figures in reports. Program MAKEPS(MAKE PostScript) translates the "LAB" format into a Postscript file, which can then be copied to a Postscript laser printer to obtain a hard copy for reporting purposes.

3.5 Near Field Structure for the Three Antenna Types

This section presents the near field of the three antennas types, in an *xz* plane and in a *yz* plane.

3.5.1 Fields in an *xz* Plane

Fig. 3.14 shows the *xz* plane selected for the examination of the near field. It is located one cm from the case of the handset of Fig. 3.1, on the side where the operator's head is located. The plane of points is centered on the base of the antenna, and is 50 by 50 cm in extent. The field strength contours show the value of E_z when the antenna is a quarter-wave monopole, fed at its base, and radiating 700 milliwatts. Contours are separated by 3 decibels. The largest field strengths are found near the feed point of the antenna, of 48 dB relative to 1 volt/metre field strength. Note that the field strength is equally large near the bottom of the case. The field strength is also large near the tip of the antenna, in excess of 39 dB. Recall in Fig. 3.7(a) that the current is strong near the feed point, and turns a corner as it flows from the top of the case onto the antenna, giving rise to large field strengths. The field is strong near an open circuit such as the tip of the antenna, or the bottom of the case. Hence by reducing the currents on the case we might expect to reduce the field strengths around the case.

Fig. 3.17 shows the field strength associated with the half-wave monopole when the feed point is at the centre of the antenna. It is seen that the field strength near the feed point is in excess of 42 dB. The field is about 33 dB near the tip of the antenna, less than at the tip in Fig. 3.16. The field at the top and bottom of the case is about 45 dB, almost the same as in Fig. 3.16. Thus, the quarter-wave monopole and the centre-fed half-wave monopole have very similar near fields, as well as having similar far field patterns.

In contrast, Fig. 3.18 shows the field strengths for the end-fed half-wave monopole. The field at the feed point at the top of the case is about 45 dB, similar to that for the previous two antennas. The field at the tip of the antenna is about 42 dB, but note that the tip of this long antenna is farther from the user's head than that of the quarter-wave monopole of Fig. 3.16. Recall from Fig. 3.7(c) that the currents on the case of the handset were considerably less for the end-fed half-wave monopole than for the other two antennas. This is seen in the near fields associated with the case. Thus the field strength at the bottom of the case is about 33 dB, compared to 45 dB for the other two antennas.

3.5.2 Fields in a *yz* Plane

Fig. 3.19 shows the *yz* plane chosen for examination. The plane is centered on the antenna vertically, but the handset lies entirely to the right of the points making up the plane. The case is separated by 1/2 cm from the closest point on the plane. Thus the plane of points encompasses the region of space where the operator's head would be located. We can model the head as an ellipse very roughly 15 cm wide and 22 cm tall, centered about $z = -5$ cm and $y = 17.5$ cm in Figs. 3.19, 3.20 and 3.21. Thus the head occupies roughly the region $10 < y < 25$ cm and $-16 < z < 6$ cm in these figures. The bottom of the head coincides with the bottom of the handset; the top of the head lies halfway up the quarter-wave monopole in Fig. 3.20; the ear lies in the top third of the handset case.

Fig. 3.20 shows the near field of the quarter-wave monopole in this *yz* plane, and should be correlated with Fig. 3.16. The field near the tip of the antenna is 42 dB. Near the feed point the field is in excess of 48 dB, larger than in Fig. 3.16 because we are half a centimeter closer in Fig. 3.20. The field near the centre of the case falls rapidly toward zero, as the metallic case requires that E_z be zero at its surface. The field near the bottom of the case exceeds 45 dB. As we move away from the case into the space to be occupied by the user's head, the field strength falls rapidly. The fields tend to be larger in the bottom half of the plane of Fig. 3.20, and drop off more rapidly with distance from the antenna in the top half of the figure. The region occupied by the user's head sees field strengths from 48 dB close to the top of the handset to about 30 dB at the right hand side of the user's face.

Fig. 3.21 shows the fields associated with the half-wave monopole when the feed point is at its centre. The field reaches 42 dB near the feed point, about the same as seen near the tip of the monopole in Fig. 3.20. The field near the top and the bottom of the case is about 45 dB, again similar to that of Fig. 3.20. The field in the bottom half of Fig. 3.21 is very much the same as in the bottom half of Fig. 3.20. In the top half of the figure, the field due to the quarter-wave monopole decreases more rapidly with distance than that of the centre-fed half-wave monopole.

Fig. 3.22 shows the near fields of the half-wave monopole when it is end-fed. The field strength at the top of the case, near the feed point, is in excess of 48 dB, similar to that of the other two antennas. The field at the tip of the antenna is about the same strength as the field at the tip of the quarter-wave antenna of Fig. 3.20, but the tip is now farther from the user's head. The field at the bottom of the case is very considerably less, about 33 dB in Fig. 3.22 compared to 45 dB in Fig. 3.20.

These differences are seen in comparing the near field of the quarter-wave monopole in Fig. 3.20 to those of the end-fed, half-wave monopole in Fig. 3.22. The field strength over the bottom half of the plane in Fig. 3.22 decreases from 24 dB at right to 21 dB at left; in comparison in Fig. 3.20 the field strength over roughly the same region decreases from 38 to 24 dB, and so is much stronger. It is interesting that in the top half of the plane, the field strengths associated with the half-wave monopole are stronger than those of the quarter-wave monopole. Thus, the field of the quarter-wave antenna has decreased to about 18 dB at 25 cm horizontally from the antenna tip, but only to about 27 dB the same distance from the tip of the half-wave antenna.

In the region $10 < y < 25$ cm and $-16 < z < 6$ cm occupied by the user's head, the field strengths in Fig. 3.22 vary from 48 dB near the earpiece, but only 33 dB near the chin, and fall off more rapidly with distance than in Fig. 3.20, being at about 21 dB at the right hand side of the user's head.

Note that we have investigated E_z because we expect a vertically-oriented monopole antenna to radiate primarily the *z* component of the electric field. We could also investigate E_x and E_y. Thus **these "radial" components of field are expected to be large near the feed point and near the tip of the antenna.** They will also be large near the top and the bottom of the case.

3.6 Comparison of the Three Antennas

This chapter has compared the performance of three different antenna designs, each mounted on the same handset. The quarter-wave monopole is the simplest, presenting a low impedance at the feed point at the base of the antenna. The second antenna is a half-wave monopole, but it is fed at its centre point. It is found that the impedance at the feed point is high and that there is strong coupling to the case, so that the current flow on the case is about the same

for the quarter-wave monopole and for the half-wave centre-fed monopole when the radiated power is the same. The third antenna is a half-wave monopole fed at the connection point to the case, and is found to couple less strongly to the handset case.

The far field was examined over the whole radiation sphere and it was found that the quarter-wave monopole, and the half-wave centre-fed monopole have very similar radiation patterns. The end-fed half-wave monopole has more suitable radiation patterns for a portable radio than do the other antennas.

The near fields of these two antennas were examined in an *xz* plane and in a *yz* plane. It was found that the quarter-wave monopole and the centre-fed half-wave monopole have very similar near fields, including the fields at the bottom of the handset case. The end-fed half-wave monopole has about the same field strength at the feed point as do the other two antennas. Although the field strength at the tip of the antenna is similar to that at the tip of the quarter-wave monopole, the tip of the half-wave monopole is farther from the user's head. The end-fed half-wave monopole couples less strongly to the handset case than does the quarter-wave monopole and so the field strength at the bottom of the case is about 12 dB less.

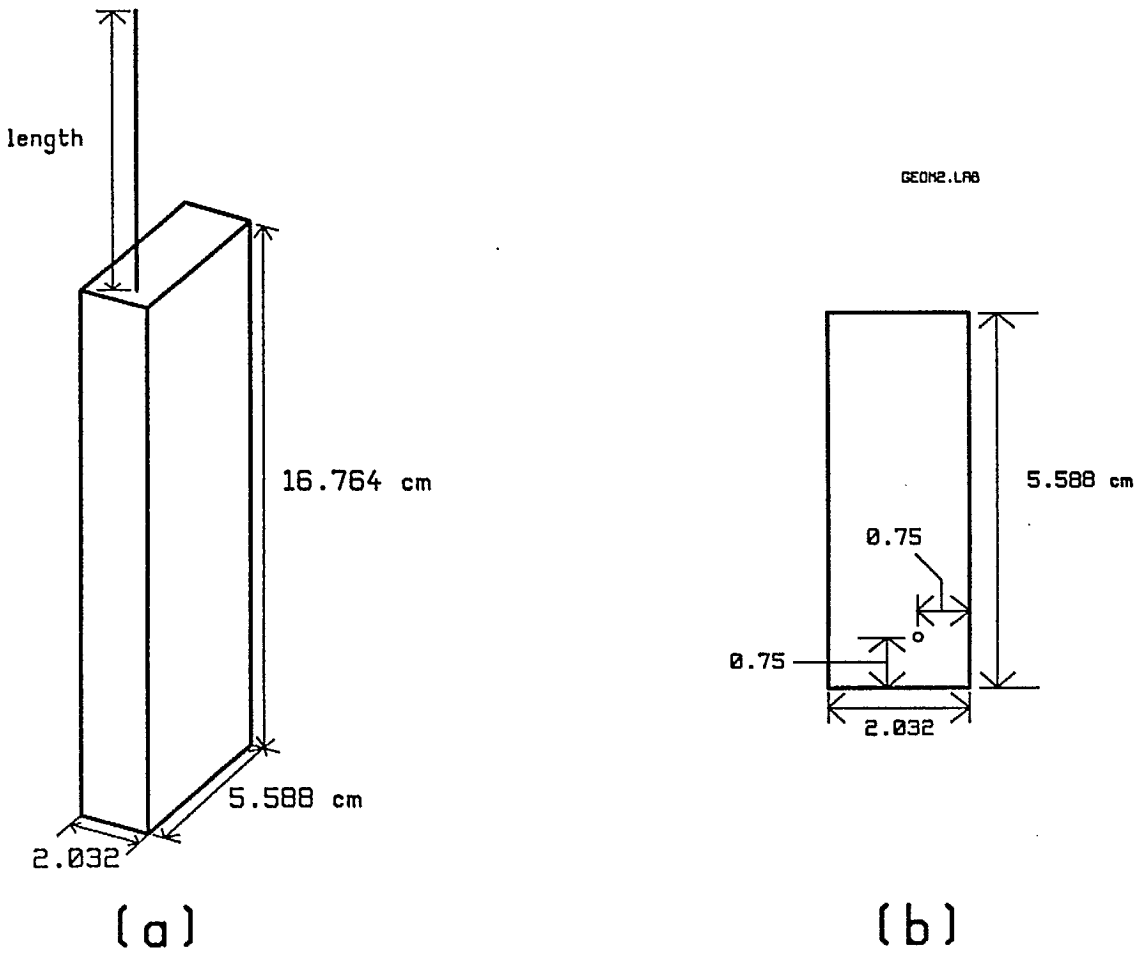

Fig. 3.1 The dimensions of the cellular telephone set used in Chapter 3 to compare the performance of the three antenna types: quarter-wave, end-fed; half-wave center-fed; and half-wave end-fed.

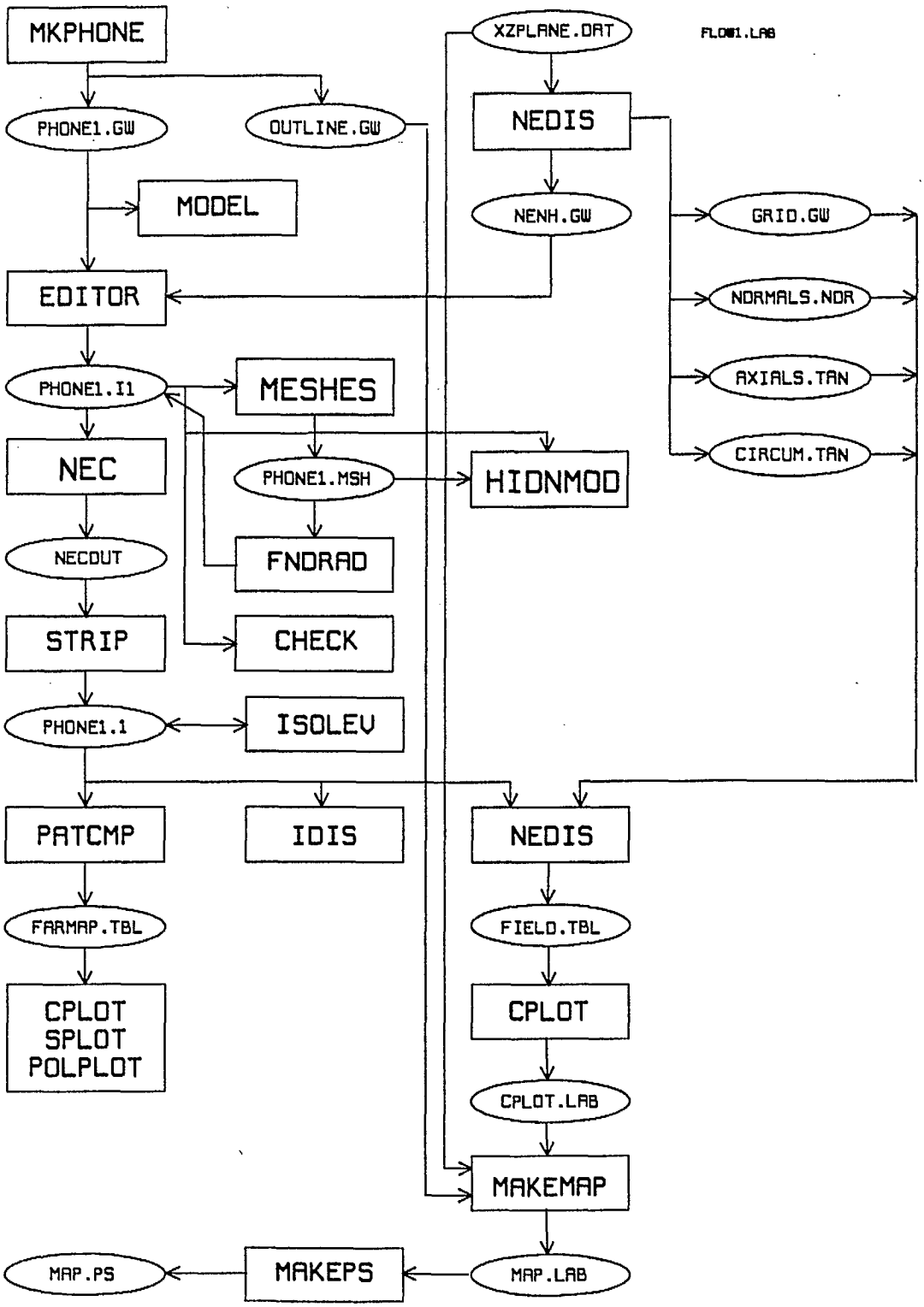

Fig. 3.2 Software flowchart showing the programs(rectangles) and data files(ellipses) used with wire-grid models to obtain far-field patterns, current distributions, and near-field maps of the fields of a cellular telephone.

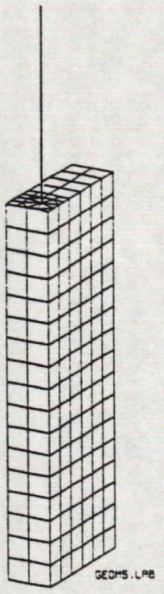

Fig. 3.3 Wire-grid model of the cellular telephone of Fig. 3.1 having 620 segments, of average length 0.93 cm.

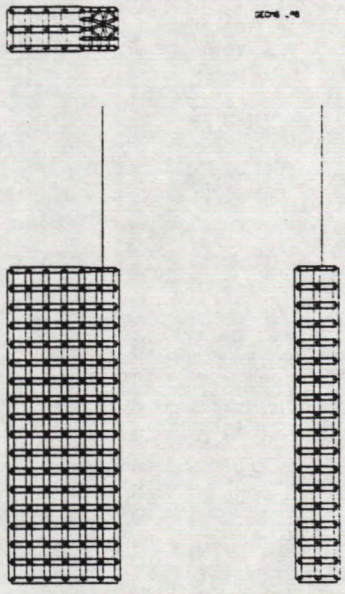

Fig. 3.4 Three views of the wire-grid model, showing the thickness of the wires and the feed region at the base of the monopole.

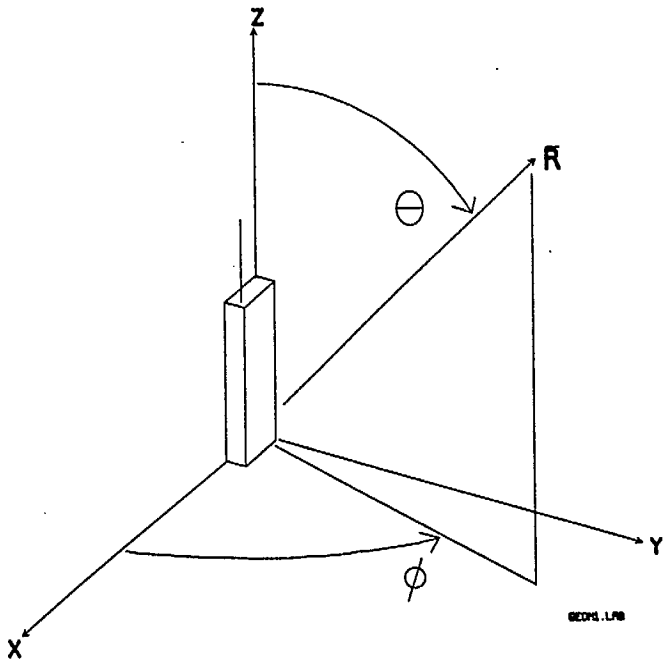

Fig. 3.5 The position of the cellular telephone in the *xyz* coordinate system, and the definition of the spherical angles θ and ϕ.

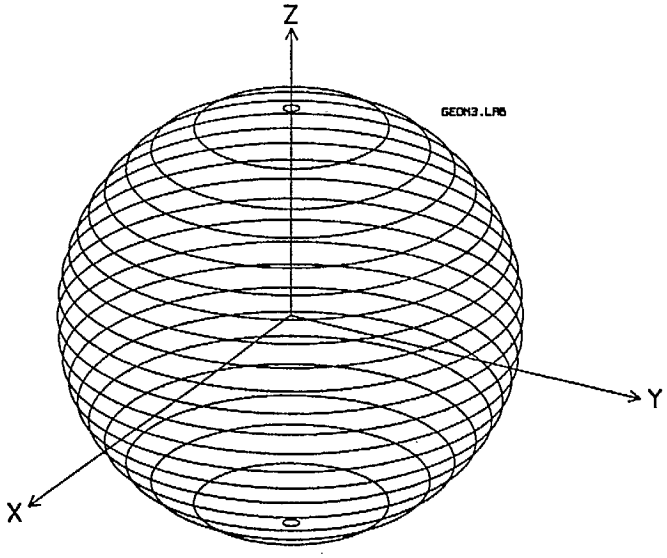

Fig. 3.6 The radiation sphere, showing the set of "conical cuts" for θ =0, 25, 37, 45, 53, 60, 66, 72, 78, 84, 90, 96, 102, 108, 114, 120, 127, 135, 143, 155, and 180 degrees, each for $0 \leq \phi \leq 360$.

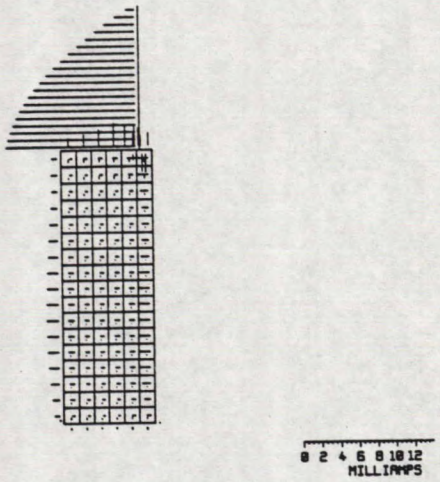

(a) quarter-wave monopole, base-fed.

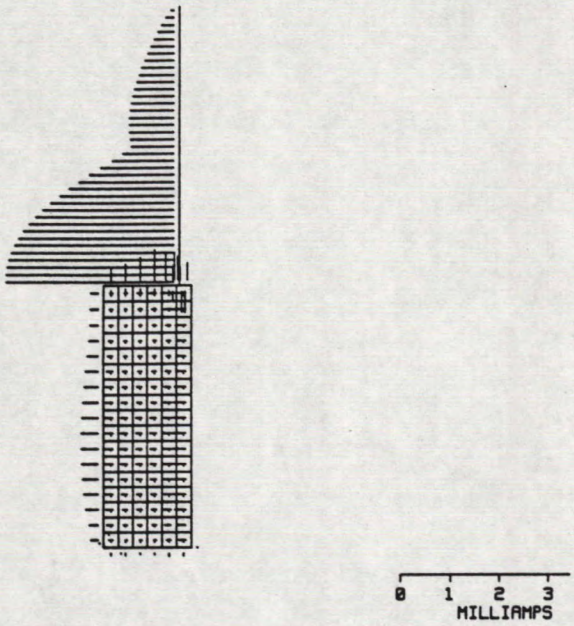

(b) half-wave monopole, centre-fed.

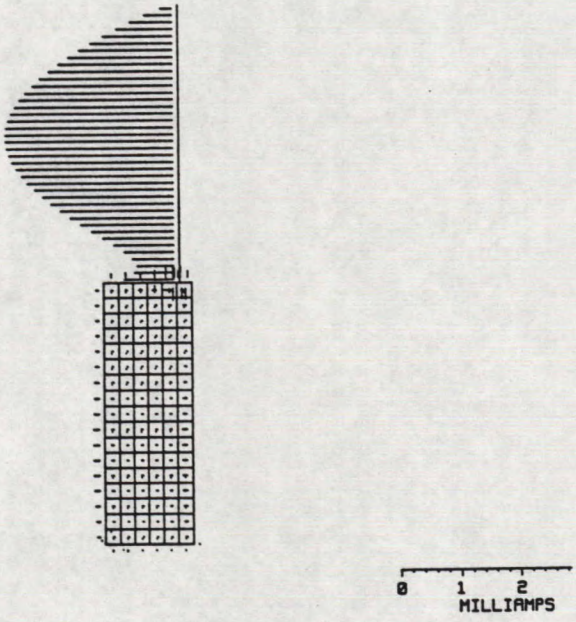

(c) half-wave monopole, base-fed.

Fig. 3.7 The current distribution on the cellular telephone set with three different antenna configurations.

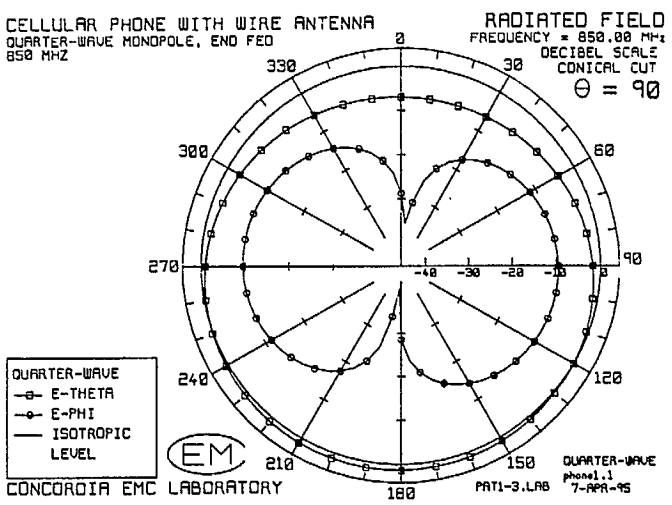

(a) $\theta = 90$ azimuth plane.

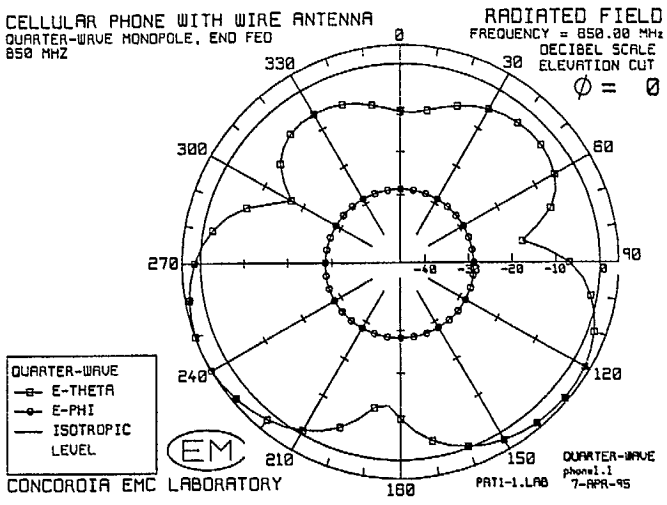

(b) $\phi = 0$ elevation plane.

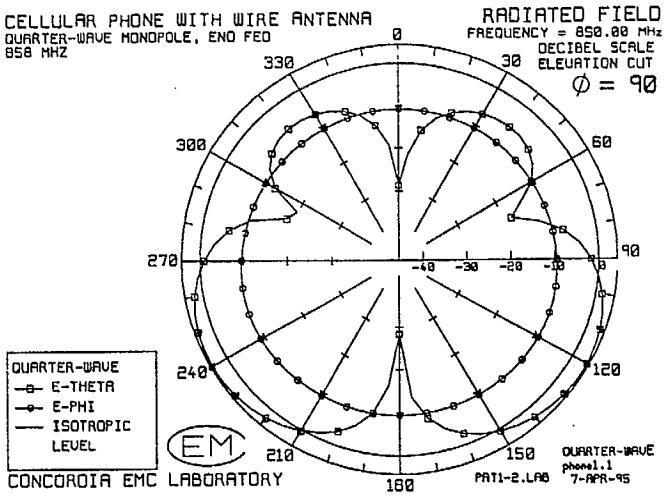

(c) $\phi = 90$ elevation plane.

Fig. 3.8 The radiation patterns of the cellular telephone with the quarter-wave monopole, base-fed.

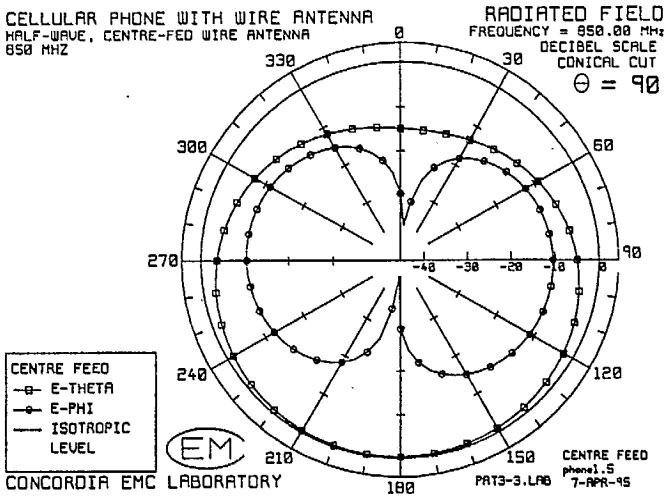

(a) $\theta = 90$ azimuth plane.

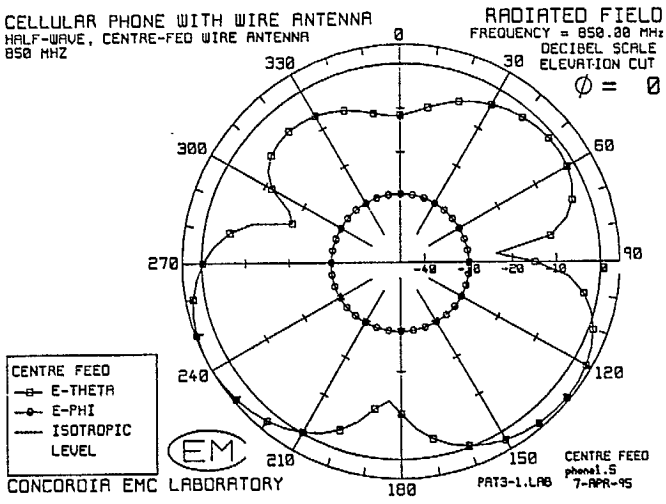

(b) $\phi = 0$ elevation plane.

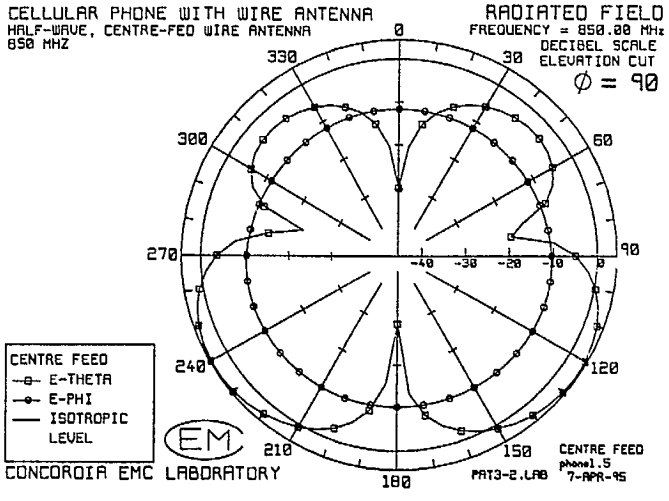

(c) $\phi = 90$ elevation plane.

Fig. 3.9 The radiation patterns of the cellular telephone with the half-wave monopole, centre-fed.

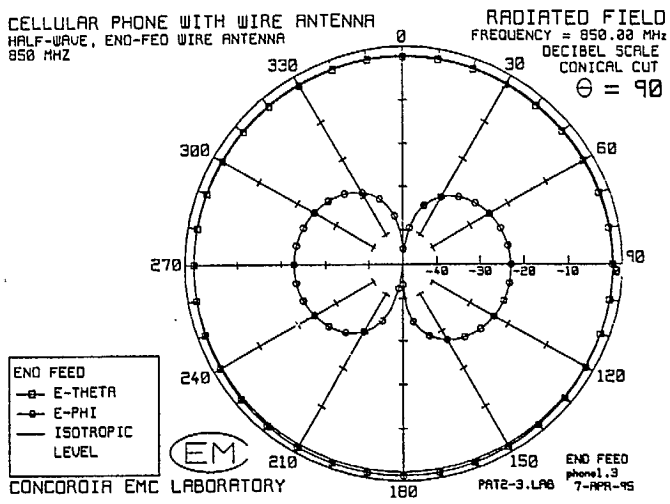

(a) $\theta = 90$ azimuth plane.

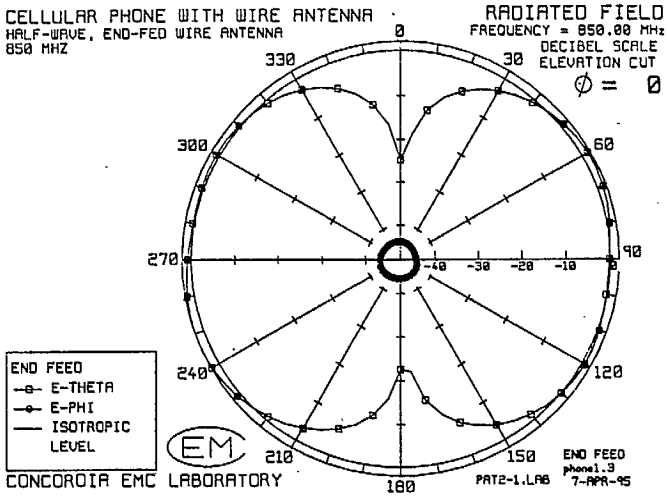

(b) $\phi = 0$ elevation plane.

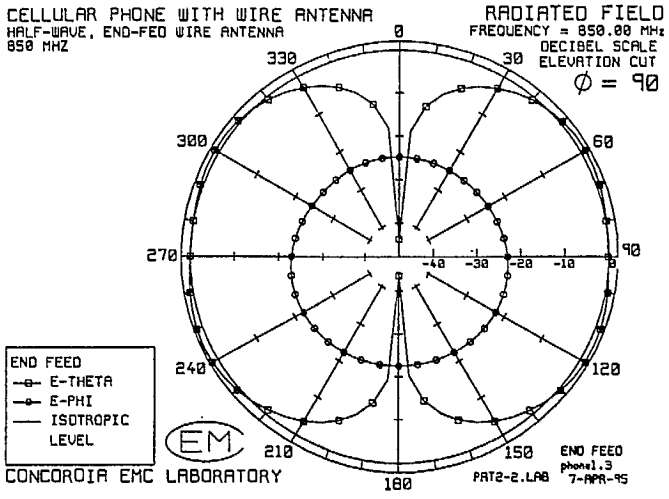

(c) $\phi = 90$ elevation plane.

Fig. 3.10 The radiation patterns of the cellular telephone with the half-wave monopole, base-fed.

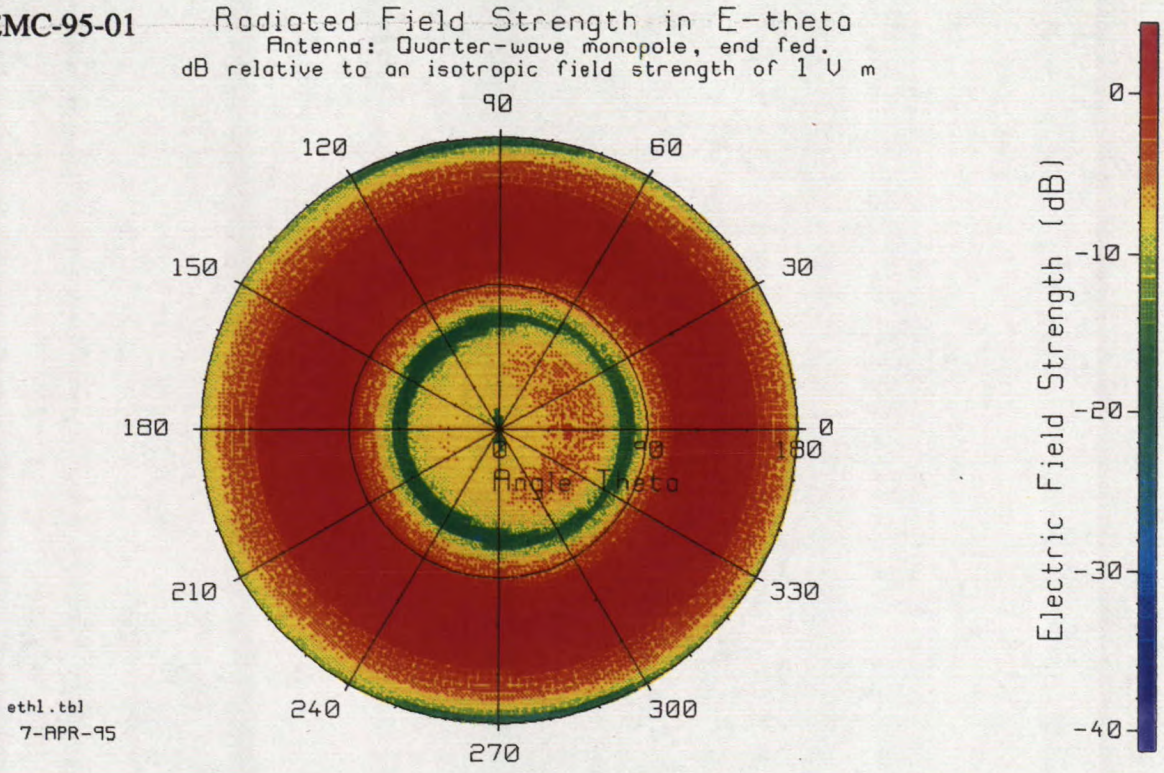

(a) Field strength in E_θ.

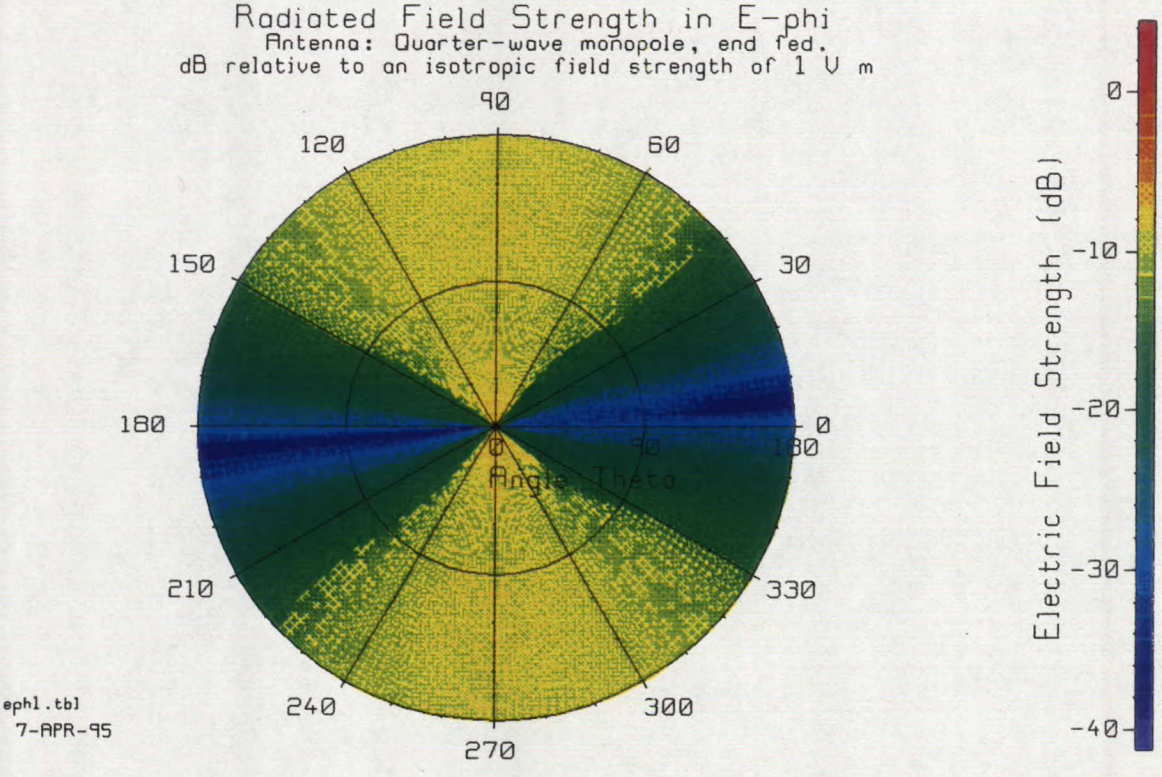

(b) Field strength in E_ϕ.

Fig. 3.11 The field strength over the radiation sphere of the cellular telephone with the quarter-wave monopole, base-fed.

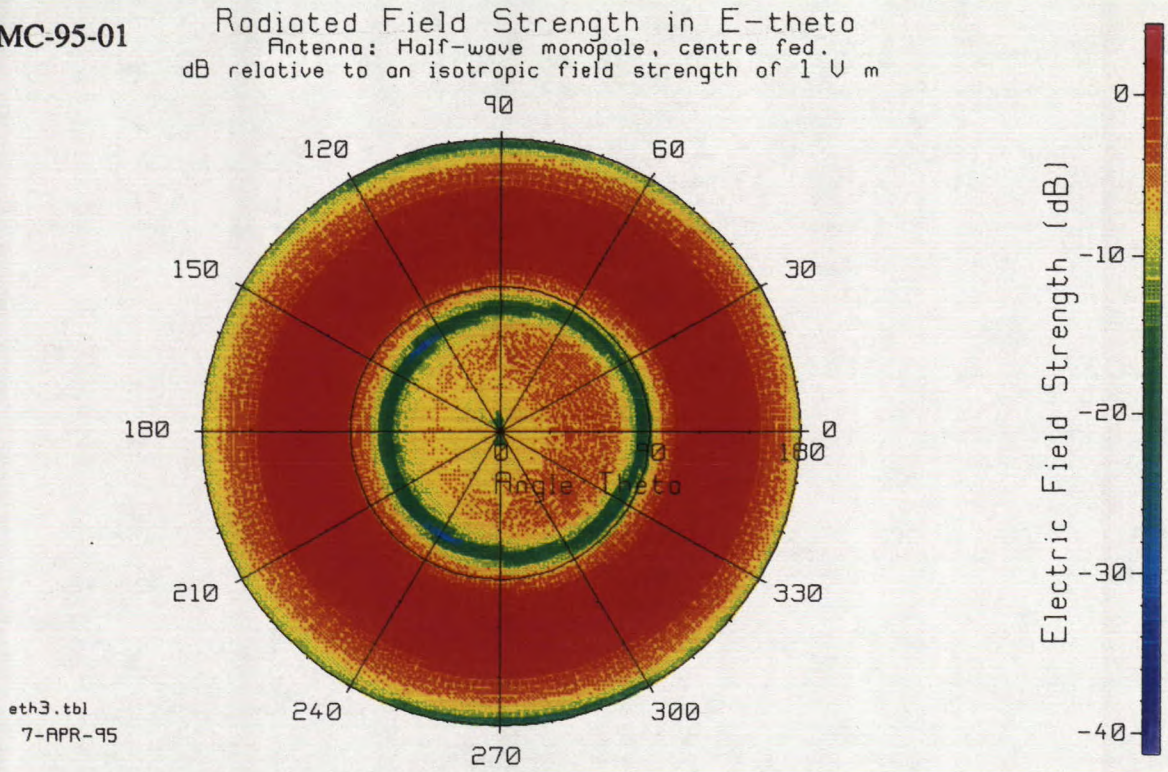

(a) Field strength in E_θ.

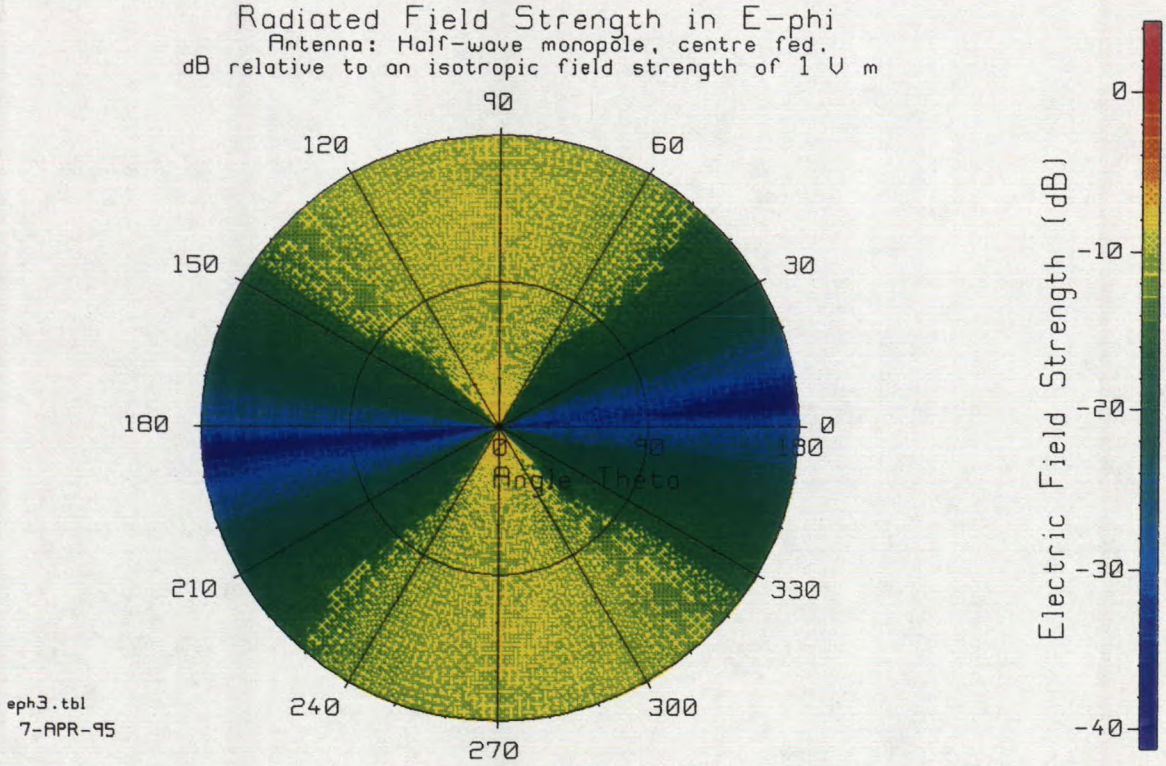

(b) Field strength in E_ϕ.

Fig. 3.12 The field strength over the radiation sphere for the cellular telephone set with the half-wave monopole, center-fed.

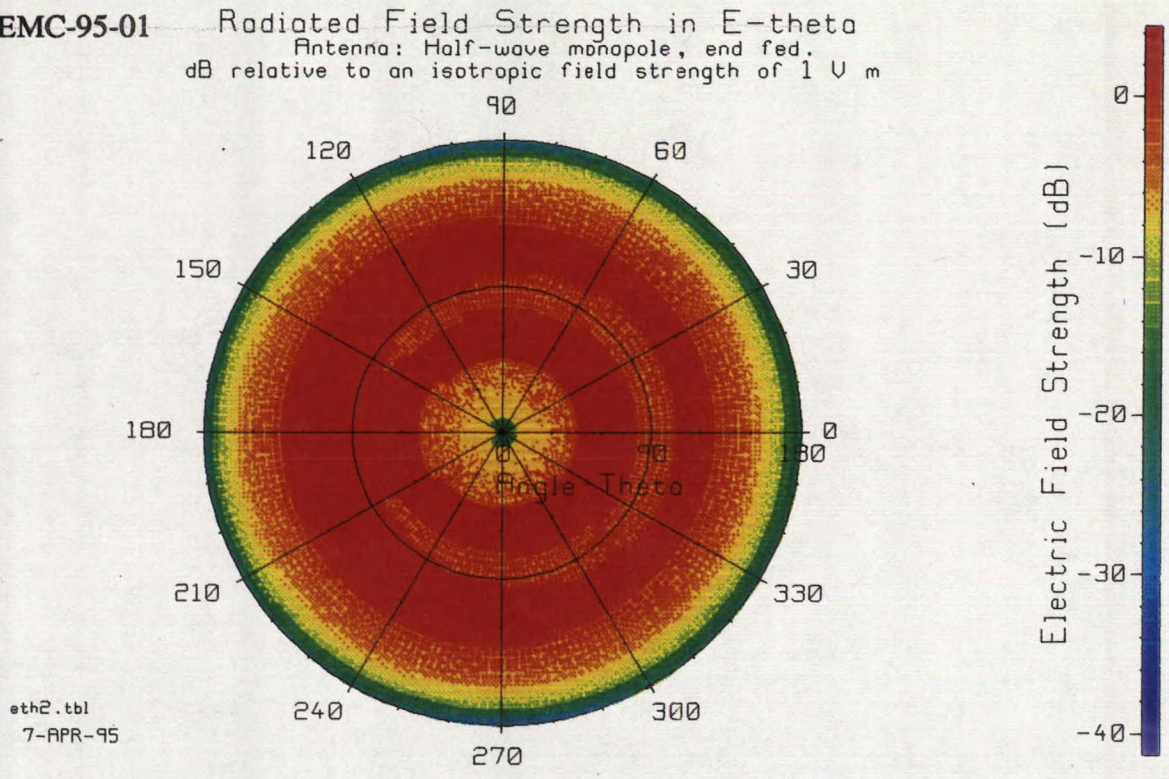

(a) Field strength in E_θ.

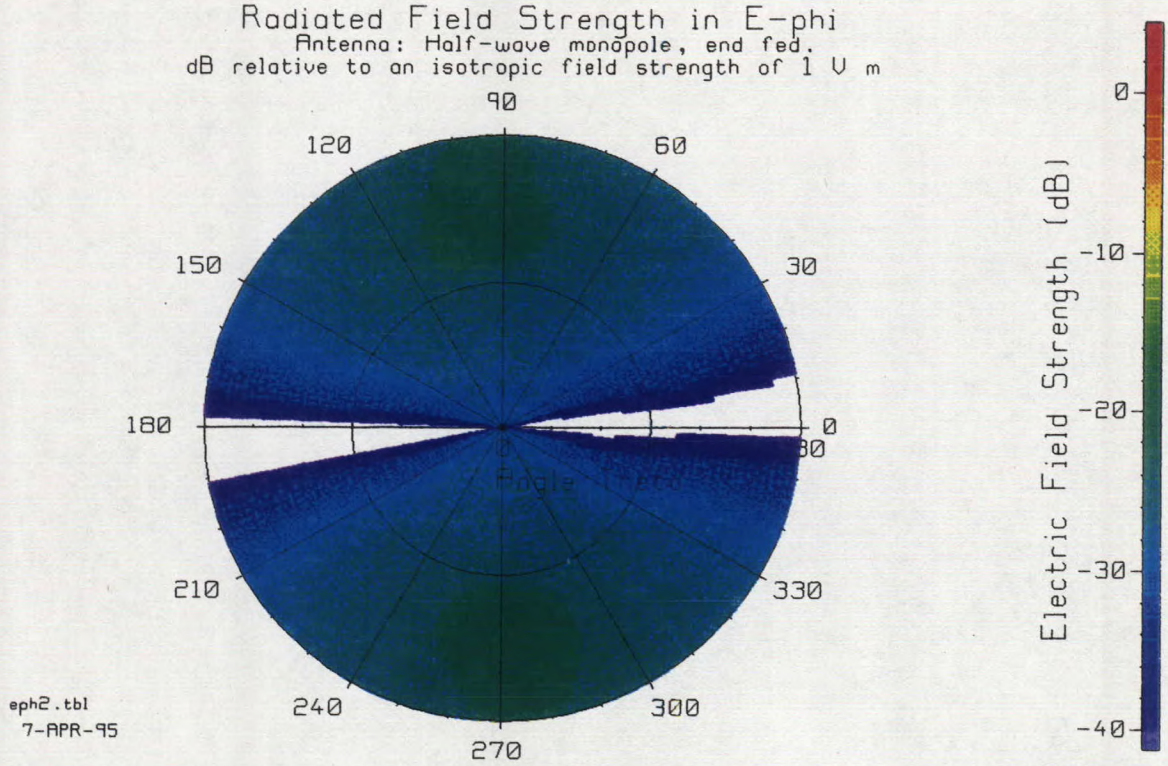

(b) Field strength in E_ϕ.

Fig. 3.13 The field strength over the radiation sphere for the cellular phone with the half-wave monopole, base-fed.

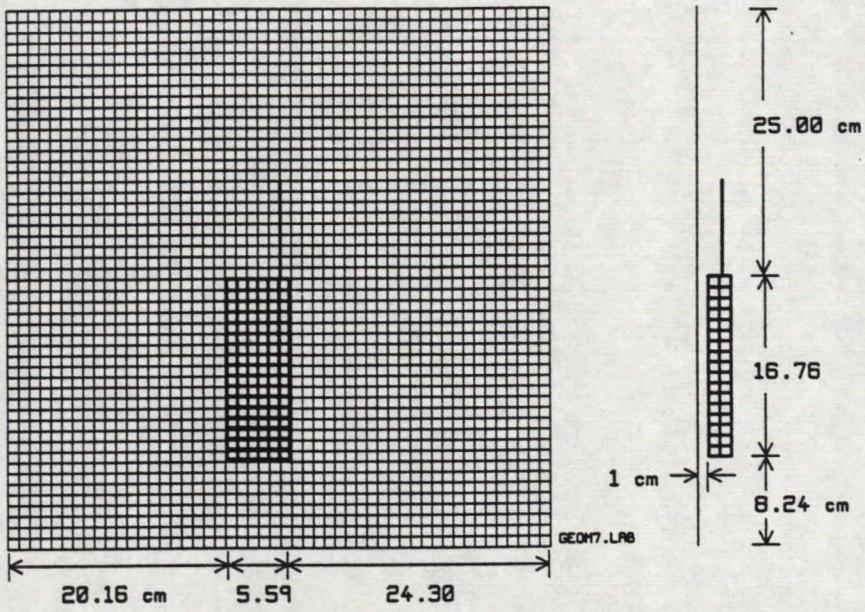

Fig. 3.14 A grid of 51 by 51 points spaced 1 cm apart that will be used to examine the near field of the cellular telephone set. The grid lies in a plane parallel to the *xz* plane, 1 cm from the case of the cellular telephone set.

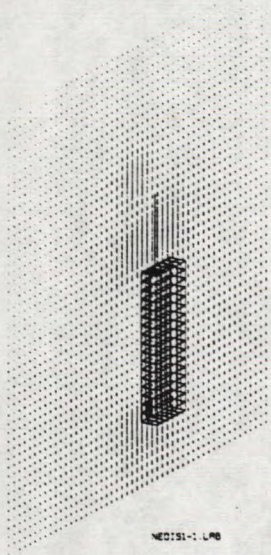

Fig. 3.15 The field strength E_z of the cellular telephone for the quarter-wave, end-fed monopole, plotted with program NEDIS. The field at each grid point is represented as a line segment of length proportional to the field strength.

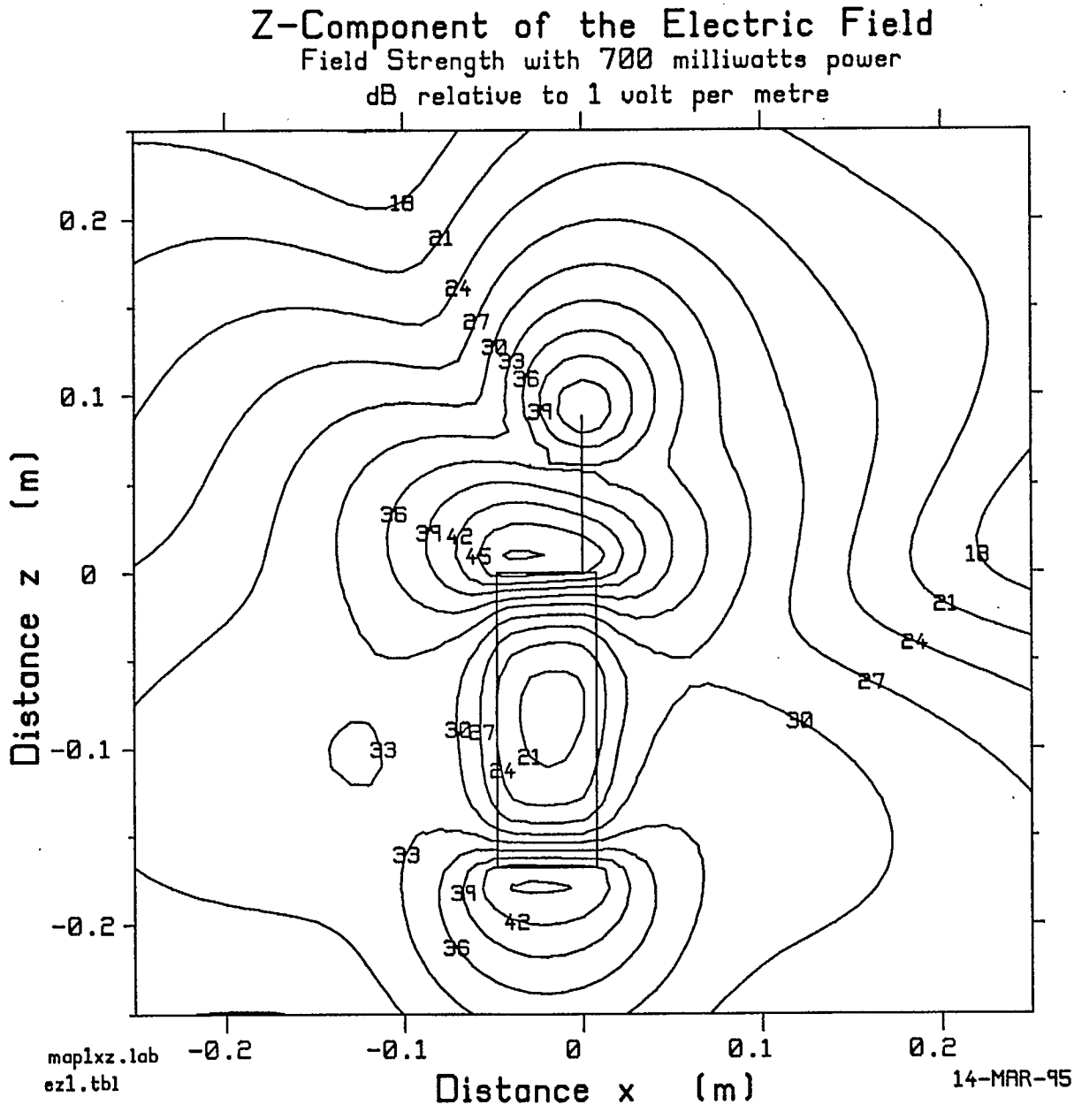

Fig. 3.16 Contour map in the *xz* plane of the field strength E_z of the cellular telephone with the quarter-wave, end-fed monopole over the grid of points of Fig. 3.14, at 850 MHz. The field strength contours are in dB relative to 1 volt per metre, with a radiated power of 700 milliwatts.

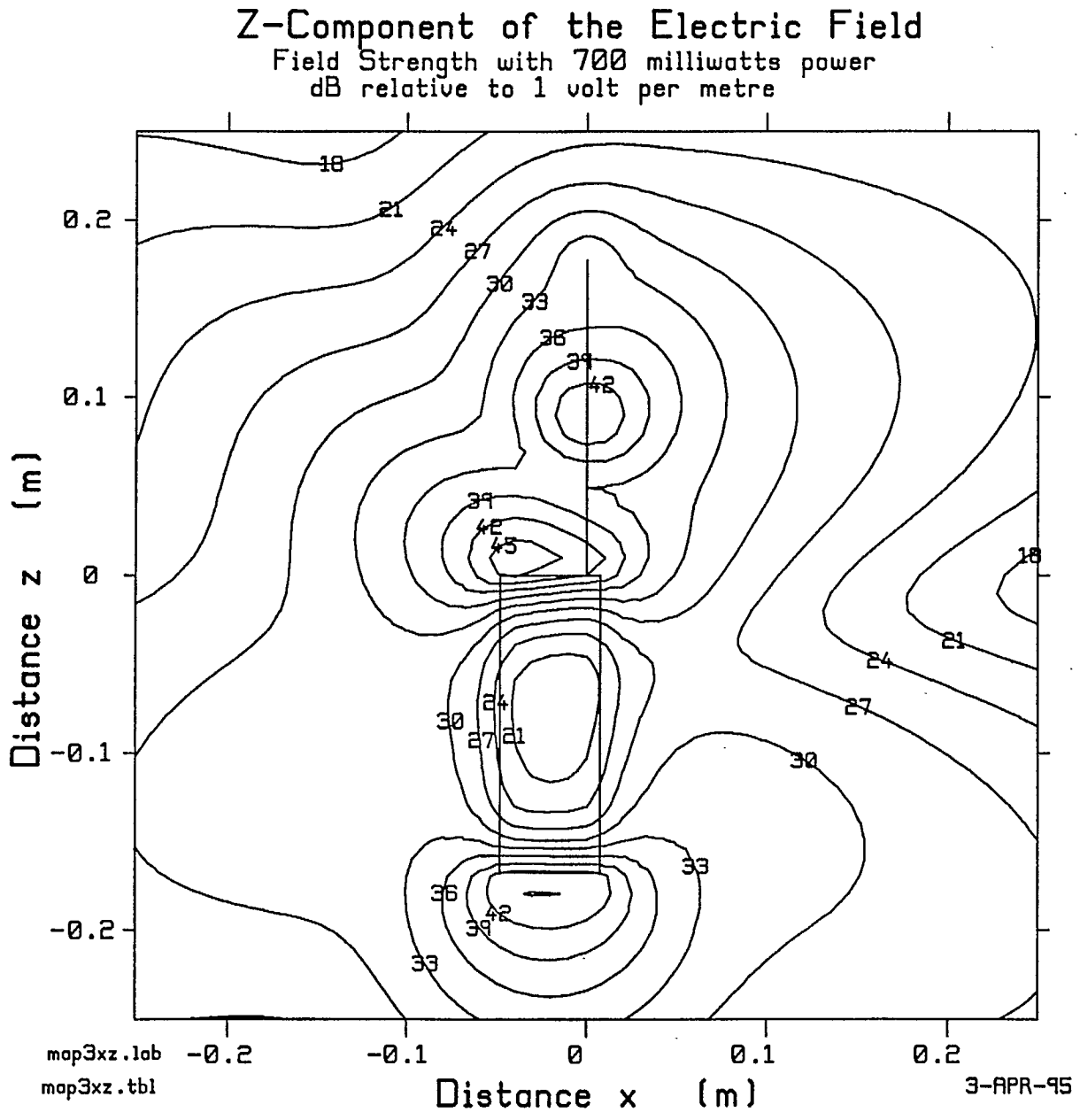

Fig. 3.17 Contour map of the field strength E_z of the cellular telephone with the half-wave monopole, center-fed.

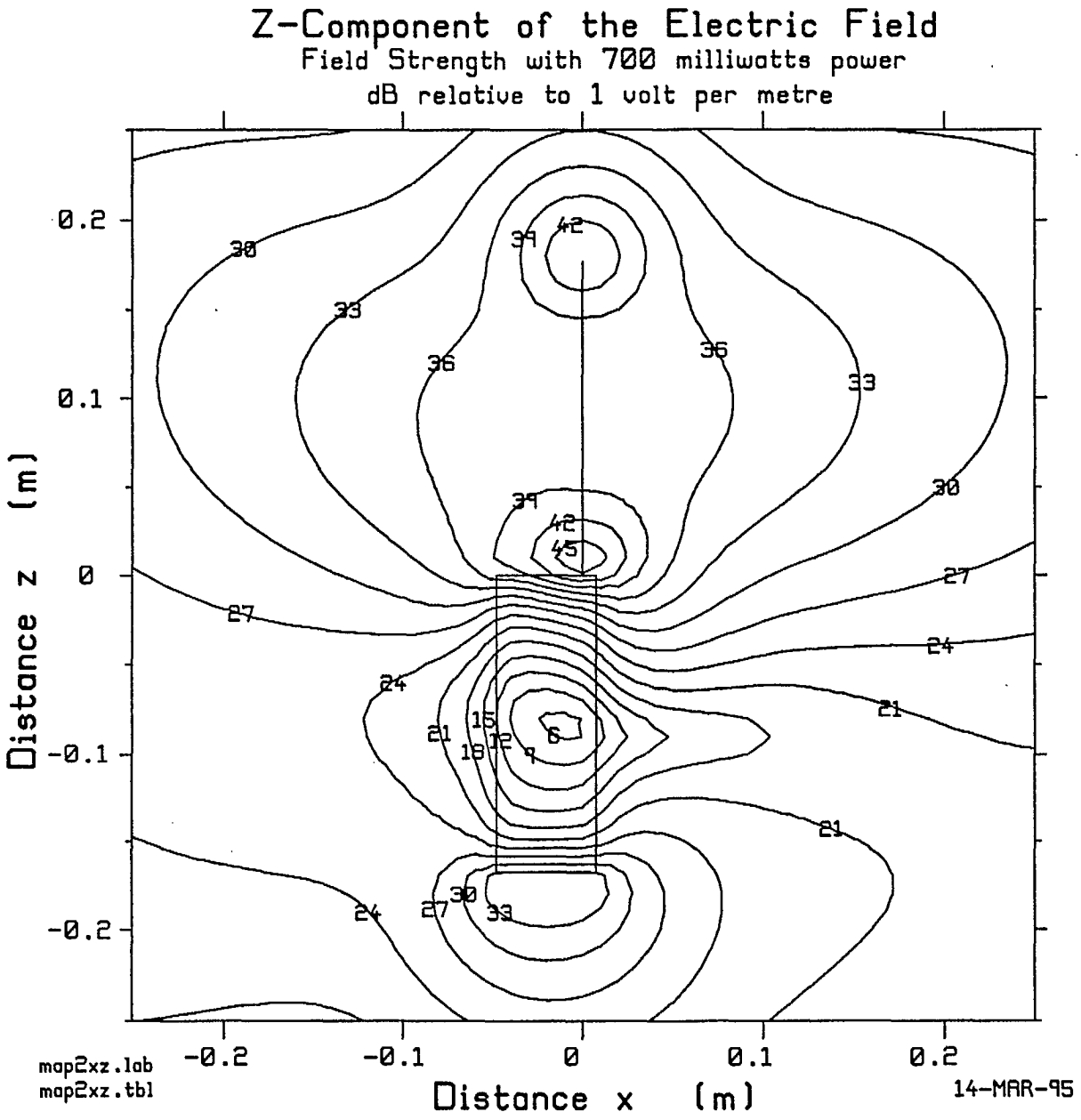

Fig. 3.18 Contour map of the field strength E_z of the cellular telephone with the half-wave monopole, end-fed.

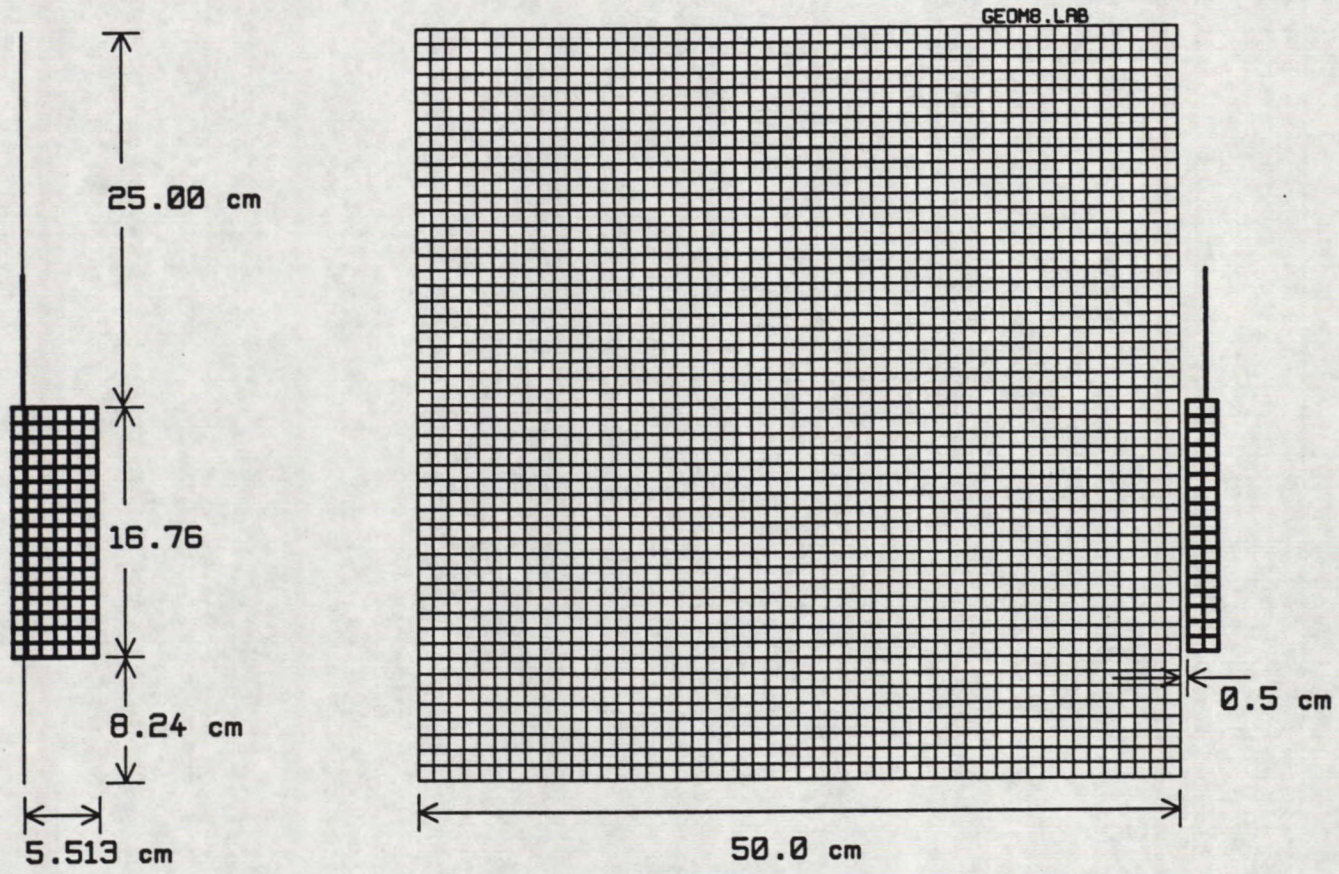

Fig. 3.19 A grid of near-field points in a *yz* plane, in the plane of the monopole antenna. The operator's head would occupy roughly the lower right-hand quarter of this grid.

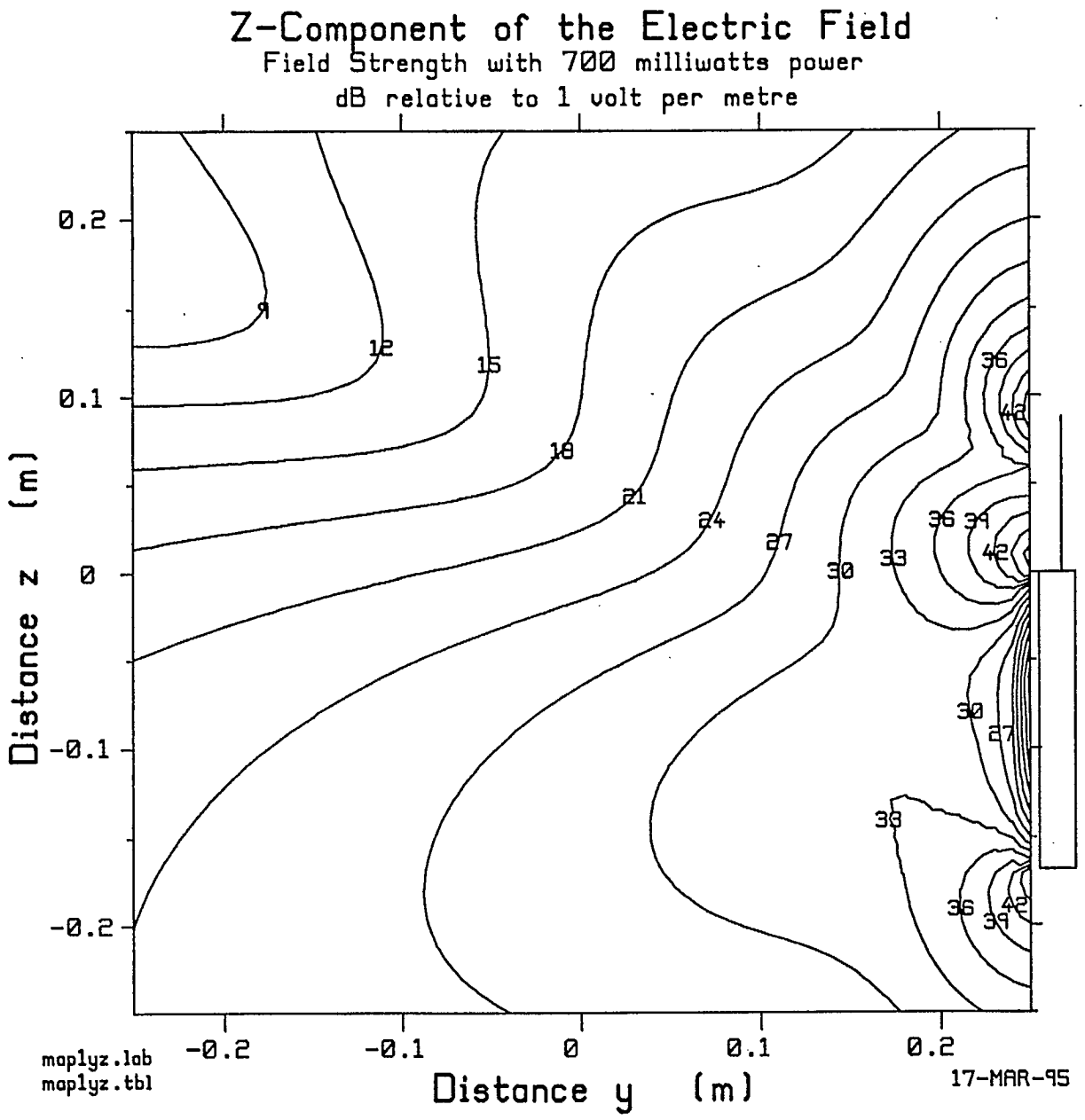

Fig. 3.20 Contour map of the field strength E_z of the cellular telephone with the quarter-wave monopole, end-fed, over the *yz* plane grid of points of Fig. 3.19.

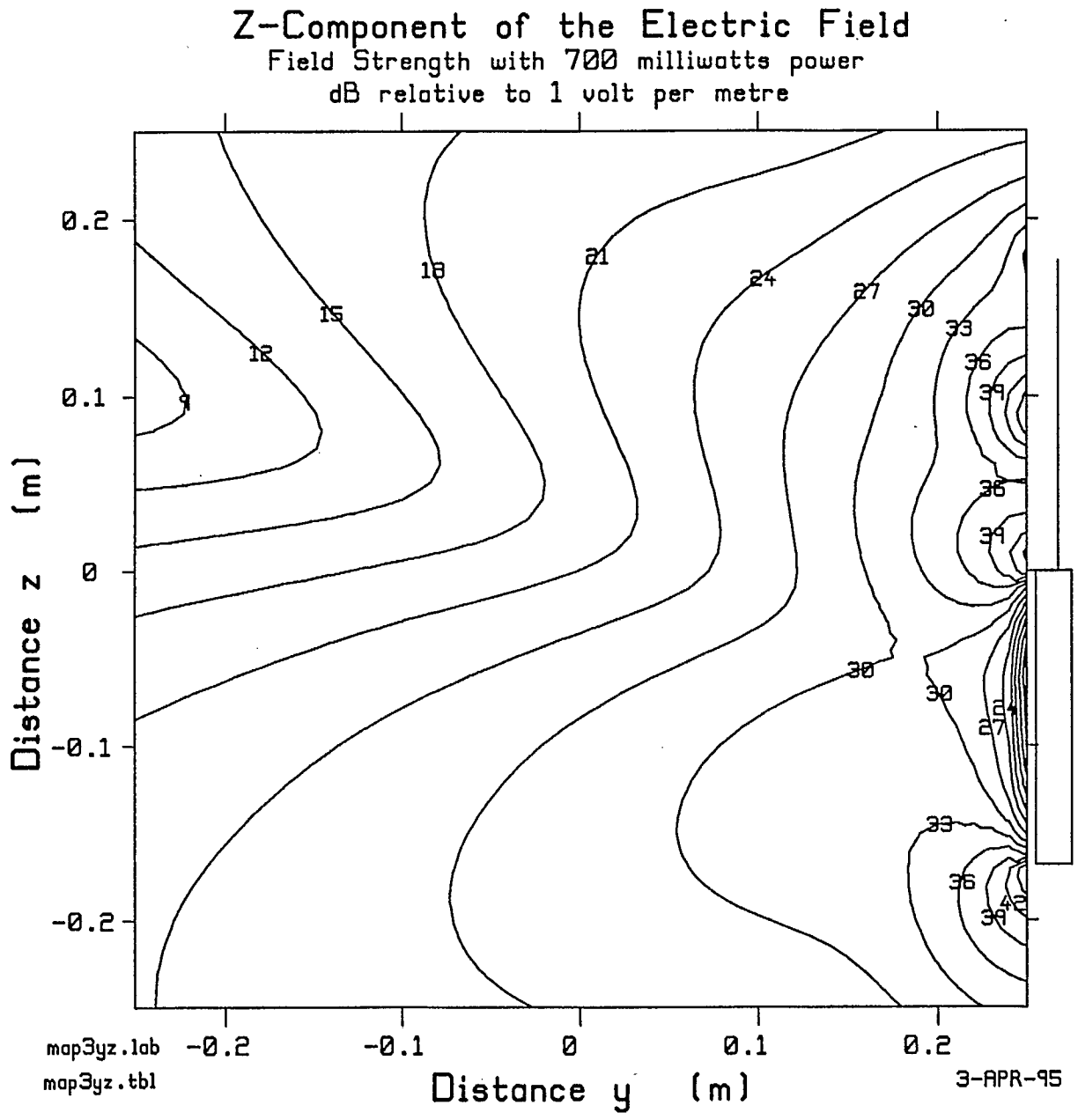

Fig. 3.21 Contour map of the field strength E_z of the cellular telephone with the half-wave monopole, center-fed, over the *yz* plane grid.

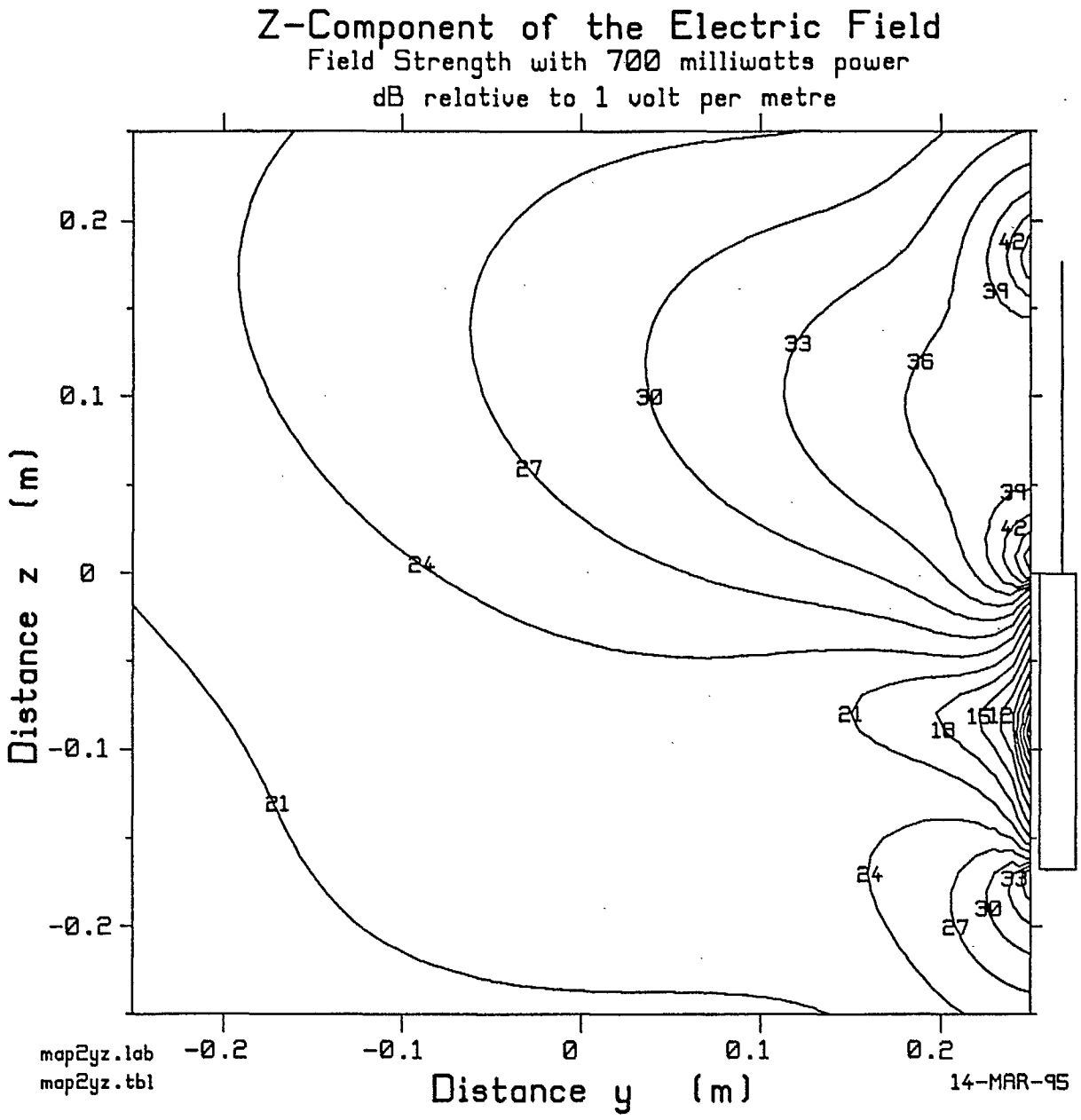

Fig. 3.22 Contour map of the field strength E_z of the cellular telephone with the half-wave monopole, end-fed, over the *yz* plane grid.

CHAPTER 4

Modelling the Handset with FDTD

4.1 Modifications to the FDTD Code to Compute Antenna Patterns

This chapter investigates the radiation patterns and near fields of a cellular telephone of the dimensions shown in Fig. 4.1 using the "finite difference time domain"(FDTD) method[2,3]. The patterns and near fields obtained by FDTD will be compared with those computed with a wire-grid model of the handset using the same dimensions, as a verification of the correctness of the FDTD computation. This chapter briefly summarizes the FDTD method. In this method space is subdivided into "cells" and each cell is filled with a material: either free-space, or a perfect conductor, or a lossy dielectric. FDTD is a time domain solution in which the time dependence of the generator is specified and time is subdivided into "steps". At each time step, the electric field is computed on each edge of each cell. To find the electric fields due to a sinusoidal generator, the generator is gradually turned on to full amplitude and the time stepping solution is carried on long enough for the fields to reach steady state.

Since space is discretized into cells of a certain size, objects must be built up or modelled out of cell-size "building blocks". The dimensions of the cellular phone used in Chapter 3, shown in Fig. 3.1, have been altered so that the handset size can be exactly represented with 6 by 2 by 19 cells of size 0.882 cm, to obtain the dimensions shown in Fig. 4.1. The antenna is a quarter-wave monopole. At 850 MHz, the 0.882 cm cell size is 0.025λ for 40 cells per free-space wavelength. The quarter-wave monopole is exactly 10 cells in length.

In the following, the FDTD method is briefly summarized, including the changes made to the existing scattering code so that it can compute antenna patterns. Fig. 4.2 summarizes the set of processing steps used to generate a cell model of the handset and antenna and to analyze it with FDTD. We will compare the far fields computed with FDTD with those found using a wire-grid model of the same handset. Finally, the near fields obtained with NEC and FDTD will be compared. Recommendations will be made for further development of the FDTD code so that it can more efficiently compute far fields.

4.1.1 The FDTD Method

This section describes program FDTDANT which is used in this report to calculate far-field radiation patterns and near field maps of a cellular telephone handset.

4.1.1.1 The FDTD Cell Space

In Yee's finite-difference time-domain formulation[2], space is subdivided into cells of size Δx by Δy by Δz. Fig. 4.3 shows one cell. The FDTD algorithm determines the electric field strength on each edge of each cell in the cell space at each time step. Integers (i,j,k) describe

the position in integer numbers of cells along the x, y and z axes, respectively. Time is subdivided into steps of length Δt, and integer n gives the time step number. The fields on the cell edges are denoted by $E_x^n(i,j,k)$, $E_y^n(i,j,k)$, and $E_z^n(i,j,k)$ in the x, y and z directions, respectively. The magnetic fields at the centers of the cell faces are also found, illustrated by H_x in Fig. 4.3.

Figure 4.4 shows the setup of a problem in FDTD schematically. The cell space consists of N_x cells in the x direction, N_y cells in y, and N_z cells in z for a total of $N_xN_yN_z$ cells. Up to about one million cells can be solved on the computers available in this project. The radiating object is located at the centre of the cell space, surrounded by a layer of free-space cells which we will call the "whitespace". The cell space is terminated on all six of its faces by an absorbing boundary which is intended to absorb all the energy incident upon it from inside the cell space. This is akin to operating a portable radio in an anechoic chamber, where the walls of the chamber are covered with absorbing material designed to dissipate the radio-frequency energy incident upon them, and not reflect it back into the room.

In the present report the radiator is the portable radio shown in Fig. 4.1, consisting of a metallic box and a monopole antenna. In future work a lossy dielectric body will be inserted adjacent to the radio, modelling the human head. All the surfaces of the radiating object must be separated from the absorbing boundary by a layer of cells filled with free-space. The FDTD algorithm, described in the following, determines at each time step the electric field along each edge of each cell, and the magnetic field at the centre of each cell face. From these near field values, the far field is found using a near-zone to far-zone transformation, by integrating the near field over an integration surface located about five cells inside the cell space. The various parts making up the FDTD method are described in the following sections.

4.1.1.2 The FDTD Algorithm

The FDTD algorithm is based on the Maxwell curl equations. Ampere's Law is given by[13]

$$\mu\frac{\partial \overline{H}}{\partial t} = -\nabla\times\overline{E}$$

and Faraday's Law by

$$\varepsilon\frac{\partial \overline{E}}{\partial t} = \nabla\times\overline{H} - \sigma\overline{E}$$

Splitting these into component equations, we obtain from Ampere's Law

$$\frac{\partial H_x}{\partial t} = -\frac{1}{\mu}\left(\frac{\partial E_z}{\partial y}-\frac{\partial E_y}{\partial z}\right)$$
$$\frac{\partial H_y}{\partial t} = -\frac{1}{\mu}\left(\frac{\partial E_x}{\partial z}-\frac{\partial E_z}{\partial x}\right)$$
$$\frac{\partial H_z}{\partial t} = -\frac{1}{\mu}\left(\frac{\partial E_y}{\partial x}-\frac{\partial E_x}{\partial y}\right)$$

and from Faraday's Law

$$\frac{\partial E_x}{\partial t} = \frac{1}{\varepsilon}\left(\frac{\partial H_z}{\partial y} - \frac{\partial H_y}{\partial z} - \sigma E_x\right)$$
$$\frac{\partial E_y}{\partial t} = \frac{1}{\varepsilon}\left(\frac{\partial H_x}{\partial z} - \frac{\partial H_z}{\partial x} - \sigma E_y\right)$$
$$\frac{\partial E_z}{\partial t} = \frac{1}{\varepsilon}\left(\frac{\partial H_y}{\partial x} - \frac{\partial H_x}{\partial y} - \sigma E_z\right)$$

where μ is the permeability, ε is the permittivity, and σ is the conductivity. Space is then divided into cells and time into steps as described above. The FDTD algorithm determines the electric field at times $t = n\Delta t$ and the magnetic field at in-between times $t = (n + 1/2)\Delta t$. The partial derivatives in the component equations are approximated with central difference formulas[2,3,51]. Thus for example, when we approximate the component equation

$$\frac{\partial H_x}{\partial t} = -\frac{1}{\mu}\left(\frac{\partial E_z}{\partial y} - \frac{\partial E_y}{\partial z}\right)$$

with central difference formulas we obtain

$$\frac{H_x^{n+1/2}(i,j,k) - H_x^{n-1/2}(i,j,k)}{\Delta t} = -\frac{1}{\mu}\left(\frac{E_z^n(i,j,k) - E_z^n(i,j-1,k)}{\Delta y} - \frac{E_y^n(i,j,k) - E_y^n(i,j,k-1)}{\Delta z}\right)$$

which is rearranged to obtain the "update equation" for H_x given by

$$H_x^{n+1/2}(i,j,k) = H_x^{n-1/2}(i,j,k) - \frac{\Delta t}{\mu}\left(\frac{E_z^n(i,j,k) - E_z^n(i,j-1,k)}{\Delta y} - \frac{E_y^n(i,j,k) - E_y^n(i,j,k-1)}{\Delta z}\right)$$

This equation permits the magnetic field H_x at location (i,j,k) at time $(n + 1/2)\Delta t$ to be calculated from its previous value, at step $(n - 1/2)\Delta t$, and the values at time $n\Delta t$ of the electric field E_y and E_z on the cell edges adjacent to the cell face where H_x is located. Similarly, we can obtain "update equations" for the other components of the magnetic field,

$$H_y^{n+1/2}(i,j,k) = H_y^{n-1/2}(i,j,k) - \frac{\Delta t}{\mu}\left(\frac{E_x^n(i,j,k) - E_x^n(i,j,k-1)}{\Delta z} - \frac{E_z^n(i,j,k) - E_z^n(i-1,j,k)}{\Delta x}\right)$$

and

$$H_z^{n+1/2}(i,j,k) = H_z^{n-1/2}(i,j,k) - \frac{\Delta t}{\mu}\left(\frac{E_y^n(i,j,k) - E_y^n(i-1,j,k)}{\Delta x} - \frac{E_x^n(i,j,k) - E_x^n(i,j-1,k)}{\Delta y}\right)$$

In the same way, we can approximate the components equations from Faraday's Law with central difference formulas to obtain update equations for the three components of the electric field, given by for the x component,

$$E_x^{n+1}(i,j,k) = \frac{\varepsilon}{\varepsilon+\sigma\Delta t}E_x^n(i,j,k) + \frac{\Delta t}{\varepsilon+\sigma\Delta t}\left(\frac{H_z^n(i,j,k)-H_z^n(i,j-1,k)}{\Delta y}-\frac{H_y^n(i,j,k)-H_y^n(i,j,k-1)}{\Delta z}\right)$$

for the y component,

$$E_y^{n+1}(i,j,k) = \frac{\varepsilon}{\varepsilon+\sigma\Delta t}E_y^n(i,j,k) + \frac{\Delta t}{\varepsilon+\sigma\Delta t}\left(\frac{H_x^n(i,j,k)-H_x^n(i,j,k-1)}{\Delta z}-\frac{H_z^n(i,j,k)-H_z^n(i-1,j,k)}{\Delta x}\right)$$

and for the z component,

$$E_z^{n+1}(i,j,k) = \frac{\varepsilon}{\varepsilon+\sigma\Delta t}E_z^n(i,j,k) + \frac{\Delta t}{\varepsilon+\sigma\Delta t}\left(\frac{H_y^n(i,j,k)-H_y^n(i-1,j,k)}{\Delta x}-\frac{H_x^n(i,j,k)-H_x^n(i,j-1,k)}{\Delta y}\right)$$

These equations permit computing the value of each component of the electric field at time $n\Delta t$ from its previous value, at time $(n-1)\Delta t$, and the values of the magnetic field at time $(n-1/2)\Delta t$ on the cell faces adjacent to the edge where the electric field component is located.

Yee's FDTD method has been called a "leap frog algorithm"[3] because at time $n\Delta t$, we update the electric field from its previous value, then we advance time by one-half a step to $(n+1/2)\Delta t$, and update the magnetic field, then advance time to $(n+1)\Delta t$ and repeat the cycle by updating the electric field once again. The algorithm "leap frogs" in space, too, because each field component is updated from its previous value and from the dual field at locations one-half cell away. Note that although we know all three components of the electric field and all three components of the magnetic field, we do not know them at coincident points in space. Thus in Fig. 4.3, the precise position at which the fields are computed is different for all six components of the field. Further, E and H are not known at exactly the same instants of time.

The present project is based on the Penn State FDTD-C code[6]. This is a program intended for computing the scattered field of metallic and dielectric objects due to an incident plane wave, and hence the radar cross-section. The code includes the near-to-far-zone transformation[16], and implements the Liao absorbing boundary[53,54,55]. For the present project, this FDTD code has been modified and renamed "FDTDANT", to permit the computation of the fields of an antenna excited by a voltage generator, as described below.

4.1.1.3 Materials and the FDTD Algorithm

In Fig. 4.4 all the cells in the "whitespace" region are free-space cells with permittivity ε_0, permeability μ_0, and zero conductivity. The telephone handset and its antenna lies entirely within the central box labelled "radiating object". A perfect conductor is modelled in FDTD by implementing the boundary condition that the tangential electric field at the surface of a perfect conductor is equal to zero. Also, all the field components inside a perfect conductor are zero. Thus, the code initializes the problem by setting up "identification arrays" for all the cell edges, which identify the type of material associated with each cell edge. All the cell edges which lie within or on the surface of the handset box are identified as perfectly-conducting, or "material type #1" within the program, where type #0 is free space. Then in updating an electric field component, the code checks the identification array to determine the material type. If the type is free-space, then the update equations given above are used. If the type is perfect conductor, the field is set equal to zero to satisfy the boundary condition.

To model dielectric materials, the above scheme is extended to include further material types, type #2, #3, and so forth. Thus for each new pair of permittivity and conductivity encountered, a new material type is defined, and cell edges that lie within that material are identified with the type number. Then when the update equation is evaluated for that cell edge, the program uses the associated material parameters. Note that this allows different values of conductivity and permittivity in each spatial direction so that anisotropic materials can be represented, though this is not required in the present project.

A complication is associated with interfaces between two material types. Ref. [56] reviews the treatment of the permittivity and the conductivity for updating the electric field for field components that lie near a material interface. As discussed in Ref. [57], cell edges on an interface between two different dielectric materials should use the average of the permittivity of the two materials, and of the conductivity of the two materials, to update the field. This requires the code to examine the regions of dielectric materials specified by the user to identify interfaces, and then define a new material type for each interface, having the average parameter values. Subsequently these new values must be used to update field components on the interfaces between materials. This has not yet been implemented in the FDTDANT code.

4.1.1.4 Cell Size, Time Step and Bandwidth

The FDTD algorithm becomes unstable if the time step is greater than the Courant limit, given by[3,58]

$$\Delta t_{\max} = \frac{1}{c\sqrt{\left(\frac{1}{\Delta x}\right)^2+\left(\frac{1}{\Delta y}\right)^2+\left(\frac{1}{\Delta z}\right)^2}}$$

The speed-of-propagation of waves through the FDTD cell space has been shown to be dependent upon the direction of propagation[58]. The speed is most uniform when the time step equal to the Courant limit, and so $\Delta t = \Delta t_{\max}$ will be used here. As the frequency is increased, the anisotropy in the speed of propagation becomes greater, and so there is a limiting frequency at which the speed of propagation is sufficiently non-uniform that the results of an FDTD computation are seriously degraded in accuracy. The usual rule-of-thumb in the literature [3,58] is that the cell size must be smaller than one-tenth of the wavelength at the highest frequency. If cubical cells are used, $\Delta x = \Delta y = \Delta z$, as in this report, then the frequency in the FDTD calculation is limited to a bandwidth of frequencies less than

$$f_{\max} = \frac{u}{10\Delta x}$$

where u is the speed of propagation in the material. For problems involving free space cells and perfect conductors, $u = c$ where c is the free-space speed of light. When lossy dielectrics are present, then u is the slowest speed of propagation. For low loss dielectrics of high permittivity, u is usually determined by the material with the largest permittivity.

It is well-known that the excitation function for the FDTD cell space must not contain frequencies above the bandwidth of the algorithm, or else unreliable results will be obtained[3]. Thus, it is not permissible to excite the cell space with an impulse voltage generator, having zero value for all time steps except one, at which its value would be unity. Such a generator implies frequencies well above the bandwidth of the grid. Instead if a pulse excitation is desired, then a

Gaussian pulse is used, which rises smoothly from zero to unity, then falls smoothly back to zero. The rate at which the pulse rises and falls is chosen such that the frequency content of the Gaussian pulse lies within the bandwidth of the FDTD algorithm.

When a sinusoidal generator is used, the sinusoid cannot be turned on abruptly, as the sudden start contains frequency components above the bandwidth of the FDTD algorithm. Instead, the amplitude of the sinusoid is gradually increased from zero over several cycles, by multiplying the sinusoid by a Gaussian pulse, chosen as mentioned above to imply a frequency content within the FDTD bandwidth.

4.1.1.5 The Absorbing Boundary

The FDTD calculation proceeds by setting all the field components to zero throughout the cell space, and starting at zero time. The calculation proceeds by updating the electric field at each time step as described above. As the voltage generator gradually "turns on" the field propagates away from the generator and spreads out to encompass the wire antenna and the handset. The FDTD method solves the transient problem involving turning on the generator and computing the time dependence of the fields over the surface of the hand set and on the wire antenna. After a certain number of time steps, the field has propagated across the whitespace cells and encounters the boundary of the cell space.

The electric field components on the outer boundary cannot be updated with the equations given above, for they require a knowledge of magnetic field values that lie outside the cell space. In Yee's paper[3], the computation could only be carried for as many time steps as it took for the field to reach the outer boundary, for no method was available to update the field at the boundary. Consequently, a different set of update equations is needed for electric fields which lie on the outer boundary of the cell space. In early applications of FDTD, an "absorbing boundary condition"(ABC) was derived based on the concept that the source of the field is a point source so the field incident on the boundary is a spherical wave[59]. Indeed, at each time step each point on the radiating body behaves as a point source, and so the field incident on the boundary is a superposition of many spherical waves. The update equations for the boundary were designed to absorb a spherical wave, but only to first-order accuracy.

FDTD approximates the partial derivatives with central difference formulas, which have second order accuracy[51], and hence an ABC with second-order accuracy is desired. Mur[60] provided a practical set of update equations which absorb plane waves, to second-order accuracy. It has been demonstrated[61] that absorbing boundary conditions such as Mur's have a very small reflection coefficient for one particular angle of incidence, but are much poorer for other angles of incidence. Indeed, the "perfect absorption" angle can be designed into the coefficients used in the update equations for the boundary. At other angles, the reflected field can be as little as 20 dB below the field incident on the boundary, where 50 dB or more would approach the accuracy of the single-precision calculations commonly used with FDTD. Hence the poor performance of the absorbing boundary has been a limitation in the accuracy of FDTD calculations.

The deleterious effect of reflections from the boundary can be reduced by moving the boundary farther away from the radiating object. This tends to reduce the strength of the fields incident on the boundary, due to the inverse distance attenuation of the radiated field strength, and also to reduce the strength of the reflected field on the surface of the object for the same reason. A whitespace layer as thick as 35 cells has sometimes been necessary to achieve good performance of the FDTD method in sensitive situations[57] involving materials of high permittivity in resonance, resulting in oscillations with little damping that continue for many, many cycles.

Many different second order absorbing boundary conditions have been proposed. In this project the Liao second-order absorbing boundary condition[53] has been used, as implemented in the FDTDC code by Luebbers and Steich[55]. The Liao ABC offers better performance than does the Mur boundary. Experiments in solving scattering problems with various thicknesses of the whitespace layer have shown that the Liao boundary often leads to sufficiently accurate results with whitespace layers as thin as 15 cells, whereas the Mur boundary requires 20 or even 30 cell thicknesses for the same accuracy. But as mentioned above, in dealing with sharply-resonant scatterers, sometimes thirty-five cells of whitespace were needed to sufficiently reduce the effect of boundary reflections.

There has been very considerable research in the community to develop a better absorbing boundary condition. Railton[61] compared a variety of second-order ABCs and showed that some appear to be superior to others for a plane wave normally incident upon the boundary. But, when examined as a function of the angle of incidence, most demonstrate zero reflection for one particular angle but much higher reflection elsewhere. He compared ABCs by averaging the reflection coefficient over a range of angles and found that there is not a great deal to choose among the various second order ABCs available. Mei and Fang[62] described a "superabsorbing" boundary, which starts with any one of the second order ABCs and applies a correction to reduce the error. The technique is much more complex than a simple second order ABC and has not gained wide acceptance. A recently-published approached to an absorbing boundary condition in two dimensions by Berenger[63] leads to a wave impedance at the boundary that is independent of frequency and of the angle of incidence of the outgoing wave. Berenger's two-dimensional ABC decreases reflections by as much as 1/3000th compared to the Mur absorbing boundary, and reduces grid noise energies by 10^{-7}. Katz, Thiele and Taflove[64] extend Berenger's work to three dimensions, and claim a reduction of grid noise due to the absorbing boundary to 1/100th of that found with the Mur boundary. This greatly increases the dynamic range of FDTD computations, by as much as 40 dB.

In the present work, the Liao absorbing boundary as implemented in the FDTDC code has been used.

4.1.1.6 Near-to-Far Zone Transformation

The FDTD algorithm computes the near fields throughout the FDTD cell space. In order to find the associated far fields, Ref. [52] describes a near-field to far-field transformation which is based on the equivalence principle[50,65]. If the electric field and the magnetic field are known everywhere over a closed surface, then the fields outside the surface can be obtained by defining equivalent electric and magnetic currents flowing over that surface, then treating these currents as the sources of the far field. The field due to these currents is found by superposition, by integration over the closed surface. For far field points, the far fields are most easily found by using the equivalent currents to find the electric and magnetic radiation vectors[50], taking advantage of the fact that the far field point is much farther away than the size of the integration surface. The fields are then found from the vector potentials.

To implement the near-to-far zone transformation for FDTD, Ref. [52] defines the integration surface to be the parallelepiped shown schematically in Fig. 4.4, which lies five cells from the absorbing boundary inside the cell space. The magnetic equivalent current flowing over the surface is given by[52]

$$\overline{M}_s = -\hat{n} \times \overline{E}(t)$$

and the electric equivalent current is given by

$$\overline{J}_s = \hat{n} \times \overline{H}(t)$$

where $\overline{E}(t)$ and $\overline{H}(t)$ are the electric and magnetic fields on the integration surface. The retarded electric radiation vector is given by[52]

$$\overline{W}(t) = \frac{1}{4\pi R c} \frac{\partial}{\partial t} \int_s \overline{J}_s \left(t + \frac{\overline{r}' \cdot \hat{r}}{c} - \frac{R}{c} \right) ds'$$

where $\overline{r}'$ is the location on the integration surface at which the current is evaluated, $\hat{r}$ is the vector pointing toward the location of the observer in the far field, and R is the distance from the origin to the observer. The magnetic radiation vector is given by

$$\overline{U}(t) = \frac{1}{4\pi R c} \frac{\partial}{\partial t} \int_s \overline{M}_s \left(t + \frac{\overline{r}' \cdot \hat{r}}{c} - \frac{R}{c} \right) ds'$$

These must be resolved into θ and ϕ components at the observer in the far field, and then the components of the far zone electric field are given by[50]

$$E_\theta = -\eta W_\theta - U_\phi$$

and

$$E_\phi = -\eta W_\phi + U_\theta$$

This near zone to far zone transformation is implemented in the FDTDC code from Penn State[6].

The FDTDC code is oriented toward excitation by a Gaussian pulse, and the computation of the time response due to a Gaussian pulse at each far zone field point. Thus the code is set up to save all the time samples of E_θ and E_ϕ at each far zone point. Then the far zone electric field time functions are Fourier-transformed to find the frequency dependence of the far zone field. Dividing by the Fourier transform of the excitation field allows the radar cross-section as a function of frequency to be conveniently calculated for perfectly-conducting targets and for non-dispersive high-permittivity dielectric targets[3,57]. This is an efficient scheme when only one or a few far field points are being studied and when the excitation is a pulse and we are seeking the frequency dependence of the fields. As discussed below in Section 4.1.5, the FDTDC approach uses excessively large amounts of computer memory when we want to compute the full set of conical cut radiation patterns.

4.1.2 Modeling the Antenna and Voltage Generator

Modelling wire antennas with FDTD has been investigated in Refs. [66] and [67]. The antenna is considered to be a highly-conducting wire, and so the component of the electric field tangent to the wire axis must be set to zero. The problem is set up so that the wire antenna lies parallel to a coordinate axis, which is the z axis for the handset of Fig. 4.1. The wire's location must be coincident with a line of cell edges, and then the electric field on each cell edge is set to zero at each time step, by marking that cell edge as material type #1, "perfectly conducting". Refs. [66] and [67] give formulas for finding the input impedance of the antenna, accounting for the radius of the wire.

Ref. [68] deals with modelling a portable radio with a monopole antenna using FDTD. Two types of generator representations are investigated and the input impedance and far field patterns are compared with measurements. Both a radio consisting of perfectly-conducting box and one with a dielectric covering are studied.

The present work uses the simpler voltage generator representation from Ref. [68]. The voltage generator is implemented by dividing the desired excitation voltage $v(t)$ by the cell size, Δz here, to obtain the source field

$$E_{sz}^{n}(i_s, j_s, k_s) = -\frac{v(n\Delta t)}{\Delta z}$$

where (i_s, j_s, k_s) is the location of the excited cell edge. Then at each time step, the field on that cell edge is set equal to E_{sz} evaluated at that time step. The FDTDC code was modified to accept wire antennas in the input data, to implement the wire by marking the appropriate field components to be set to zero along the length of the wire, and by implementing the voltage generator at the base of the wire. The revised code was named FDTDANT.

The FDTDC code is set up to excite the cell space with a plane wave with a Gaussian pulse time dependence, and to calculate and save the radiated field at a few far field points at all the time steps. The far field time record is then Fourier-transformed to determine the frequency dependence of the scattered field. In the present project, the plane wave generator has been replaced by a voltage source at a designated location at the base of the wire antenna. The Gaussian pulse time dependence was replaced with a sinusoidal generator in the FDTDANT code. The sinusoidal source must be "turned on" or increased in amplitude gradually, to avoid exciting frequency components outside the frequency range of the FDTD cell space. The solution is then time-stepped until steady state is reached, as suggested in Refs. [67] and [68]. Then the amplitude of the field at each near field point and far field point is determined by examining the field strength over the last half-cycle of the sinusoid and finding the maximum value.

4.1.3 FDTD Problem Setup

To set up a problem for solution by FDTD the first choice that the user must make is the cell size. This is governed by two considerations, the first being the fidelity to which the geometry of the radiating object is to be represented, and the second being the maximum frequency for which the FDTD algorithm is expected to obtain reasonably accurate results. In the present problem, the frequency is 850 MHz, and so the cell size for tenth-wavelength cells in free space is 3.53 cm. This is too coarse to model the 1.76 cm thick handset in Fig. 4.1. The cell size was thus set at one-half the case thickness, or 0.882 cm. The handset case is then represented as a block of 6 by 2 by 19 cells of perfectly-conducting material. The cell size was thus set at one-

fortieth wavelength by the need for fidelity in modelling the case. The quarter-wave antenna is represented by setting the electric field to zero along ten consecutive cell edges in the z direction coincident with the location of the antenna wire.

The next choice is the size of the cell space. The quarter-wave antenna in Fig. 4.1 will be represented as a line of 10 cell edges in series, and so the overall size of the radiating object, case plus antenna, is 6 cells in x, 2 cells in y, and 29 cells in z. To this must be added the thickness of the whitespace layer all around the radiating object. For the present purpose, this was set to 10 cells, although more would be desirable for the best accuracy. The small whitespace was dictated by the enormous storage required to calculate the far-zone fields, as discussed below. Thus the overall cell space size is $N_x = 26$, $N_y = 22$ and $N_z = 49$ cells for a total of 28,028 cells. This is a small FDTD cell space.

The time step was chosen to be the Courant limit, which for cubical cells is given by

$$\Delta t = \frac{\Delta x}{\sqrt{3}\,c}$$

With $\Delta x = 0.882$ cm, the time step is $\Delta t = 17$ picoseconds, approximately. At a frequency of 850 MHz, the period of the sinusoid is 1,177 ps, or about 69 time steps per period. The user must decide at the outset how many time steps are needed to reach steady state. For the present purpose this was set at 512, or 7.4 periods of the sinusoid. The first two periods are used in turning on the sinusoid, so about 5 periods are available to reach steady state. The transient field at some points should be examined to ensure that steady state is being reasonably achieved.

4.1.4 Dispersive Materials and Sinusoidal Excitation

In biological tissues, the electrical parameters vary significantly with frequency, and the simple approach assuming frequency-independent electrical parameters is not sufficient to compute the fields over a wide bandwidth using a Gaussian pulse excitation. There are two possibilities for dealing with this dispersive behavior. One is to modify the FDTD algorithm to represent the dispersive nature of biological materials. Thus Ref. [36] uses one time constant to represent simple materials, Ref. [38] extends this to multiple time constants for more complex materials, and Ref. [37] deals with materials requiring a resonant frequency and a damping constant to represent their relaxation behavior. A more complete discussion of materials can be found in Ref. [9], reproduced in Appendix A. Implementation of this frequency-dependent form of FDTD would considerably slow down the algorithm, but allows results to be obtained over a wide bandwidth in a single computation.

The more common approach to dealing with dispersive materials is to retain the simple form of FDTD assuming a constant permittivity and conductivity, and to set the parameters to values appropriate for the frequency band of interest. The FDTD code is then run with a sinusoidal generator, and the time-stepping algorithm is continued until steady state is reached. Essentially, we are using a time-domain method as if it were a frequency-domain method, to obtain results one frequency at a time. For results at another frequency, the electrical parameters are set to new values, and the code is run again. In the present study we will use a sinusoid at a single frequency as the generator, and run the code for each frequency of interest separately.

If a narrow bandwidth is being studied, in which the permittivity and conductivity can be considered essentially constant, then a Gaussian pulse can be modulated with a sinusoid at the centre of the frequency band to obtain an excitation which has energy only in the frequency band of interest, and the frequency response can be obtained in a single run of the code.

4.1.5 Computing the Conical Cut Radiation Patterns

To study the far field of a telephone handset comprehensively in all directions, it is convenient to compute the far fields on the set of circles illustrated in Fig. 3.5, called the "conical cut" radiation pattern set, at angles θ =0, 25, 37, 45, 53, 60, 66, 72, 84, 90, 96, 102, 108, 114, 120, 127, 135, 143, 155 and 180. This is a set of 21 radiation patterns usually evaluated at five degree intervals in ϕ, for a total of 1533 points. In addition two elevation patterns are computed, for 146 points, and both E_θ and E_ϕ are evaluated, requiring storage for 3358 field values. The FDTDC code is oriented toward retaining all the time samples of both components of the electric field at each far field point. In the FDTDC code, all the time samples for each component of the vector potentials at all the time steps and for each of the two far field components at all the time steps must be stored. This requires 8 real variables at each far field point, and so for 512 time steps and 3358 far field points, for a total of 55 megabytes of memory. This uses most of the 72 megabytes on the available computers, and so severely limits the size of problem that can be solved. For the present, this is how we are computing the far field patterns.

This difficulty can be fully overcome by taking advantage of the fact that we are using the FDTD program with a sinusoidal generator at a single frequency, essentially to compute frequency domain results. Thus all we need to save is the amplitude and phase of the equivalent current at each point on the integration surface at steady state, requiring a modest amount of computer memory. Then the near-to-far zone transformation can be done in the frequency domain to obtain the far field patterns, which is a quick and efficient operation. Programming this into the FDTDANT code is recommended for the next stage in this project.

4.1.6 Software Setup for FDTD Studies

Fig. 4.2 is a flow chart of the software setup used in association with the FDTD program. As described above, the FDTD cell model is defined in a "build file" shown as "PHONE.BLD" in Fig. 4.2. The build file defines the number of cells in the cell space, sets the cell size in meters, defines a line of cell edges oriented in the z-direction as a "wire" to model the cell phone's monopole antenna, and defines a parallelepiped of cells as filled with a perfect conductor to represent the handset. The total number of time steps is set. The voltage generator is set to be the cell edge at the base of the monopole, and the frequency is given. The build file defines which radiation patterns are to be computed. Finally, the build file specifies planes over which the program will write the electric field strength for further study.

When program FDTDANT is run, it reads the "build file" and assembles the "model" by remembering which cell edges belong to cells filled with perfectly-conducting material, and which edges lie along the monopole. On these cell edges, the FDTDANT code enforces the boundary condition that the electric field component along the cell edge must be equal to zero at all time steps. The cell edge which represents the voltage generator is considered to have a known, specified field imposed along it, equal to the field strength of the generator, which is a sinusoid in this work.

To help the user to verify that the handset geometry is correctly coded in the build file, the FDTDANT program is set up to create two output geometry files in the format of GW cards, which can be examined with program MODEL, which was discussed in conjunction with wire-grid modelling in Chapter 3. The first geometry file is part of the code's principal output file, PHONE.DAT. For each cell edge that the program designates internally as perfectly conducting, the program writes one GW card corresponding to a wire positioned along the cell edge. This set of GW cards defines the object being studied precisely and can be examined with MODEL and compared with the desired dimensions as a verification. Since the GW cards are created directly from FDTDANT's internal designation of material properties, used to carry out the time stepping

solution, if we verify the geometry by examining the PHONE.DAT geometry file then we can have great confidence that the geometry is indeed correct. In addition, FDTDANT creates an outline of the handset in file OUTLINE.GW, also in the GW card format. This file is useful for superimposing the handset geometry on near field maps, as described below.

4.1.6.1 Diagnostic Tools

The cell model can be examined on computer graphics using program HDNFDTD. HDNFDTD displays the FDTD model from the information in the build file. HDNFDTD was developed to display aircraft models being used to calculate radar cross-section. The three-dimensional aircraft shape is represented with a staircase approximation built up out of FDTD cells. HDNFDTD allows the user to judge the extent to which the FDTD cell model is a reasonable approximation of the actual aircraft. The current version of HDNFDTD needs to be updated to handle wire antennas, and to use color to display regions with differing permittivity. Thus, HDNFDTD is of limited usefulness in the present project, and it is recommended that it be adapted to the needs of this project in the next phase.

CELMODEL is another diagnostic tool developed to aid in constructing FDTD models of aircraft. CELMODEL reads a build file and estimates the bandwidth of the FDTD model it describes. CELMODEL finds the size of the whitespace, that is, the minimum distance between the extreme dimensions of the model and the boundary of the cell space, on all six sides of the cell space. CELMODEL allows the user to adjust the position of the model within the cell space so the whitespace is of equal thickness on all sides. Also, the cell space size can be redefined, by specifying a new whitespace thickness. The build file is rewritten with the model centered within the new cell space.

The main function of CELMODEL is to draw a cross-section of the model in a specified plane, xy, xz or yz, showing which cells are filled with perfectly-conducting material. Examining the cross-sections lets the user judge the degree to which the staircase approximation of the three-dimensional shape is reasonable. A improved version of CELMODEL would allow the user to adjust the model by superimposing a cross-section of the true three-dimensional shape, and to toggle cells between "free-space" and "perfectly-conducting", to adjust the model. This function is currently supported by an associated program called GWTOFDTD[69].

CELMODEL needs to be developed to support the current project so that: (i) it can display wire antennas; (ii) it can color code the various dielectric materials encountered in modelling a human head; and (iii) provide an estimate of the bandwidth over which a model is valid, based on the material properties of the cells. The program would then provide a valuable tool for examining cell models prior to the execution of the FDTDANT code.

4.1.6.2 Running FDTDANT

The FDTDANT program actually computes the near field components E_x, E_y, and E_z on each cell edge throughout the cell space at each time step. This report uses a sinusoidal voltage generator at the base of the cell phone's monopole antenna. As discussed above, the generator gradually "turns on", reaching its full amplitude after about 140 time steps. The calculation is continued for a sufficient number of time steps to reach "steady state", about 512 time steps for the perfectly-conducting handset in free space that is studied here. The amplitude of the sinusoidal field strength at any point is determined by searching the time samples for the largest value of the field strength over the last half-period of the sinusoidal excitation.

To compute far field radiation patterns, the present version of the FDTDANT code saves the full set of time samples at each far field point, which requires a great deal of computer memory, as discussed above. Then at each far field point, the program searches through the last half-cycle of time samples for the largest value. This is very inefficient both in computation and in storage, and should be replaced by a frequency-domain near-to-far zone transformation, as mentioned above. Thus the current version of the code is only practical for small cell spaces and modest numbers of time steps, not sufficient to analyze complex dielectric structures. The program takes about 12 hours to calculate the conical cut set of radiation patterns for a cell space of about 25 by 30 by 50 cells, using 512 time steps, on a DECStation 5000 workstation. Most of this execution time is spent in the near-to-far zone transformation.

4.2 Handset Dimensions for FDTD

The objective of this chapter is to compare the radiation patterns and near fields of a telephone handset computed with FDTD with those computed by wire-grid modelling with the NEC code. The telephone handset studied in Chapter 3 cannot be precisely represented by integer numbers of cells, and so its dimensions were altered to obtain the handset in Fig. 4.1. With these dimensions and a cell size of 0.882 cm, the handset is represented with a perfectly-conducting box 6 by 2 by 19 cells in size, and the quarter-wave monopole antenna by 10 cell edges in series. Then at 850 MHz, the cell size is .025λ for 40 cells per free-space wavelength.

The size of the cell space was set by identifying the overall size of the handset and antenna as 6 cells in x, 2 cells in y, and 29 cells in z. The whitespace layer was set at 10 cells on all sides, which is thin compared to whitespaces that have been used in scattering studies using perfectly-conducting targets as in Ref. [70] and high-permittivity dielectric targets, in Refs. [57]. As discussed above in Section 4.1.5, the computation of the set of conical cut radiation patterns uses a very large amount of computer memory in the present version of FDTDANT, and so a small cell space was required to make the problem fit into the computer memory. Thus the overall cell space size is $N_x = 26$, $N_y = 22$ and $N_z = 49$ cells for a total of 28,028 cells.

With the cell size set at $\Delta x = 0.882$ cm, the Courant limit time step is approximately $\Delta t = 17$ picoseconds. At a frequency of 850 MHz, the period of the sinusoid is 1,177 ps, or about 69 time steps per period. The first two cycles of the sinusoid are used to "turn on" the generator by gradually increasing the amplitude, requiring about 140 time steps. The total number of steps was set at 512, or 7.4 periods of the sinusoid, allowing about 5 periods for the problem to reach steady state.

4.3 Radiation Patterns of the Handset

This section describes the scaling of the radiation patterns computed with FDTD to the same radiated power as those computed with NEC, and the comparison of patterns computed with FDTD and with NEC on the basis of equal radiated power using PATCMP. The far fields computed with FDTD and NEC will then presented, both for azimuth and elevation radiation patterns and over the whole radiation sphere using color maps.

To compute the far field patterns at 850 MHz with FDTDANT, the voltage generator is sinusoidal and the time stepping solution is obtained with the FDTD algorithm. The FDTDANT code saves the field strength as a function of time at every far field point in the conical cut radiation pattern set. After enough time steps to reach steady state, the amplitude of the field at each far field point is determined by finding the largest magnitude of the field strength over the last half-cycle of the sinusoid.

The output file of FDTDANT in Fig. 4.2 is arranged in the same format as the output file obtained from the NEC program. The first part of the file shows the geometry of the FDTD model, in the format of one GW card for each cell edge on which the electric field is set to zero. These GW cards define the case and the antenna of the handset. The output file then contains the radiation patterns for the set of conical cuts shown in Fig. 3.6. Writing the output from FDTDANT in the same format as that obtained from running NEC is convenient because the same set of programs used for examining far fields obtained from wire-grid modelling can be used to study fields computed with FDTD.

4.3.1 Power Scaling

To compare the radiation patterns and near fields of the FDTD model for the cellular telephone of Fig. 4.1 with a wire-grid model of the same handset, it is necessary to scale the radiation patterns and near fields so that both models radiate the same power. This is done here by computing the set of conical cut radiation patterns shown in Fig. 3.6 both with NEC and with the FDTDANT program. The program ISOLEV is used to calculate the radiated power by integrating the power density over the radiation sphere, for the NEC computation and for the FDTD computation. Because FDTDANT's output has the same format as that obtained with NEC, we can use ISOLEV with no modifications on the FDTD data. Once the radiated power is known, the field strengths are easily rescaled to any desired radiated power level. Also, program PATCMP can be run to compare radiation patterns computed with FDTD to those computed with a wire-grid model, as presented below.

4.3.2 Examining the Far Fields with PATCMP

The PATCMP program is designed to compare radiation patterns computed by two different methods or to compare computed radiation patterns with measured radiation patterns. PATCMP compares patterns on the basis of equal radiated power, and expects to find the radiated power explicitly in each data file, usually written there by program ISOLEV as described above. PATCMP scales both sets of input data to the same power then plots the desired radiation pattern from each file on the same polar axis for comparison.

There are two options for power scaling. Either we can scale the power for the NEC computation and for the FDTD computation so that it is 700 milliwatts in both cases. Then we are comparing the absolute field strength at some fixed distance in the far field of the antenna, for example, in millivolts per meter at one kilometer. Alternatively, we can scale the power in both files so that the isotropic field strength, defined above in Section 3.2.6, is the same for both files. In this report we will scale both the NEC and the FDTD computations to an isotropic field strength of 1 volt/metre, then display field strengths in decibels above 1 volt/metre. PATCMP will be used below to compare the far field patterns computed with FDTD with those computed with NEC for the same handset geometry.

In Chapter 3 the field strengths over the whole radiation sphere were displayed in a polar color map format created with program POLPLOT. PATCMP creates the "table file" for input to POLPLOT, either E_θ or E_ϕ, over the whole radiation sphere, scaled to an isotropic field strength of 1 volt/metre. This file can also be used with CPLOT to create field maps in a rectangular format, and SPLOT to display the field strength as a surface above the (θ, ϕ) plane. Here we will use POLPLOT to display the field strength in a polar format as a function of θ on the radial axis and ϕ on the angle axis, as was done in the previous chapter.

4.3.3 Far Fields: FDTD and NEC

The handset of Fig. 4.1 differs somewhat from that of Fig. 3.1 as the dimensions were adjusted so that the case measures 6 by 2 by 19 cells, with 10 cells for the antenna. Thus in Chapter 3 the handset is 5.588 by 2.032 by 16.764 cm, here the handset is substantially thinner, 1.76 cm, and a little narrower, 5.35 cm, but about the same height, 16.76 cm. Here the antenna is located exactly one cell size or 0.882 cm from the three adjacent edges of the case, instead of 0.75 cm from the edge of the case and from the back of the case, as in Chapter 3. The MKPHONE program described in Chapter 3 was used to create a wire-grid model of the cellular phone of Fig. 4.1, and NEC was run to compute the currents, the set of conical cut radiation patterns, and hence with ISOLEV the radiated power. NEC takes 26.7 minutes to compute the currents, the far fields, and one plane of near field points on a DECStation 5000 workstation. In comparison FDTDANT takes about 12 hours to calculate the conical cut radiation patterns for a cell space of about 25 by 30 by 50 cells, using 512 time steps. Much of that time is associated with the inefficient near-to-far-zone transformation.

4.3.3.1 Radiation Patterns

Fig. 4.5 compares the far fields computed with FDTD with those computed with NEC, both scaled to an isotropic field strength of 1 volt/metre or 0 dB. The FDTD data is the dashed curves, and the NEC data the solid lines. The azimuth or $\theta = 90$ pattern in Fig. 4.5(a) shows remarkably good agreement between the two methods, in both the principal polarization, E_θ, and the cross polarization, E_ϕ. The elevation pattern for $\phi = 0$ in Fig. 4.5(b) show some differences, in the minimum at 85 degrees, where the FDTD computation shows a deeper minimum, about -20 dB for FDTD compared to about -15 dB for NEC. The field differs in the minimum at 300 degrees as well, being shallower for FDTD than for NEC. Because the antenna is centered on the case in a back-to-front sense, the same distance from the back of the case as from the front, there is no cross-polarized field in the $\phi = 0$ pattern. Fig. 4.5(c) shows the $\phi = 90$ elevation cut. The E_θ polarization agrees well, with some difference in the minimum. The E_ϕ polarization agrees very well.

The handset discussed in this chapter uses a quarter-wave monopole antenna, and the radiation patterns in Fig. 4.5 are very similar to those presented in Chapter 3 for the same antenna.

4.3.3.2 Field Strength over the Radiation Sphere

Figs. 4.6 and 4.7 show the field strengths over the radiation sphere for the NEC computation and the FDTD computation, respectively, using the polar format presented in Section 3.3.2 above. The color patterns seen are remarkably similar, considering the hugely different methods used to solve Maxwell's Equations to obtain the data. Comparing the E_θ patterns in part (a) of the two figures shows that both NEC and FDTD predict that the handset radiates the main lobe in a circle centered at roughly $\theta = 135$ degrees, pointing downward, which is seen as the wide red circle in the two figures. There is a minimum at $\theta = 80$ degrees, which shows as a green circle surrounded by yellow on both sides. This minimum is deeper from $\phi = -30$ (330) degrees to $\phi = 30$ degrees in the FDTD computation than in the NEC computation. Thus in the NEC computation, the green circle at $\theta = 80$ degrees breaks up into yellow from -30 to +30 degrees,

whereas the green color is quite continuous over the full circle in the FDTD computation. The cross-polarized fields in part (b) of the two figures are also remarkably similar in pattern and level.

This section has demonstrated excellent agreement between the far fields computed with a wire-grid model using the NEC program and those computed with FDTD using time-stepping to steady state.

4.4 Software Setup for Constructing Maps of the Near Field

Although the FDTDANT program calculates the field strength on all cell edges in the cell space, it is not convenient to save this huge amount of data. Instead, the user designates planes for which the program will write out the near field amplitudes. Thus here we will examine the field component E_z in an xz plane spaced one cell away from the case of the handset. The plane of points is similar to that shown in Fig. 3.14, but the spacing between the plane and the handset is one cell or 0.882 cm. FDTDANT can assemble many planes of data in one run, and for each plane requested by the user, creates one "table file" of electric field as a function of position on the plane. In Fig. 4.2 the table file has been labelled "Ecppnnn.TBL", where "c" is the field component, x, y or z; "pp" is the plane cut, xy, xz or yz; and "nnn" is an integer giving the plane number in the cell space. Thus, EZXZ010.TBL contains E_z in an xz plane at the y location 10 cells from $y = 0$. These table files of field strength as a function of position are displayed with either CPLOT to obtain contour maps, or SPLOT to graph the field strength as a surface above the plane.

4.4.1 Scaling the Power to 700 Milliwatts

After FDTDANT is run to obtain a "table file" such as EZXZ010.TBL of E_z over an xz plane, the field can be displayed with program CPLOT. CPLOT composes a contour map of the field strength on the xz plane. The field strengths in the table files created by FDTDANT are scaled to a voltage generator of 1 volt, rather than to a radiated power of 700 milliwatts. CPLOT cannot itself rescale the power to 700 milliwatts. Thus program PWRSCALE was written to rescale table files to 700 milliwatts. The radiated power is found from the conical cut radiation patterns and written into the PHONE.DAT file by program ISOLEV. PWRSCALE reads the radiated power from the PHONE.DAT file and rescales the field strengths in the "table file" EZXZ010.TBL so that the fields correspond to a radiated power of 700 milliwatts.

4.4.2 Creating a Contour Map with CPLOT

Once the "table file" has been rescaled with PWRSCALE, program CPLOT is used to create a contour map of the scaled electric field as a function of position on the plane, such as E_z as a function of x and z. CPLOT is used to change the data in the "table file" EZXZ010.TBL into decibels, and to draw a contour map with the contour interval set to 3 dB. CPLOT lets the user position labels on the contour map, giving the strengths of the contours. CPLOT lets the user compose titles for the graph, and write labels on the axes. CPLOT scales distance along the

horizontal axis and along the vertical axis so that the graph fills the area of the computer screen, so inherently uses different scale factors for the two distance axes. CPLOT is used to store an image of the field map in the file "CPLOT.LAB".

4.4.3 Creating Scaled Near Field Maps

We want to plot field strength contours as a function of distance on the *xz* plane surrounding the telephone set. Program FDTDMAP was written to resize the contour map in the CPLOT.LAB file so that the horizontal and vertical axes have the same scale factor, and to superimpose the outline of the telephone handset. This is done by FDTDMAP by reading the header of the table file, which contains a copy of the original build file "PHONE.BLD". FDTDMAP reads the table file header to determine the cell size and the plane being graphed, *xz* or *yz*. FDTDMAP then rescales the image in CPLOT.LAB so that distance on the page is proportional to position with the same scale for the horizontal and vertical axes. FDTDMAP uses the OUTLINE.GW file to superimpose an image of the handset onto the field map, correctly scaled and positioned to correspond to the contour lines. A field map created this way will be examined in the following section.

4.5 Near Field Computed with FDTD

Fig. 4.8 shows the near field of the telephone handset shown in Fig. 4.1 as computed with the NEC program and created with program MAKEMAP in Fig. 3.2. The map is similar to that shown in Fig. 3.16, for the handset geometry of Fig. 3.1, with a quarter-wave monopole antenna. Note that the plane of Fig. 3.16 is 1 cm from the handset case whereas the plane in Fig. 4.8 is 0.882 cm from the case. Fig. 4.8 shows a similar configuration of field strength contours to those of Fig. 3.16. The field strengths in Fig. 4.8 are larger than those in Fig. 3.16. Near the tip of the antenna, the field is 45 dB in Fig. 4.8, compared to 42 dB in Fig. 3.16. The field at the top of the case is 48 dB, whereas the field in Fig. 3.16 reaches 48 dB only over a very small region. The field at the bottom of the case is 45 dB in Fig. 4.8, but only reaches 45 dB in Fig. 3.16 over a small region. The differences are due to the closer spacing of the plane of points to the handset case in Fig. 4.8, 0.882 cm, compared to that in Fig. 3.16, which used a spacing of 1 cm.

Fig. 4.9 shows the contour map computed with FDTDANT and created with the software setup of Fig. 4.2 using PWRSCALE and FDTDMAP. The region over which the field strength has been computed is determined by the size of the cell space, 26 by 2 by 49 cells. Hence a cross-section of the cell space in an *xz* plane measures 26 by 49 cells, with the handset occupying 6 by 19 cells, and the monopole antenna 10 cells long. A thicker whitespace layer would lead to a larger contour map.

Comparing the contour maps computed with NEC in Fig. 4.8 and with FDTDANT in Fig. 4.9 show that they are very similar. The field near the tip of the antenna is 45 dB. The field near the top of the handset is 48 dB and the shape of the 48 dB contour is very similar in both figures. The field near the bottom of the handset case is 45 dB and is very similar in both figures. The field to the left of the handset in the figures is very flat, and the NEC calculation shows the 33 dB contour extends to enclose a considerable area in this region, whereas in the FDTDANT computation the 33 dB contour breaks into two, one centered on the bottom of the handset, and the other halfway up the left side of the picture.

4.6 Conclusion

This chapter has presented several modifications to the Penn State FDTDC program, developing the program so that it can solve a radiating antenna problem consisting of a monopole antenna on a perfectly conducting handset. The new program, called FDTDANT, was used to calculate the far fields and the near fields of a representative telephone handset. This chapter has described a software system which permits the comparison of far fields and near fields on the basis of equal radiated power. A method of constructing scaled contour maps of the near field has been constructed and presented in this chapter.

This chapter has compared fields computed with FDTD with those from a wire-grid model of the same handset. In the far field very good agreement was obtained. Some differences were noted in the depth of the minima in the radiation patterns, with the FDTD calculation showing a deeper minimum. The near fields of the two computations were compared and found to be in excellent agreement in an xz plane.

In testing the FDTDANT code with a sinusoidal generator, a serious limitation was identified concerning the algorithm used to compute the far field. Various other code developments were also identified in this chapter to permit efficient and convenient FDTD computations of the near and far fields of telephone handsets near models of the human head. These developments will be summarized as recommendations for further work in the next chapter.

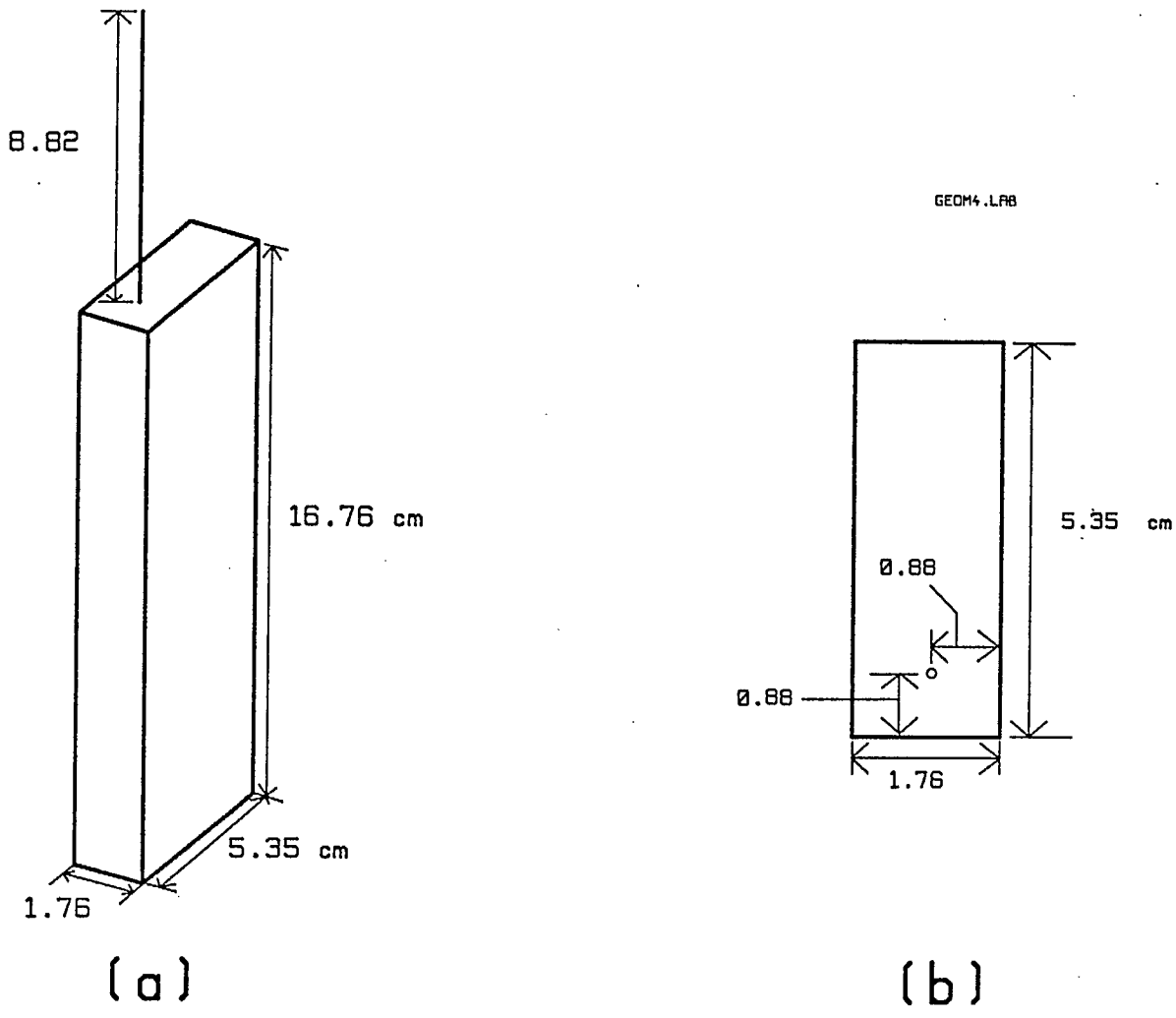

Fig. 4.1 The dimensions of the cellular telephone handset used to compare FDTD computations with wire-grid computations, with a quarter-wave monopole, end-fed.

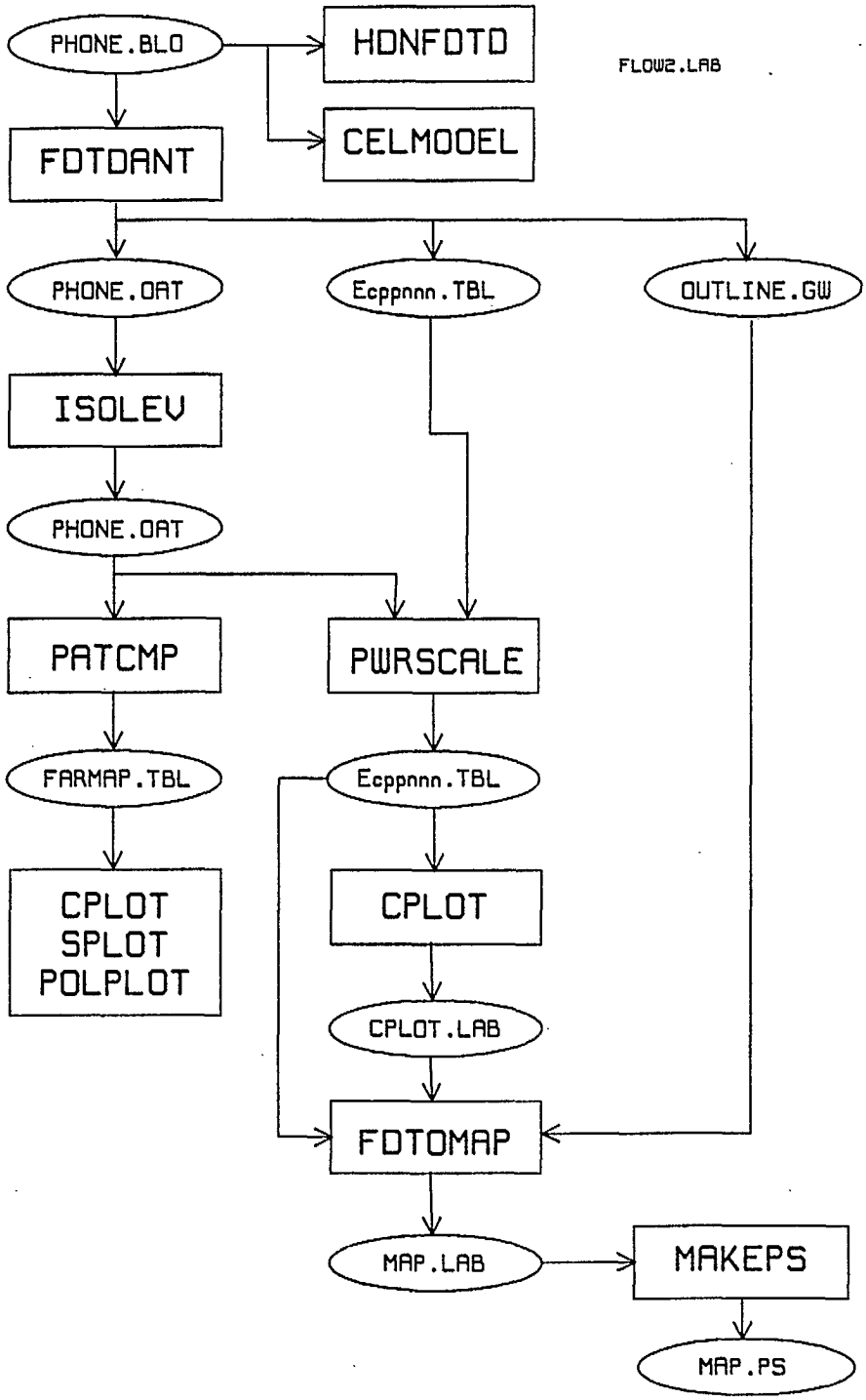

Fig. 4.2 Flowchart showing the programs(rectangles) and data files(ellipses) used with FDTD models to obtain far-field patterns, to scale the power to 700 milliwatts, and to plot near-field maps of the fields of a cellular telephone.

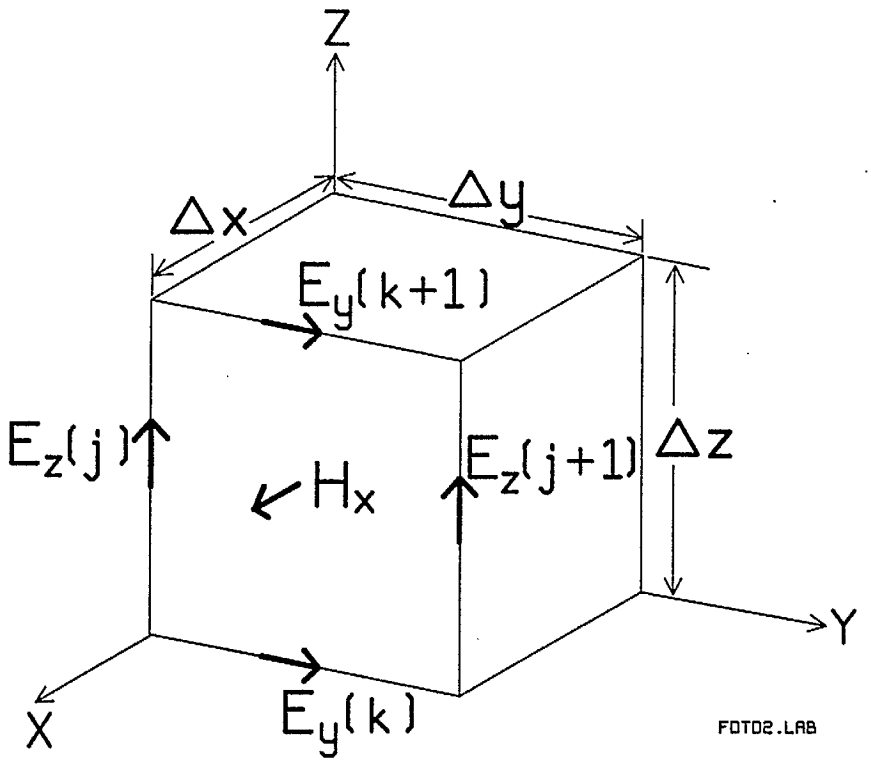

Fig. 4.3 One cell in the FDTD cell space, showing the cell size, Δx by Δy by Δz, the electric field components along the cell edges, and the magnetic field components perpendicular to the centers of the cell faces.

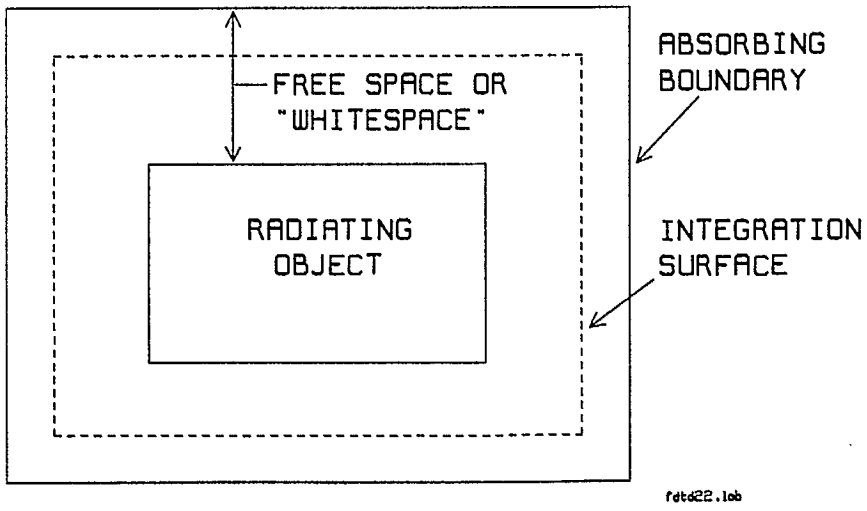

Fig. 4.4 A sketch of a cross-section of the FDTD cell space, showing: the central box which entirely encloses the cellular telephone and its antenna; the layer of free-space cells or "whitespace" separating the radio from the outer "absorbing boundary" of the cell space; and the integration surface five cells inside the cell space, used to compute the far fields.

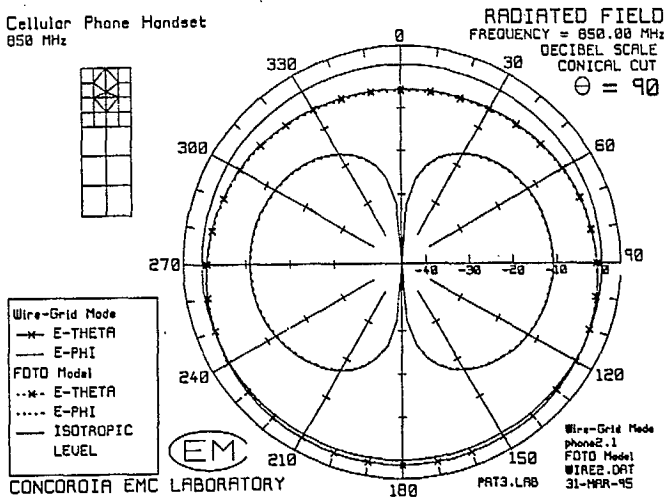

(a) $\theta = 90$ azimuth plane.

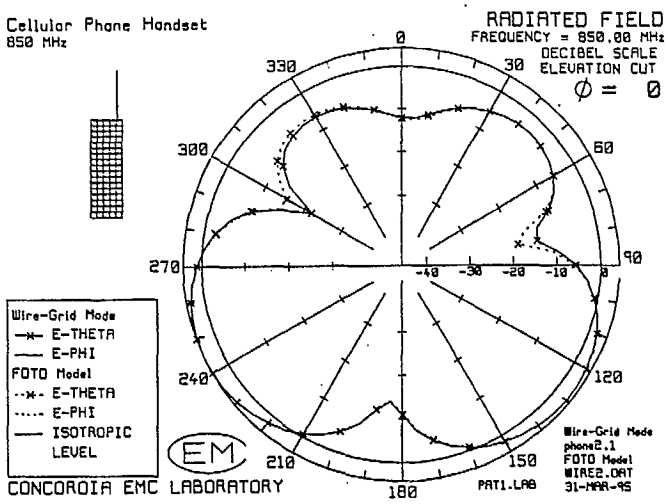

(b) $\phi = 0$ elevation plane.

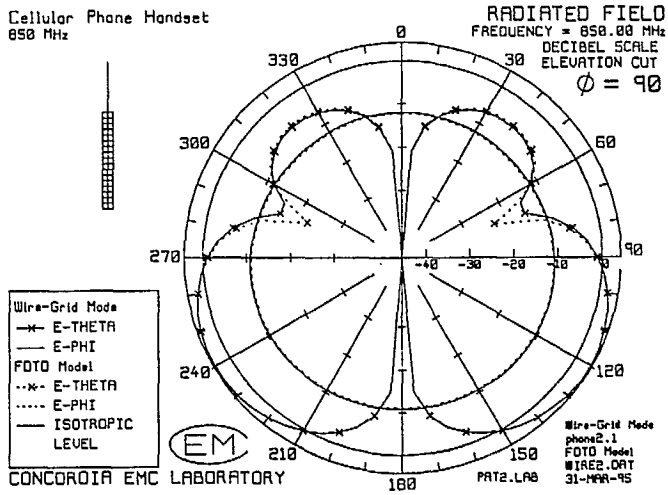

(c) $\phi = 90$ elevation plane.

Fig. 4.5 Comparison of the far-field radiation patterns of the cellular telephone of Fig. 4.1 obtained by wire-grid modelling with the NEC program and by FDTD.

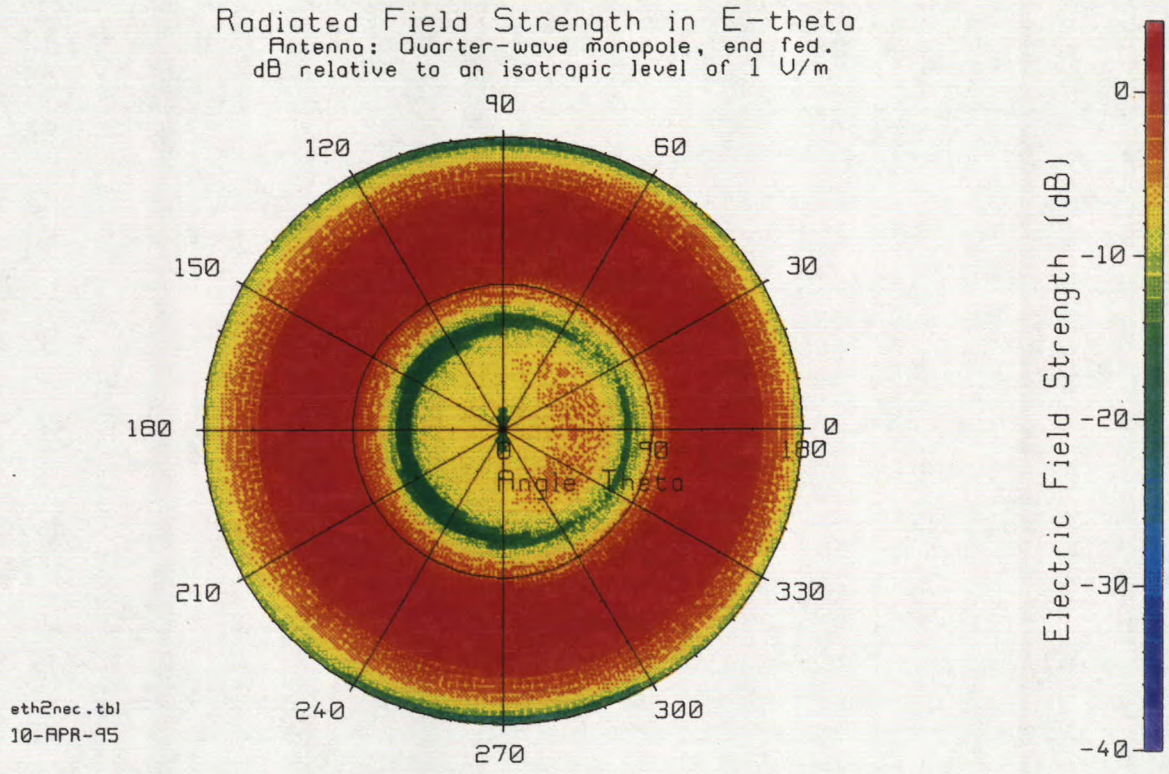

(a) Field strength in E_θ.

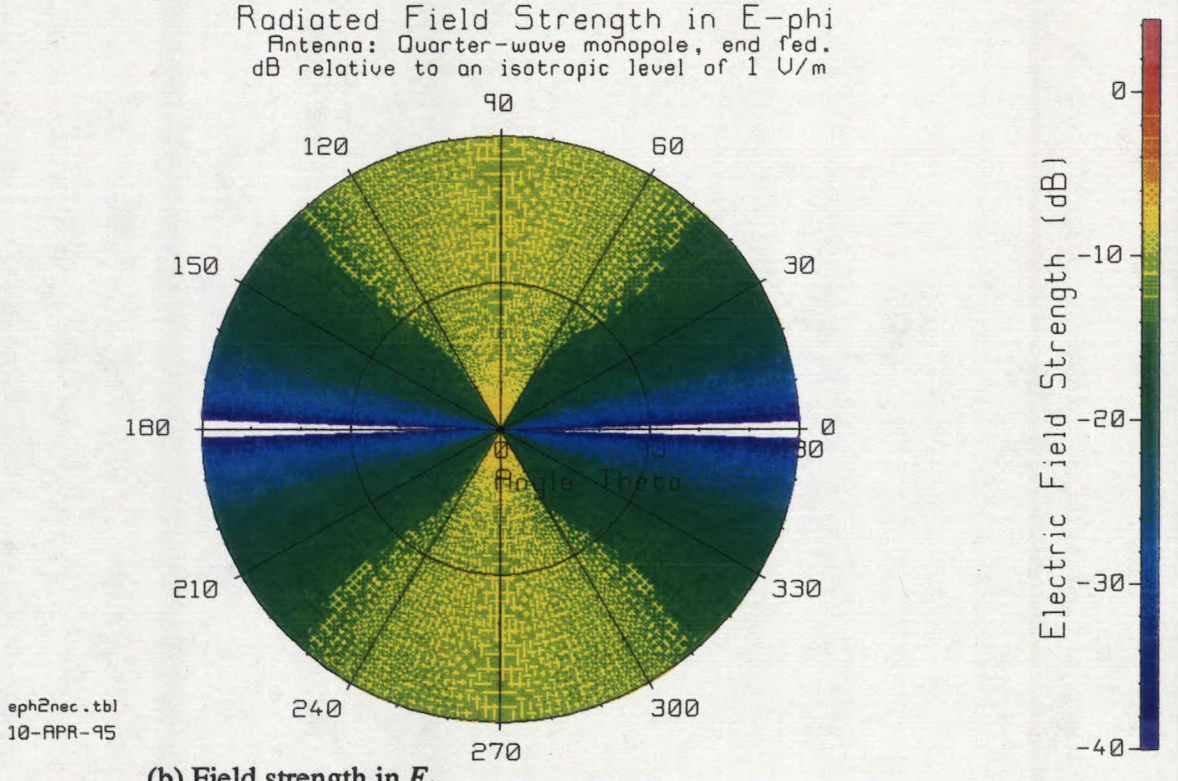

(b) Field strength in E_ϕ.

Fig. 4.6 The field strength over the radiation sphere of the cellular telephone, computed with the NEC program.

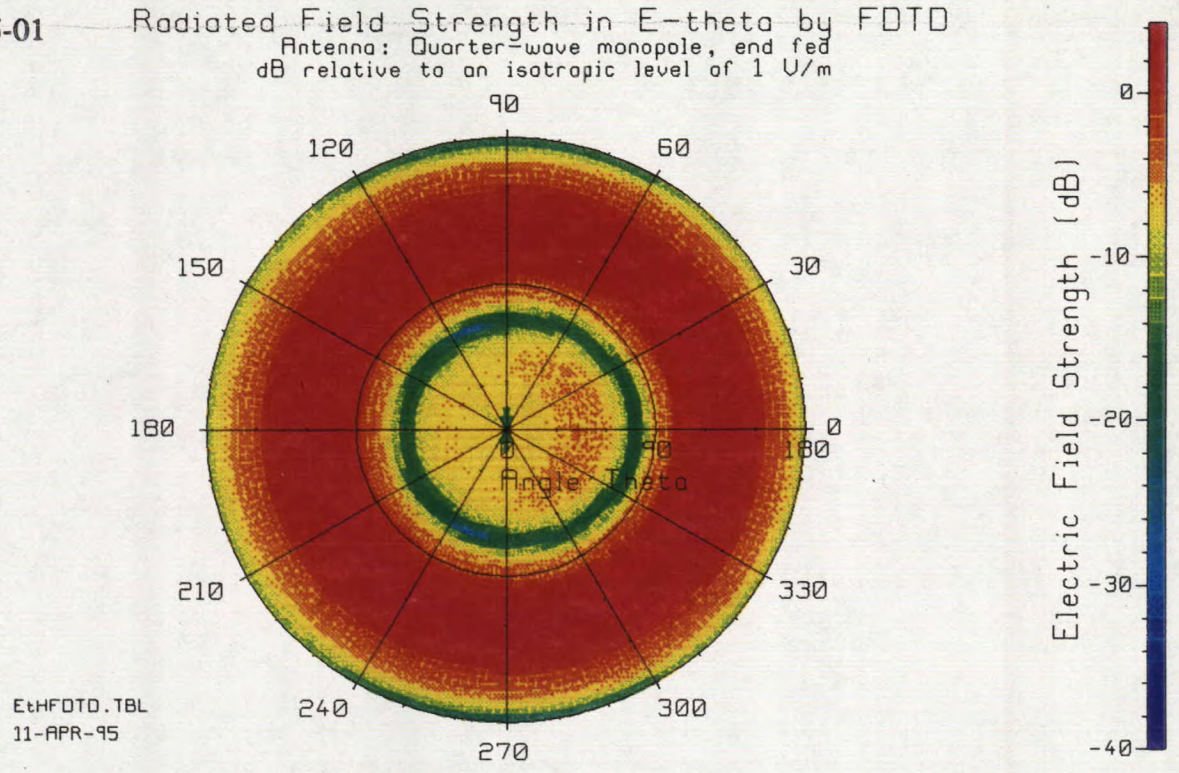

(a) Field strength in E_θ.

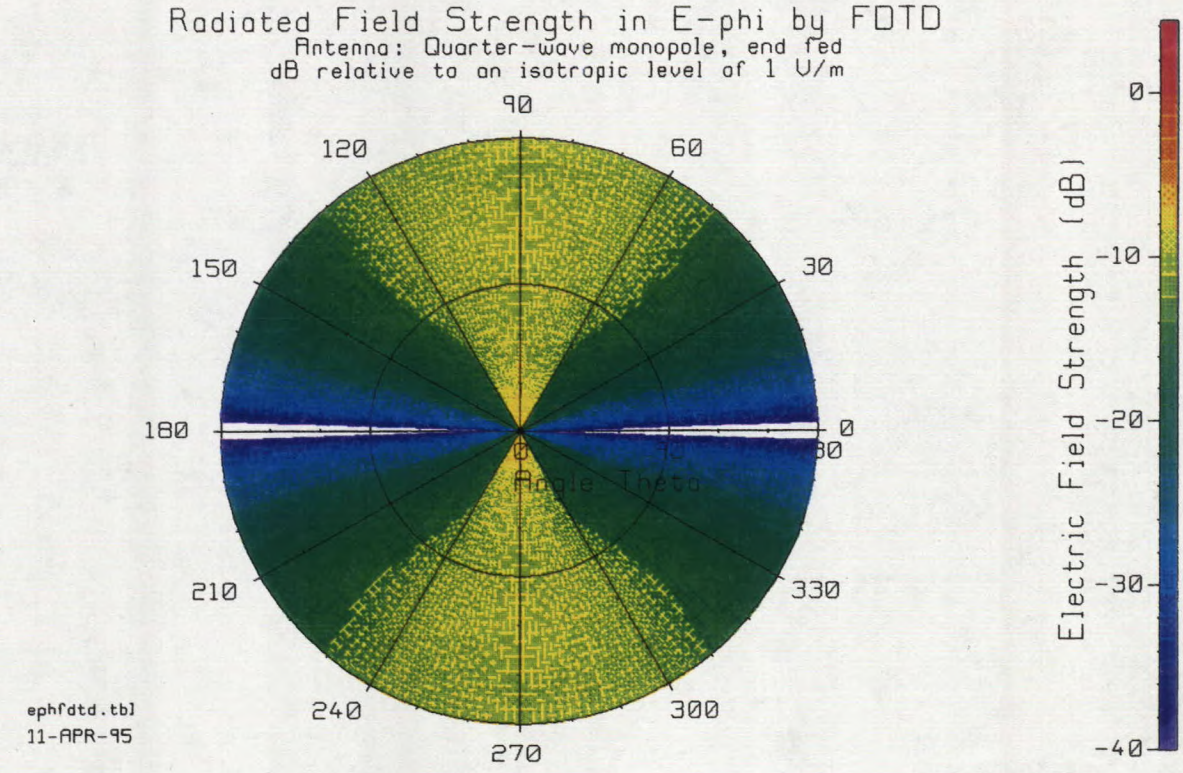

(b) Field strength in E_ϕ.

Fig. 4.7 The field strength over the radiation sphere of the cellular telephone, computed with FDTD.

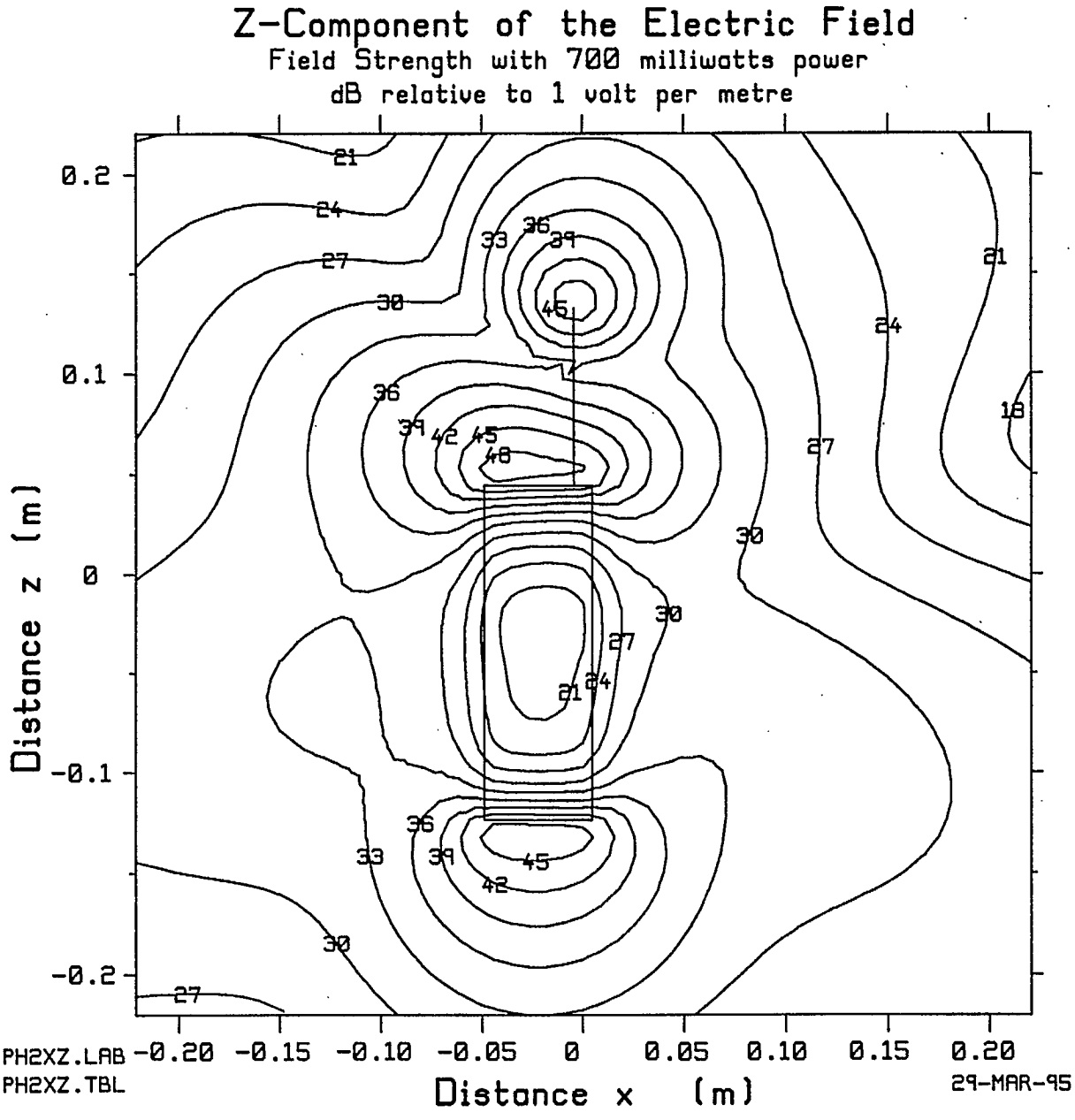

Fig. 4.8 The field strength of the cellular telephone of Fig. 4.1 over the near-field grid of points in the *xz* plane similar to that shown in Fig. 3.14, spaced by 0.882 cm from the case, computed with the NEC program.

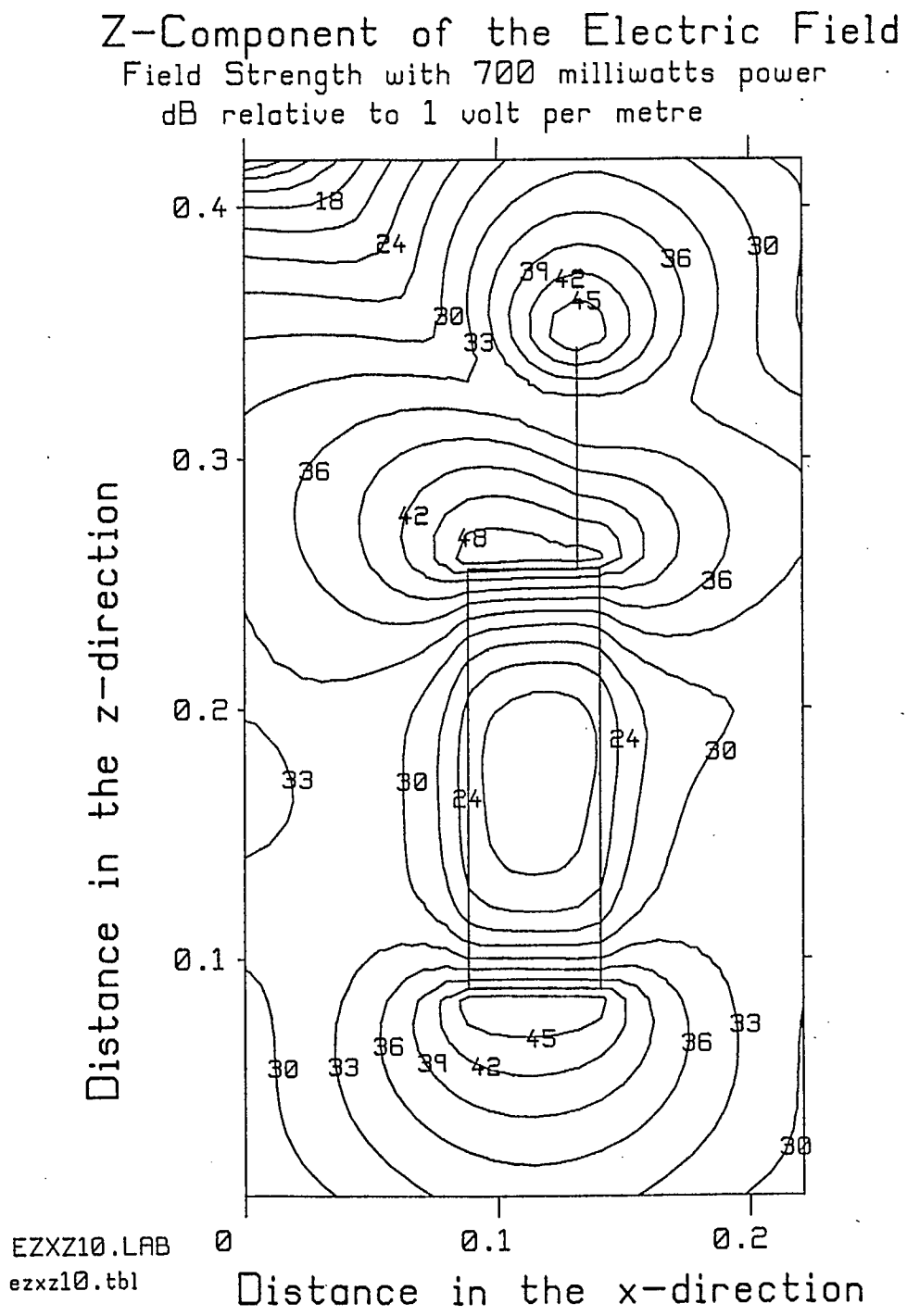

Fig. 4.9 The field strength of the cellular telephone of Fig. 4.1 over an *xz* plane grid of points 0.882 cm from the handset case, computed with FDTD.

CHAPTER 5

Recommendations for Further Work

5.1 Measurements and Validation

This section discusses measurements that can be carried out to provide reference data for validating the computations presented in this report, and for validating new computations involving dielectric objects near the handset.

5.1.1 Computations and Measurements for the Handset Alone

This report has presented maps of the field strength of a handset consisting of a metal box with a monopole mounted on top. Excellent agreement between quite dissimilar computational methods, wire-grid modelling and FDTD, was demonstrated. We have very high confidence in the computations presented here, which can thus serve as a basis for establishing a measurement method for the near and far fields of a portable radio.

It is recommended that a portable radio handset of dimensions similar to that of Fig. 4.1 be constructed. The near fields of the handset should be measured on *xz* and *yz* planes. All three components of the field are of interest, not simply E_z as studied in this report. The measurement system must operate at a known power level, so that comparisons between measurements and computations be done at the same radiated power level.

Ref. [71] discusses the measurement of the conical-cut set of far field patterns for a portable radio handset. The far fields of the portable radio should be measured for the conical-cut set of patterns, both to serve as a check of the power level, and to provide pattern data for comparison with the computations. Establishing agreement between the measurements and the computations for the simple handset-only case clearly demonstrates the validity of both the measurements and the computations.

5.1.2 Simulations with a High-Permittivity Dielectric Body

To approach the modelling of the human head with confidence, it is necessary to establish agreement between measurements and computations for simpler structures. Thus Ref. [21] uses a dielectric sphere as a representation of the human head. The sphere diameter is 18 cm, and is uniformly filled with dielectric using relative permittivity $\varepsilon_r = 50.5$ and conductivity $\sigma = 1.2$ S/m for muscle at the operating frequency of 900 MHz. FDTD is used to compute the far field patterns and input impedance, which are compared with measurements.

The first structure recommended is a simple dielectric parallelepiped or box, of overall volume comparable to a human head. It is recommended that a hollow plexiglas box be constructed, of dimensions 12 by 16 by 16 cm, having the same volume as the 18 cm diameter sphere used in Ref. [21]. The box will be filled with liquid such as salt water that has a high-permittivity and a loss tangent similar to that of tissue. Or, the liquid can be a muscle-equivalent or a brain-equivalent such as those discussed in Ref. [32]. It is essential that the permittivity and conductivity be well-known, to avoid the complication of computing for an object of unknown electrical properties! The near field must be measured on planes close to the surfaces of the dielectric box, both on the same side as the portable radio and on the opposite side, where the field strengths will be much lower. If possible, the far fields on the conical cut pattern set should be measured. We would expect to be able to establish excellent agreement between computation and measurement.

A second simple configuration is that of a sphere representing a head, as used in Ref. [21]. A hollow plexiglas sphere can be made, and filled with a tissue-equivalent liquid of known properties. Again the near field is to be measured in planes close to the surface of the sphere. Again, the conical-cut pattern set should be measured. A sphere is more challenging to model with FDTD than a simple box, especially if the plexiglas wall is to be included in the FDTD model. This structure provides a tool for checking the validity of the code that will be written to deal with changes in permittivity between cells of an object of complex shape, as discussed below in Section 5.2.3.

5.1.3 Measurements with Phantoms

It would be very useful to carry out measurements of the near and far fields of a "head phantom", that is, a full-size model of a human head made with materials that have the same electrical properties as the tissues they represent. Head phantoms are commercially available and it is recommended that a head phantom be purchased for use in this project. It is important that the geometry of the head phantom be accurately known, for it will be necessary to construct an FDTD cell model of the phantom. Thus, cross-sections of the phantom must be available, identifying the regions of dielectric material in each cross-section. The electrical properties of the various dielectrics must be known.

Another possible measurement using a phantom is that done at the Dept. of Health and Welfare in conjunction with the verification of the field strength radiated by commercial cellular telephone handsets, which is very similar to the method described in Ref. [28]. In this measurement, the head and torso of a person are constructed as a thin-walled fiberglass shell. The phantom is mounted as if the person were lying on his left side. The cellular telephone is located under the left side of the phantom's head. The right side of the head has been cut away. The fiberglass shell is filled with a liquid with the same electrical properties as brain tissue. A probe is inserted into the liquid and can measure two orthogonal components of the electric field. A robot manipulator arm moves the probe to cover a plane of points within the head, and several or many planes can be measured to map the field strength throughout the head.

To model this configuration with FDTD, it would be necessary to know the geometry of the head-and-shoulders phantom well enough to construct a cell model. This requires knowing the cross-section dimensions at quite closely spaced cross-sections. The electrical parameters of the fiberglass must be known, as well as those of the brain-equivalent liquid. The phantom would be operated near a simplified handset such as used in this report. FDTD could then be used to calculate the field strength inside the brain and a comparison made with the measured data. This would provide an excellent validation of the FDTD computation method.

5.1.4 Measurement with a Person

It may be useful to do a measurement of the far fields of a handset held by an actual person. Someone standing on a turntable holding a handset can be rotated to measure a radiation pattern as a function of angle ϕ. It would be necessary to have a probe antenna mounted such that the probe position could be changed to vary angle θ. It would also be necessary to have a probe arrangement that could either measure both E_θ and E_ϕ simultaneously, or a probe that could be rotated ninety degrees to change between E_θ and E_ϕ.

It may also be useful to scan the near field in planes close to the head of a person holding a cellular phone. To model these near and far field measurements, the cell model of the head would be scaled to approximately the size of the subject's head. The cellular phone model would need to be as good a representation of the actual handheld radio as possible. The angle that the cell phone is held relative to the head is an important parameter in trying to calculate the fields measured with an actual person.

5.2 Computation Development

This section describes developments to the FDTDANT program which will permit the study of the near fields and radiation patterns of the telephone handset near a representation of the human head in a computationally efficient manner.

Chapter 4 described the development of the FDTDANT code from the Penn State FDTDC code for the computation of the scattering of plane waves from metallic and dielectric bodies. The principal changes were as follows. First, a wire antenna feature was added, allowing the electric field to be set to zero along a row of cell edges to represent a thin, highly conducting wire. Second, a voltage generator feature was included, allowing the wire antenna to be excited at its base by a voltage generator with sinusoidal time variation, that gradually turns on. The solution is then time-stepped to steady state. The program was modified so that it calculates the far field at 73 points on each of the conical cut radiation patterns. The program was modified to allow the user to output the amplitude of the near field in specified planes. The program determines the field amplitudes by searching the last half-cycle of time samples for the largest magnitude. The output file of the FDTDANT program was arranged to simulate an output obtained from a run of the NEC program, so that the same display software can be used to examine the fields. Thus, the PHONE.DAT output file contains an image of the handset and antenna written in the form of GW cards, and contains the radiation patterns in the format accepted by ISOLEV and PATCMP. FDTDANT was arranged to write a "table file" of near field points for display by CPLOT, for each plane of near field values selected by the user.

5.2.1 Development of the Diagnostic Tools

Fig. 4.2 in Chapter 4 shows the diagnostic tools HDNFDTD and CELMODEL, which were written to aid in developing cell models of aircraft for analysis with FDTD. HDNFDTD shows the FDTD cell model by representing each block of cells filled with perfectly conducting material as a solid box. This is useful for visualizing the shape of the object described in the "build file". To make HDNFDTD useful for the present purpose, the program should be modified so that it can show a wire antenna by showing the line of cell edges on which the program will enforce the zero-electric field boundary condition. The location of the generator could be

highlighted. To display complex dielectric objects, it would be useful to add a color-coding scheme to HDNFDTD, so that blocks of cells associated with each type of dielectric are drawn in different colors.

Program CELMODEL is oriented toward showing cross-sections of an aircraft in xy, xz or yz planes in the cell space. The present version of the program fills cells that are perfectly-conducting with color. The program should be developed to show the location of the wire antennas. The program should recognize cells filled with dielectric materials and distinguish the dielectric types by color.

CELMODEL reports the highest frequency at which the model is useful, estimated by setting the cell size to one-tenth of the free-space wavelength. The program should be improved to find the shortest wavelength by searching all the dielectrics present, and base the bandwidth estimate on that wavelength. CELMODEL reports the minimum thickness of the whitespace surrounding the model and lets the user adjust the whitespace thickness if desired. Further editorial features would be very useful. For example the user could be allowed to toggle cells on and off for the various material types, to edit the model geometry.

It might also be useful to extend CELMODEL's functions to let the user superimpose on the cell model a wire-grid model from a GW card file. This might be useful in that a reference geometry could be stored in the GW card format, and superimposed on the staircasing approximation in the FDTD model, to permit adjustments to get the best possible fit.

5.2.2 FDTD Modifications for Radiated Power and Far Fields

In Chapter 4, the method used in FDTDC to compute the far fields was examined. It was noted that FDTDC, hence FDTDANT, saves all the time samples at each far field point, and then searches the last half cycle of time samples for the largest magnitude to obtain the "steady state" amplitude of the sinusoidal field. It was demonstrated that this requires 55 megabytes of storage for the conical cut set of radiation patterns, with a modest 512 time steps!

The first recommendation is that the FDTDANT code be developed to determine and save the amplitude and phase of the tangential electric field and the tangential magnetic field flowing over the integration surface used for the near-to-far zone transformation. Then the far fields should be calculated by a frequency-domain implementation of the near-to-far zone transformation, as a post-processing step after the time stepping calculation is completed. This will speed up the FDTD program considerably, by eliminating the far zone calculations presently required at each time step. The fields on the integration surface only need be examined during the last half-cycle of time steps, to determine the amplitude and phase. Further, a near-to-far zone computation in the frequency domain is quick and efficient.

An added advantage of this approach is that the power density can be integrated over the near-zone integration surface to determine the power radiated directly, rather than indirectly via the conical cut set of far zone patterns. Thus the FDTDANT program can itself find the power radiated and scale the field strengths to 700 milliwatts, eliminating the need for the ISOLEV processing step and for the PWRSCALE processing step in Fig. 4.2.

5.2.3 Dealing with Multiple Dielectrics

The FDTD algorithm permits the user to assign a value of permittivity and conductivity to each cell throughout the cell space. Metallic objects such as a wire antenna or the handset studied in this report, are represented by enforcing the boundary condition of zero electric field on

all cell edges that lie inside or on the surface of the metallic object. Dielectric objects, such as a model of the human head, are represented by assigning an appropriate permittivity and conductivity to each cell, depending on the type of tissue present at the location of the cell. The whole radiating body, handset plus head, must be surrounded by a layer of free-space cells separating its surfaces from the outer boundary of the cell space. These free-space cells support near fields that surround the handset and head.

In constructing a model of the head, the cell size is often coarser than the resolution of the anatomical information upon which the model is based, and so one cell contains more than one type of tissue. Then the material properties of the cell are sometimes assigned by taking an average of the properties of the tissue within the cell, weighted by volume[11,25,30]. Thus cells represent the average properties of the materials within them at a given frequency. The procedure of volume-averaging material properties over all the tissues within a cell leads to a unique set of material properties for every cell within the head model. The FDTD code must then be set up to handle a great many different material types, perhaps many thousand.

The permittivities and conductivities assigned to all the cells are used to update the electric field components that lie along the edges of the cells. Since the field component being updated lies along a cell edge, the value of permittivity and conductivity that needs to be used in the update equation must account for the properties of the four cells surrounding the cell edge. The appropriate value of the material properties has been investigated in conjunction with the modelling of thin resistive sheets in waveguide, and the results available in the literature are summarized in Ref. [56]. In modelling scattering from dielectric parallelepipeds by FDTD[57], it was found that the electric field components on cell edges that lie on the surface of the parallelepiped must be updated with the average value of the parallelepiped permittivity and that of free space, which is consistent with the results obtained by several of the investigators discussed in Ref. [56]. It was verified by measurement that the resonant frequencies of a dielectric parallelepiped are correctly computed with FDTD when the update equations use the average permittivity on the surface of the parallelepiped.

A model of a human head is much more complex than a simple solid box filled with a homogeneous dielectric. Almost every cell throughout the head model will have a unique permittivity and conductivity, depending upon the volume average of the materials within it. Consequently, every cell edge will require unique values of permittivity and conductivity to be used in its update equations. The FDTDANT code must be modified to include a pre-processing step which examines every cell edge throughout the cell space and determines the appropriate values for the permittivity and conductivity based on the material properties of the four neighboring cells. These values need to be stored in arrays, which will considerably increase the storage requirements of the program. Then at each time step the appropriate value of permittivity and conductivity is readily available, and the speed of execution of the program will be little changed.

5.2.4 Graphical FDTD

The FDTDANT code is readily modified to create a graphical display of the field strength in each cell as a function of time during the course of the FDTD computation. Thus, the program will draw a specified cross-section of the cell space, showing the telephone handset, the monopole antenna, and the head, and then will show the field strength in each cell on a false color scale. At each time step the field in each cell is updated, and so the user sees the fields as a function of time on the computer screen. When the computation is concluded, the graphical display can be updated with the amplitude of the field in each cell at steady state. The value of such a display is that it provides insight into the nature of radiation from a portable radio and its interaction with the human head. For the portable radio alone, we can see waves radiated from the feed point, radiated from the tip of the antenna, and radiated from the base of the handset case,

which interact to create the near and far fields of the radio. When the head model is introduced, we can see the penetration of the electromagnetic energy into the head, and the formation and location of hot spots where the field strength is strong. It is recommended that FDTDANT include this graphical display feature.

5.3 Steady State with High-Permittivity Dielectrics

This report determines the amplitudes of the fields at steady state due to a portable radio excited by a sinusoidal generator at a given frequency. The approach used in this report and often used in the literature[67,68,21,11] is to use FDTD to compute the transient solution at each time step as the generator is gradually turned on, and to continue the time-stepping solution for a sufficient number of time steps to reach steady state. The success of this approach depends on the time constants associated with the radiating object, which, of course, are not known in advance. If the object has short time constants, then few time steps are needed to reach steady state, and the time-step-to-steady-state approach is practical. Time constants are short when the handset is an efficient radiator of the field, for then energy coupled to the antenna and handset is quickly radiated away. Conversely, time constants become long when energy can become trapped on or inside an object of resonant size, and for these cases time-stepping to steady state may require far too many time steps.

Ref. [57] studied scattering from dielectric parallelepipeds with high-permittivity and low losses. The relative permittivity in Ref. [57] was ε_r =37.84 and 79.46, which are in the range found for biological tissue. However, the ceramic materials studied had very low loss due to dissipation, with loss tangents of the order of 1/2000. Biological materials have much higher losses. In Ref. [57] the rectangular-box parallelepiped geometry is strongly resonant, and at resonance the parallelepiped is a very poor radiator of energy trapped inside it. The resulting resonance peaks in the frequency response are very high Q, that is, have very low damping[72] and so the time constant associated with the ringing-down of the oscillation inside the resonator is very long. It was found in Ref. [72] that as many as 140,000 time steps were required to compute the full transient response of a high-permittivity dielectric resonator. Ref. [72] used a signal-processing technique based on Prony's method[73] to trace the transient to zero based on an FDTD computation using 8192 time steps.

Biological materials have permittivities in the range studied for dielectric resonators, but are much lossier. The human head is not a perfectly regular structure, and so is not expected to have high-Q resonances as does a parallelepiped. However, resonance of anatomical structures with reasonably regular shapes, such as the eyes or the brain, may play a significant role in the interaction of portable radios with humans[12]. Ultimately we wish to determine the largest field strength within the head; resonance tends to build up the strength of oscillations over time and hence it is crucial to be sure that we have used enough time steps to reach steady state, even for resonant sub-structures of the head.

Because biological materials are much lossier than the ceramic used in the resonator study, we expect more internal energy dissipation and so shorter time constants. Further, the head does not contain perfectly-regular cavities and so is not likely to support the very high-Q resonances of a parallelepiped or sphere. Thus, it may not require many thousands of time steps to reach steady state. It is not obvious from mere inspection of the field strength as a function of time whether steady-state has indeed been reached, or whether there is a transient with a long time constant active in the solution, thus requiring further time-stepping. It is recommended that the signal-processing method used in Ref. [72] be extended to provide a tool for examining the tran-

sient response due to a sinusoidal generator, to determine whether steady state has been reasonably achieved, and if not, to extrapolate the field strength to steady state and estimate the resulting field amplitude.

5.3.1 Examining the Specific Absorption Rate

Although the overall objective of this project is to determine the radiation patterns of a portable radio held by a user against the head, the FDTD method also permits the calculation of the specific absorption rate(SAR) as power absorbed per kilogram mass of tissue throughout the head. The SAR depends on the conductivity of the tissue at each point inside the head, and on the current density, which in turn depends on the three components of the electric field.

It is recommended that the FDTDANT code include a post-processing subroutine for evaluating the SAR in each cell throughout the head model. The program must determine the SAR and write "table files" of SAR in the planes specified by the user. It may be useful to have the FDTDANT code determine the cell in which the SAR is largest, and automatically generate table files for all three planes intersecting the cell of largest SAR.

5.4 Handset with Full-Head Model

Ref. [11] presented a cell model of a human based on the cross-sectional anatomy in Ref. [4] that was used in Chapter 2 of this report to develop a cell model of the head. In Ref. [11] at 100 MHz, 2.62 cm cubical cells were used, and at 350 MHz, 1.31 cm cubes were used. Fourteen different tissue types were examined. Much the same model has been the basis of more recent papers, such as Ref. [30] presenting an FDTD analysis over a wide bandwidth, accounting for the dispersive properties of the tissues. More recent work[25] has used the same anatomy atlas[4] on a 6.56 millimeter grid to construct a more detailed model of the head, supplemented with magnetic resonances(NMR) images. The full head model uses 24 by 33 by 31 cells, for a total of 24,552 cells. In Ref. [26], NMR images consisting of 109 slices of the head form the basis of a head model using cells of dimension 2.5 by 2.5 by 3.3 millimeters. The head is illuminated by a dipole at 915 MHz and the field strength throughout the head is calculated.

The preliminary studies discussed above are intended to first establish a close correspondence between FDTD calculations and measurements for the handset alone, and then between computations and measurements for a handset near a dielectric parallelepiped "head", and then a spherical "head". Having established that we can correctly compute the fields for these simplified geometries, we are ready to make use of the full head model developed in Chapter 2.

The head model presented in Chapter 2 is based on the cross-sectional anatomy atlas[4] used by other authors[11,25,30]. About half of the head cross-sections in Ref. [4], namely those through the brain, are spaced by approximately 6.35 mm, and the remainder for the lower part of the head, by about 12 mm. These cross-sections were digitized on a grid of cell size 3.3 mm. Twenty-seven different kinds of tissue were identified. The result is a head model containing 64x72x76 cells, for a total of 350,208 cells.

The next stage in this project is to develop the FDTDANT program so that it will accept as input a "build file" containing 27 or perhaps 30 different dielectric materials, each with a different permittivity and conductivity. The program must then read the description of the head model from the build file and store the electrical parameters of each cell. The program will also read the portable radio description, which should be modified to be a more realistic handset model including the plastic case of the handset. It may be useful to include the operator's hand in the model, which must be constructed from the cross-sectional anatomy data.

Once the head model and the handset model have been input, the FDTDANT program must sort through the model to identify the permittivity and conductivity needed to update the electric field on each cell edge, accounting for the material properties of the four adjacent cells. The program must use an average of the material properties of these four adjacent cells to update the electric field on the cell edge. This average must be computed and stored for each cell edge. This process increases the number of material types the program must deal with but is necessary to obtain correct results at the interfaces between dissimilar dielectrics.

The program can then proceed to calculate the fields due to a sinusoidal oscillator, time-stepping to steady state. The last step is to output the fields in desired planes, containing cross-sections of the head in critical regions, and to use the frequency-domain near-zone to far-zone transformation to calculate the conical cut radiation pattern set.

It may be useful to reduce the roughly 350,000 cell head model using 3.3 mm cells to a coarser model with 6.6 mm cells, by replacing blocks of eight cells with a single cell, to obtain a simplified model with about 44,000 cells. This model can form the basis of initial comparisons and investigations, and then the finer model used to obtain results with a finer resolution as needed.

5.5 External Code Acquisition and Testing

Penn State now offers for sale a code called XFDTD which may be capable of the calculations required in the next stage of this project. The description of XFDTD suggests that the program may be useful for examining and modifying the FDTD cell model of the handset and head using computer graphics. The program permits the calculation of near fields, of far zone radiation patterns, and of antenna input impedance, and of gain. The program includes the calculation of the SAR for each cell in the cell space. Thus XFDTD offers features that may be useful for this project.

It is recommended that the XFDTD code be purchased for the LINUX operating system to be executed on a Pentium computer. XFDTD's graphical input and display features may provide a useful addition to our capabilities for creating input geometries and for examining near and far fields. Running XFDTD in parallel with the FDTDANT code will provide additional confidence that the modifications made to create FDTDANT have been correctly implemented.

The source code for XFDTD is offered and should be purchased so that XFDTD can be customized to support the specific needs of this project. For example, XFDTD only supports 14 material types; this will have to be greatly increased. XFDTD must use the average material types at interfaces between dielectrics; if not it must be modified to do so. It is not clear that XFDTD overcomes the limitation of the older FDTDC code when the far field is required at a great many points. It may be possible to use the frequency-domain near-to-far-zone transformation in conjunction with XFDTD as well as with FDTDANT.

The purchase of XFDTD is not expected to remove the need to develop the FDTDANT code. Rather, XFDTD provides an additional capability for supporting the needs of this project.

5.6 Conclusion

This report has described the work done in the second year of this project. In this time period two parallel efforts were made. A detailed cell model of the human head was developed from anatomical cross-sections, including the writing of the software required to create the head model. And the FDTDANT code was developed to support the calculation of the near-zone and

far-zone fields of a portable radio, and was validated by comparison with calculations made by the well-established wire-grid modelling method. Limitations to the FDTDANT code were identified and suggestions made to overcome these limitations.

The project is poised for a very productive third year. Much of the necessary background work has been completed, and in the third year computations of the near and far fields of a portable radio alone, of the radio with a simplified head, and of the radio with the full head model can be carried out. The parallel measurement project should provide reference data for validating the computations, and lend great confidence to the results being obtained.

5.7 Acknowledgements

The authors wish to acknowledge the contribution of Wilf Lauber of the Communications Research Centre for posing the problems investigated in this report, and for his encouragement during the course of the work. The authors are indebted to research assistant Mina Danesh, who developed the software needed to "digitize" the cross-sectional anatomy of the head, and to create a cell model of the head from the digitized information. Her dedication to the project is greatly appreciated.

REFERENCES

1. S.J. Kubina and C.W. Trueman, "Computational Studies for Prediction of Energy Deposition in Humans Exposed to RF Fields from Cellular Phones", Final Report prepared for the Communications Research Centre, Ministry of Industry, Science and Technology, Contract No. MIST/CRC 36001-3-3603, Technical Note No. TN-EMC-94-01, Electromagnetic Compatibility Laboratory, Concordia University, March 31, 1994.

2. K.S. Yee, "Numerical Solution of Initial Value Problems Involving Maxwell's Equations in Isotropic Media", IEEE Trans. on Antennas and Propagation, Vol. AP-14, No. 3, pp. 302-307, May, 1966.

3. K.S. Kunz and R.J. Luebbers, "The Finite-Difference Time-Domain Method for Electromagnetics", CRC Press, Boca Raton, 1993.

4. A.C. Eycleshymer and D.M Schoemaker, "A Cross-Section Anatomy", D. Appleton and Co., New York, 1911.

5. C.W. Trueman and S.J. Kubina, "Fields of Complex Surfaces Using Wire Grid Modelling," IEEE Transactions on Magnetics, Vol. 27, No. 5, pp. 4262-4267, September, 1991.

6. J.H. Beggs, R.J. Luebbers, K.S. Kunz, H.S. Langdon, "User's Manual for Three Dimensional FDTD Version A Code for Scattering from Frequency-Independent Dielectric Materials", Electrical and Computer Engineering Department, The Pennsylvania State University, University Park, Pennsylvania, March 25, 1992.

7. H.D. Bruns, H. Singer, and T. Mader, "Field Distributions of a Hand-Held Transmitter due to the Influence of the Human Body", Proceedings of the 10th International Zurich Symposium and Technical Exhibition on Electromagnetic Compatibility, pp. 9-14, March 9-11, 1993.

8. N. Kuster, "Multiple Multipole Method Applied to an Exposure Safety Study", Applied Computational Electromagnetics Society Journal, Special Issue on Bioelectromagnetic Computations, Vol. 7, No. 2, pp.43-60, Winter 1992.

9. S.J. Kubina, C.W. Trueman, W. Lauber and S.R. Mishra, "Cellular Phones and Humans-A Neophyte Outlook", Symposium on Antenna Technology and Applied Electromagnetics(ANTEM), pp. 87-96, August 3-5, 1994, Ottawa.

10. O.P. Gandhi, Editor, "Biological Effects and Medical Applications of Electromagnetic Energy", Prentice-Hall, New Jersey, 1993.

11. D.M. Sullivan, O.P. Gandhi and A. Taflove, "Use of the Finite-Difference Time-Domain Method for Calculating EM Absorption in Man Models", IEEE Trans. on Biomedical Engineering, Vol. BME-35, No. 3, pp. 179-186, March, 1988.

12. M.J. Hagmann, O.P. Gandhi, J.A. D'Andrea and I. Chatterjee, "Head Resonance: Numerical Solutions and Experimental Results", IEEE Trans. on Microwave Theory and Techniques, Vol. MTT-27, No. 9, pp 809-813, September, 1979.

13. N. Kuster and Q. Balzano, "Energy Absorption Mechanism by Biological Bodies in the Near Field of Dipole Antennas Above 300 MHz", IEEE Transactions on Vehicular Technologies, Vol. VT-41, No. 1, pp. 17-23, February, 1992.

14. D. M. Sullivan, D. T. Borup, and O. P. Gandhi, "Use of Finite-Difference Time-Domain Method in Calculating EM Absorption in Human Tissues", IEEE Transactions on Biomedical Engineering, Vol. BME-34, No. 2, pp. 148-157, February, 1987.

15. D. Sullivan, "Three Dimensional Computer Simulation in Deep Regional Hyperthermia Using the Finite-Difference Time-Domain Method", IEEE Transactions on Microwave Theory and Techniques, Vol. MTT-38, No. 2, pp. 204-211, February, 1990.

16. Q. Balzano, O. Garay, and F. R. Steel, "Heating of Biological Tissue in the Induction Field of VHF Portable Radio Transmitters", IEEE Transactions on Vehicular Technology, Vol. VT-27, No. 2, pp. 51-56, May, 1978.

17. A.W. Guy and C-K Chou, "Specific Absorption Rates of Energy in Man Models Exposed to Cellular UHF Mobile-Antenna Fields", IEEE Trans. on Microwave Theory and Techniques, Vol. MTT-34, No. 6, pp. 671-680, June, 1986.

18. H. Schmidt, "On the Radiation and Loss Characteristics of Handheld-User Systems using Spherical Scanning", Conférences Journées Internationales de Nice sur Les Antennes(JINA), pp. 386-389, Nov. 8-10, 1994, Nice, France.

19. M. Hirose and M. Miyake, "A New Structure of Antenna System in a Handset Enhancing Antenna Gain by Passive Loading - The Case for 1/4 Monopole Antenna", IEICE Trans. Commun., Vol. E77, No. 7, pp. 956-960, July 1994.

20. A. Bahr and I. Wolff, "Numerical Investigation of Antenna Concepts for Hand-Held Portable Telephones Including Effects from the Human Body", 1994 International Symposium Digest, IEEE Antennas and Propagation Society, pp. 363-366, Seattle, Washington, June 19-24, 1994.

21. J. Toftgard, S.N. Hornsleth, and J. Bach Andersen, "Effects on Protable Antennas of the Presence of a Person", IEEE Trans. on Antennas and Propagation, Vol. 41, No. 6, pp. 739-746, June, 1993.

22. L. Martens, "Electromagnetic Field Calculations for Wireless Telephones", Radio Science Bulletin, No. 217, pp. 9-11, December, 1994.

23. J-C Wang and H-Y Chen, "Current and SAR Induced in a Human Head Model by the Electromagnetic Fields Irradiated from a Cellular Phone", International Symposium on Electromagnetic Environments and Consequences(EURO Electromagnetics), Book of Abstracts, Bordeaux, France, May 30-June 4, 1994.

24. M.A. Jensen and Y. Rahmat-Samii, "Performance Analysis of Antennas for Hand-Held Transceivers Using FDTD", IEEE Trans. on Antennas and Propagation, Vol. 42, No. 8, pp. 1106-1112, August, 1994.

25. M.A. Jensen and Y. Rahmat-Samii, "EM Interaction of Handset Antennas and a Human in Personal Communications", Proc. IEEE, Vol. 83, No. 1, pp. 7-17, January, 1995.

26. S. Gutschling and T. Weiland, "Detailed SAR Distribution in High-Resolution Human Head Models", Proceedings of the 11th International Zurich Symposium on Electromagnetic Compatibility, pp. 291-296, March 7-9, 1995, Zurich.

27. The MAFIA Collaboration, "User's Guide MAFIA Version 3.x", CST GmbH, Lautenschlagerstr.38, D64289, Darmstadt.

28. K. Meier, O. Egger, T. Schmid and N. Kuster, "Dosimetric Laboratory for Mobile Communications", 11th International Zurich Symposium and Technical Exhibition on Electromagnetic Compatibility, pp. 297-300, Zurich, March 7-9, 1995.

29. M. Danesh, "Absorption of RF Energy by the Human Head", Technical Report prepared for course ENGR 410, Dept. of Electrical and Computer Engineering, Concordia University, September, 1994.

30. C.M. Furse, J.-Y. Chen and O.P. Gandhi, "The Use of the Frequency-Dependent Finite-Difference Time-Domain Method for Induced Current and SAR Calculations for a Heterogeneous Model of the Human Body", IEEE Trans. on Electromagnetic Compatibility, Vol. EMC-36, No. 2, pp. 128-133, May, 1994.

31. A. Taflove and M. E. Brodwin, "Computation of the Electromagnetic Fields and Induced Temperatures within a Model of the Microwave-Irradiated Human Eye", IEEE Transactions on Microwave Theory and Techniques, Vol. MTT-23, No. 11, pp. 888-896, November, 1975.

32. G. Hartsgrove, A. Kraszewski, and A. Surowiec, "Simulated Biological Materials for Electromagnetic Radiation Absorption Studies", Bioelectromagnetics, Vol. 8, pp. 29-36, 1987.

33. M. A. Stuchly and S. S. Stuchly, "Dielectric Properties of Biological Substances - Tabulated", Microwave Power, 15(1), pp. 19-26, 1980.

34. W. T. Joines, Y. Zhang, C. Li, and R. L. Jirtle, "The Measured Electrical Properties of Normal and Malignant Human Tissues From 50 to 900 MHz", Medical Physics, Vol. 21, No. 4, pp. 547-550, April 1994.

35. D.M. Sullivan, "A Frequency-Dependent FDTD Method for Biological Applications", IEEE Trans. on Microwave Theory and Techniques, Vol. MTT-40, No. 3, pp. 532-539, March, 1992.

36. R. Luebbers, F.P. Hunsberger, K.S. Kunz, R.B. Standler and M. Schneider, "A Frequency-Dependent Finite-Difference Time-Domain Formulation for Dispersive Materials", IEEE Trans. on Electromagnetic Compatibility, Vol. 32, No. 3, pp. 222-227, August, 1990.

37. R. Luebbers, D. Steich and K. Kunz, "FDTD Calculation of Scattering from Frequency-Dependent Materials", IEEE Trans. on Antennas and Propagation, Vol. AP-41, No. 9, pp. 1249-1257, September, 1993.

38. R. Luebbers and F. Hunsberger, "FDTD for N-th Order Dispersive Media", IEEE Trans. on Antennas and Propagation, Vol. AP-40, No. 11, pp. 1297-1301, November, 1992.

39. O.P. Gandhi, B-Q Gao and J-Y Chen, "A Frequency-Dependent Finite-Difference Time-Domain Formulation for General Dispersive Media", IEEE Trans. on Microwave Theory and Techniques, Vol. MTT-41, No. 4, pp. 658-665, April, 1993.

40. W.D. Hurt, "Multiterm Debye Dispersion Relations for Permittivity of Muscle", IEEE Trans. Biomed. Eng., Vol. BME-32, pp. 60-63, January, 1985.

41. C.W. Trueman and S.J. Kubina, "The Radar Cross-Section of Aircraft, Ships and Missiles at HF Frequencies", Final Report, DREO Contract No. W7714-9-9216/01-SZ, Defence Research Establishment Ottawa, Technical Note Number TN-EMC-92-06, Electromagnetic Compatibility Laboratory, Concordia University, September 10, 1992.

42. K.S.H. Lee, L. Marin and J.P. Castillo, "Limitations of Wire-Grid Modelling of a Closed Surface", IEEE Trans. on Electromagnetic Compatibility, Vol. EMC-18, No. 3, pp. 123-129, August, 1976.

43. A. Ludwig, "Wire-Grid Modelling of Surfaces", IEEE Trans. on Antennas and Propagation, Vol. AP-35, No. 9, pp. 1045-1057, September, 1987.

44. R. Paknys, "The Near Field of a Wire-Grid Model", IEEE Trans. on Antennas and Propagation, Vol. AP-39, No. 7, pp. 994-1006, July, 1991.

45. C.W. Trueman, "Automated Radius Calculation for Wire-Grid Models," 7th Annual Review of Progress in Applied Computational Electromagnetics of the Applied Electromagnetics Computational Society, Monterey, California, March 18-22, 1991.

46. G.J. Burke, A.J. Poggio, J.C. Logan and J.W. Rockway, "NEC - Numerical Electromagnetics Code for Antennas and Scattering", 1979 IEEE International Symposium on Antennas and Propagation Digest, IEEE Publication No. 79CH1456-3AP, Seattle, Washington, June, 1979.

47. G.J. Burke and A.J. Poggio, "Numerical Electromagnetics Code - Method of Moments, Part I: Program Description-Theory", Technical Document 116, Naval Electronic Systems Command(ELEX 3041), July, 1977.

48. G.J. Burke and A.J. Poggio, "Numerical Electromagnetics Code - Method of Moments, Part III: User's Guide," Technical Document 116, Naval Electronic Systems Command(ELEX 3041), July, 1977.

49. C.W. Trueman and S.J. Kubina, "Verifying Wire-Grid Model Integrity with Program CHECK," Applied Computational Electromagnetics Society Journal, Vol. 5, No. 2, Winter, 1990, pp. 17-42.

50. C.A. Balanis, "Advanced Engineering Electromagnetics", Wiley, New York, 1989.

51. R.L. Burden, J.D. Faires and A.C. Reynolds, "Numerical Analysis", Prindle, Weber and Schmidt, Boston, 1978.

52. R.J. Luebbers, K.S. Kunz, M. Schneider and F. Hunsberger, "A Finite-Difference Time-Domain Near-Zone to Far-Zone Transformation", IEEE Trans. on Antennas and Propagation, Vol. AP-39, No. 4, April, 1991.

53. Z.P. Liao, H.L. Wong, B.P. Yang and Y.F. Yuan, "A Transmitting Boundary for Transient Wave Analysis", Scientia Sinica, Vol. XXVII, No. 10, p. 1065, October, 1984.

54. M. Moghaddam and W. Chew, "Stabilizing Liao's Absorbing Boundary Conditions Using Single-Precision Arithmetic", Proceedings of the IEEE AP-S Symposium, Vol. 1, pp. 430-433, London, Ontario, June, 1991.

55. D. Steich, R. Luebbers and K. Kunz, "Absorbing Boundary Condition Convergence Comparisons", IEEE International Symposium on Antennas and Propagation, Ann Arbor, Michigan, June 28-July 2, 1993.

56. J.G. Maloney and G.S. Smith, "A Comparison of Methods for Modeling Electrically Thin Dielectric and Conducting Sheets in the Finite-Difference Time-Domain (FDTD) Method", IEEE Trans. on Antennas and Propagation, Vol. 41, May, 1993.

57. C.W. Trueman, S.R. Mishra, C.L. Larose, and R.K. Mongia, "Resonant Frequencies and Q Factors of Dielectric Parallelepipeds by Measurement and by FDTD", to be published in the IEEE Trans. on Instrumentation.

58. A. Taflove and K.A. Umashankar, "The Finite-Difference Time-Domain Method for Numerical Modeling of Electromagnetic Wave Interactions", Electromagnetics, Vol. 10., Nos. 1-2, January-June, 1991.

59. R. Holland, L. Simpson and K.S. Kunz, "Finite-Difference Analysis of EMP Coupling to Lossy Dielectric Structures", IEEE Trans. on Electromagnetic Compatibility, Vol. EMC-22, No. 3, August, 1980.

60. G. Mur, "Absorbing Boundary Condition for the Finite-Difference Approximation of the Time-Domain Electromagnetic Field Equations", IEEE Trans. on Electromagnetic Compatibility, Vol. EMC-23, No. 4, pp. 377-382, November 1981.

61. C.J. Railton and E.M. Daniel, "A Comparison of the Properites of Radiating Boundary Conditions in the FDTD Method for Antenna and Waveguide Analysis", Program and Abstracts, 1993 URSI Radio Science Meeting, p. 63, Ann Arbor, Michigan, June 28-July 2, 1993.

62. K.K. Mei and J. Fang, "Superabsorption-A Method to Improve Absorbing Boundary Conditions", IEEE Trans. on Antennas and Propagation, Vol. 40, No. 9, pp. 1001-1010, September, 1992.

63. J.P. Berenger, "A Perfectly Matched Layer for the Absorption of Electromagnetic Waves", Jour. Comp. Phys., Vol. 114, pp. 184-200, August, 1994.

64. D.S. Katz, E.T. Thiele and A. Taflove, "Validation and Extension of the Berenger Absorbing Boundary Condition for FDTD Meshes", 1994 Abstracts and Program, URSI Radio Science Meeting, p. 167, Seattle, Washington, June 19-24, 1994.

65. R.F. Harrington, "Time Harmonic Electromagetic Fields", McGraw-Hill, 1961.

66. K. Umashankar, A. Taflove, and B. Beker, "Calculation and Experimental Validation of Induced Currents on Coupled Wires in an Arbitrary Shaped Cavity", IEEE Trans. on Antennas and Propagation, Vol. AP-35, No. 11, pp. 1248-1257, Nov. 1987.

67. J.G. Maloney, G.S. Smith, and W.R. Scott, "Accurate Computation of the Radiation from Simple Antennas Using the Finite-Difference Time-Domain Method", IEEE Trans. on Antennas and Propagation, Vol. 38, No. 7, pp. 1059-1068, July 1990.

68. R. Luebbers, L. Chen, T. Uno, and S. Adachi, "FDTD Calculation of Radiation Patterns, Impedance and Gain for a Monopole Antenna on a Conducting Box", IEEE Trans. on Antennas and Propagation, Vol. 40, No. 12, pp. 1577-1583, Dec., 1992.

69. C.W. Trueman, S.J. Kubina and B. Messier, "Creating FDTD Models of Aircraft with GWTOFDTD", 10th Annual Review of Progress of the Applied Computational Electromagnetics Socitey, pp. 53-60, Monterey, California, March 21-26, 1994.

70. S.R. Mishra, C.L. Larose and C.W. Trueman, "Precision Radar Cross-Section Measurements for Computer Code Validation", IEEE Trans. on Instrumentation and Measurement, Vol. 42, No. 2, pp. 179-185 , April, 1993.

71. T. Maeda, S. Sekine, and S. Obayashi, "High Speed Radiation Characteristics Measurement Equipment over the Solid Angle of a Sphere to Evaluate Antennas Attached to an 800 MHz Cellular Telephone", 1993 IEEE Antennas and Propagation Symposium Digest, pp. 1828-1831, Ann Arbor, Michigan, June 28-July 3, 1993.

72. C.W. Trueman, S.R. Mishra, C.L. Larose, and R.K. Mongia, "Computation and Measurement of the Resonant Frequencies and Q Factors of High-Permittivity Dielectric Resonators", Symposium on Antenna Technology and Applied Electromagnetics(ANTEM), pp. 395-402, August 3-5, 1994, Ottawa.

73. M.L. Van Blaricum and R. Mittra, "A Technique for Extracting the Poles and Residues of a System Directly from its Transient Response", IEEE Trans. on Antennas and Propagation, Vol. AP-23, No. 6, pp. 777-781, Nov. 1975.

BIBLIOGRAPHY

Fields in Man Due to Portable Radios

Q. Balzano, O. Garay, and R. F. Steel, "Energy Deposition in Biological Tissue Near Portable Radio Transmitters at VHF and UHF", Conference Record of the 27th Annual Conference IEEE Vehicular Technology Group, Orlando, Florida, pp. 25-29, March 16-18, 1977.

D. P. Nyquist, K-M. Chen, and B. S. Guru, "Coupling Between Small Thin-Wire Antennas and a Biological Body", IEEE Transactions on Antennas and Propagation, Vol. AP-25, No. 6, pp. 863-866, November 1977.

Q. Balzano, O. Garay, and F. R. Steel, "Energy Deposition in Simulated Human Operators of 800 MHz Portable Transmitters", IEEE Transactions on Vehicular Technology, Vol. VT-27, No. 4, pp. 174-181, November 1978.

R. J. Spiegel, "The Thermal Response of a Human in the Near-Zone of a Resonant Thin-Wire Antenna", IEEE Transactions on Microwave Theory and Techniques, Vol. MTT-30, No. 2, pp. 177- 185, 1982.

I. Chatterjee, Y-G. Gu, and O. P. Gandhi, "Quantification of Electromagnetics Absorption in Humans from Body-Mounted Communication Transceivers", IEEE Transactions on Vehicular Technology, Vol. VT-34, No. 2, pp. 55-61, May 1985.

M. A. Stuchly, R. J. Spiegel, S. S. Stuchly, and A. Kraszewski, "Exposure of Man in the Near-Field of a Resonant Dipole: Comparison Between Theory and Measurements", IEEE Transactions on Microwave Theory and Techniques, Vol. MTT-34, No. 1, pp. 26-31, January 1986.

R. F. Cleveland and T. W. Athey, "Specific Absorption Rate (SAR) in Models of the Human Head Exposed to Hand-Held UHF Portable Radios", Bioelectromagnetics, Vol. 10, No. 2, pp. 173-186, 1989.

N. Kuster and Q. Balzano, "Energy Absorption Mechanism by Biological Bodies in the Near Field of Dipole Antennas Above 300 MHz", IEEE Transactions on Vehicular Technologies, Vol. VT-41, No. 1, pp. 17-23, February 1992.

H-D Brüns, H. Singer, and T. Mader, "Field Distributions of a Hand-Held Transmitter due to the Influence of the Human Body", Electromagnetic Compatibility 1993, 10th International Zurich Symposium and Technical Exhibition on Electromagnetic Compatibility, March 9-11, pp. 10-14, 1993.

M. Fischetti, "The Cellular Phone Scare", Special Report/Communications, IEEE Spectrum, pp. 43-47, June, 1993.

SAR Computations in Man

C.C. Johnson and A. W. Guy, "Nonionizing Electromagnetic Wave Effects in Biological Materials and Systems", Proceedings of the IEEE, Vol. 60, No. 6, pp. 692-718, June 1972.

D. E. Livesay and K-M Chen, "Electromagnetic Fields Induced Inside Arbitrarily Shaped Biological Bodies", IEEE Transactions on Microwave Theory and Techniques, Vol. MTT-22, No.12, pp. 1273- 1280, December 1974.

K-M Chen, and B. S. Guru, "Internal EM Field and Absorbed Power Density in Human Torsos Induced by 1-500 MHz EM Waves", IEEE Transactions on Microwave Theory and Techniques, Vol. MTT-25, No. 9, pp. 746-755, September 1977.

M. J. Hagmann, O. P. Gandhi, and C. H. Durney, "Numerical Calculation of Electromagnetic Energy Deposition for a Realistic Model of Man", IEEE Transactions on Microwave Theory and Techniques, Vol. MTT-27, No. 9, pp. 804-813, September 1979.

J. F. DeFord, O. P. Gandhi, and M. J. Hagmann, "Moment-Method Solutions and SAR Calculations for Inhomogeneous Models of Man with Large Number of Cells", IEEE Transactions on Microwave Theory and Techniques, Vol. MTT-31, No. 10, pp. 848-851, October 1983.

D. T. Borup and O. P. Gandhi, "Fast-Fourier-Transform Method for Calculation of SAR Distributions in Finely Discretized Inhomogeneous Models of Biological Bodies", IEEE Transactions on Microwave Theory and Techniques, Vol. 32, No. 4, pp. 355-360, April 1984.

A. R. Guy, C-K Chou, and B. Neuhaus, "Average SAR and SAR Distributions in Man Exposed to 450 MHz Radiofrequency Radiation", IEEE Transactions on Microwave Theory and Techniques, Vol. MTT-32, No. 8, pp. 752-763, August 1984.

R. J. Spiegel, "A Review of Numerical Models for Predicting the Energy Deposition and Resultant Thermal Response of Humans Exposed to Electromagnetic Fields", IEEE Transactions on Microwave Theory and Techniques, Vol. MTT-32, No. 8, pp. 730-746, August 1984.

J. F. Deford, and O. P. Gandhi, "An Impedance Method to Calculate Currents Induced in Biological Bodies Exposed to Quasi-Static Electromagnetic Fields", IEEE Transactions on Electromagnetic Compatibility, Vol. EMC-27, No. 3, pp. 168-173, August 1985.

D. T. Borup, D. M. Sullivan, and O. P. Gandhi, "Comparison of the FFT Conjugate Gradient Method and the Finite-Difference Time-Domain Method for the 2-D Absorption Problem", IEEE Transactions on Microwave Theory and Techniques, Vol. MTT-35, No. 4, pp. 383-395, April 1987.

M. F. Iskander, S. C. Olson, and J. F. McCalmont, "Near-Field Absorption Characteristics of Biological Models in the Resonance Frequency Range", IEEE Transactions on Microwave Theory and Techniques, Vol. MTT-35, No. 8, pp. 776-780, August 1987.

M. A. Stuchly, A. Kraszewski, S. S. Stuchly, G. W. Hartsgrove, and R. J. Spiegel, "RF Energy Deposition in a Heterogeneous Model of Man: Near-Field Exposures", IEEE Transactions on Biomedical Engineering, Vol. BME-34, No. 12, pp. 944-950, December 1987.

N. Orcutt and O. P. Gandhi, "A 3-D Impedance Method to Calculate Power Deposition in Biological Bodies Subjected to Time Varying Magnetic Fields", IEEE Transactions on Biomedical Engineering, Vol. 35, No. 8, pp. 577-583, August 1988.

J-Y. Chen and O. P. Gandhi, "Electromagnetic Deposition in an Anatomically Based Model of Man for Leakage Fields of a Parallel-Plate Dielectric Heater", IEEE Transactions on Microwave Theory and Techniques, Vol. MTT-37, No. 1, pp. 174-180, January 1989.

J-Y. Chen and O. P. Gandhi, "RF Currents Induced in an Anatomically-Based Model of a Human for Plane-Wave Exposures (20-100 MHz)", Health Physics, Vol. 57, No. 1, pp. 89-98, July 1989.

F. J. C. Meyer and D. B. Davidson, "A 2D Finite Element/Boundary Element Method for Solving Electromagnetic Fields in and Around a Human Cross-Section Near a Line Source", IEEE/SAIEE AP/MTTS-93 Proceedings, pp. 12-1 12-10, August 5 1993.

Hyperthermia

J. W. Strobehn, and R. B. Roemer, "A Survey of Computer Simulations of Hyperthermia Treatments", IEEE Transactions on Biomedical Engineering, Vol. BME-31, No. 1, pp. 136-149, January 1984.

K. D. Paulsen, J. W. Strohbehn, and D. R. Lynch, "Theoretical Electrical Field Distributions Produced by Three Types of Regional Hyperthermia Devices in a Three-Dimensional Homogeneous Model of Man", IEEE Transactions on Biomedical Engineering, Vol. 35, No. 1, pp. 36-45, January 1988.

G. P. Rine, T. V. Samulski, W. Grant, and C. A. Wallen, "Comparison of Two-Dimensional Numerical Approximation and Measurement of SAR in a Muscle Equivalent Phantom Exposed to a 915 MHz Slab-loaded Waveguide", Int. J. Hyperthermia, pp. 213-225, 1990.

V. Sathiaseelan, A. Taflove, M. J. Piket-May, C. Reuter, and B. B. Mittal, "Application of Numerical Modeling Techniques in Electromagnetic Hyperthermia", Applied Computational Electromagnetic Society Journal, Special Issue on Bioelectromagnetic Computations, Vol. 7, No. 2, pp. 61-71, Winter 1992.

J. J. Mallorqui, A. Broquetas, L. Jofre, and A. Cardama, "Non-Invasive Active Thermometry with a Microwave Tomographic Scanner in Hyperthermia Treatments", Applied Computational Electromagnetic Society Journal, Special Issue on Bioelectromagnetic Computations, Vol. 7, No. 2, pp.121-127, Winter 1992.

FDTD Modelling of Antennas and Portable Radios

K. R. Umashankar, A. Taflove, and B. Becker, "Calculation and Experimental Validation of Induced Currents on Coupled Wires in an Arbitrary Shaped Cavity", IEEE Transactions on Antennas and Propagation, Vol. AP-35, No. 11, pp. 1248-1257, November 1987.

L. Chen, T. Uno, S. Adachi, R. J. Luebbers, and K. S. Kunz, "FDTD Method Analysis of a Monopole Antenna Mounted on a Conducting Rectangular Box", IEEE International Symposium on Antennas and Propagation, pp. 1670-1673, June, 1992.

R. Luebbers and K. Kunz, "Finite Difference Time Domain Calculations of Antenna Mutual Coupling", IEEE Transactions on Electromagnetic Compatibility, Vol. 34, No. 3, pp. 357-359, August 1992.

R. J. Luebbers and J. Beggs, "FDTD Calculation of Wide-Band Antenna Gain and Efficiency", IEEE Transactions on Antennas and Propagation, Vol. 40, No. 11, pp. 1403-1407, November 1992.

R. Luebbers, J. Beggs, and K. Chamberlin, "Finite Difference Time-Domain Calculation of Transients in Antennas with Nonlinear Loads", IEEE Transactions on Antennas and Propagation, Vol. 41, No. 5, pp. 566-573, May 1993.

L. Chen, T. Uno, S. Adachi, and R. Luebbers, "FDTD Analysis of a Monopole Antenna Mounted on a Conducting Box Covered with a Layer of Dielectric", IEICE Trans. Commun., Vol. E76-B, No. 12, pp. 1583-1586, December 1993.

FDTD Modelling of Curved Surfaces

C. M. Furse, S. P. Mathur, and O. P. Gandhi, "Improvements to the Finite-Difference Time-Domain Method for Calculating the Radar Cross Section of a Perferctly Conducting Target", IEEE Transactions on Microwave Theory and Techniques, Vol. 38, No. 7, pp. 919-927, July 1990.

T. G. Jurgens, K. Umashankar, and T. Moore, "Finite-Difference Time-Domain Modeling of Curved Surfaces", IEEE Transactions on Antennas and Propagation, Vol. 40, No. 4, pp. 357-366, April 1992.

P. H. Aoyagi, J-F Lee, R. Mittra, "A Hybrid Yee Algorithm/Scalar-Wave Equation Approach", IEEE Transactions on Microwave Theory and Techniques, Vol. 41, No. 9, pp. 1593-1600, September 1993.

R. Holland, "Pitfalls of Staircase Meshing", IEEE Transactions on Electromagnetic Compatibility, Vol. 35, No. 4, pp. 434-439, November 1993.

FDTD Modelling of Biological Materials

R. W. M. Lau, R. J. Sheppard, "The Modelling of Biological Systems in Three Dimensions using the Time Domain Finite-Difference Method: I. The Implementation of the Model", Phys. Med. Biol., Vol. 31, No. 11, pp. 1247-1256, 1986.

R. W. M. Lau, R. J. Sheppard, G. Howard, and N. M. Bleehen, "The Modelling of Biological Systems in Three Dimensions using the Time Domain Finite-Difference Method: II. The Application and Experimental Evaluation of the Method in Hyperthermia Applicator Design", Phys. Med. Biol., Vol. 31, No. 11, pp. 1257-1266, 1986.

P. J. Dimbylow and O. P. Gandhi, "Finite-Difference Time-Domain Calculations of SAR on a Realistic Heterogeneous Model of the Head for Plane-Wave Exposure from 600 MHz to 3 GHz", Phys. Med. Biol., Vol. 36, No. 8, pp. 1075-1089, 1991.

O. P. Gandhi, J. Y. Chen, and C. M. Furse, "A Frequency-Dependent FDTD Method for Induced-Current Calculations for a Heterogeneous Model of the Human Body", IEEE MTT-S International Microwave Symposium Digest, Albuquerque, New Mexico, Vol. III, pp. 1283-1286, June 1-5, 1992.

International Non-Ionizing Radiation Committee of the International Radiation Protection Association, "Guidelines on Limits of Exposure to Radiofrequency Electromagnetic Fields in the Frequency Range from 100 kHz to 300 GHz", Health Physics, Vol. 54, No. 1, pp. 115-123, January 1988.

"IEEE Standard for Safety Levels with Respect to Human Exposure to Radio Frequency Electromagnetic Fields, 3 kHz to 300 GHz", IEEE C95.1-1991, Piscataway, New Jersey: IEEE, 1991.

APPENDIX 1

ANTEM '94 Symposium on Antenna Technology and Applied Electromagnetics, August 2-5, 1994 Ottawa, Canada

CELLULAR PHONES AND HUMANS- A NEOPHYTE OUTLOOK

S.J. Kubina
C.W. Trueman
EMC Laboratory
Concordia University
Montreal, Quebec

W. Lauber
Communications
Research Centre
Ottawa, Ontario

S.R. Mishra
David Florida Laboratory
Canadian Space Agency
Ottawa, Ontario

Abstract-A cellular phone is a portable radio that radiates 0.6 watt from an antenna located very close to the operator's head. Concern has been expressed as to whether a cellular phone is capable of inducing damaging field strengths inside the user's head. This paper reviews the application of electromagnetic modelling techniques using the finite-difference time-domain(FDTD) method to this problem. The construction of an FDTD model of the cellular phone and of the head is discussed. The relative permittivity and conductivity of biological tissue varies with frequency, and this paper reviews modifications of the FDTD method to handle such dispersive media. Some specific applications of measurement methods and of the FDTD method to the calculation of the amount of electromagnetic power delivered to the body are discussed.

Introduction

Recently concern has been expressed by the general public and the news media over whether cellular telephones pose a health risk[1]. Cellular phones operate between 824 and 850 MHz, and radiate 0.6 watt of power. Cellular phone sets meet the existing standard for portable radio sets[2], which limit the power that the radio can cause the body to absorb. Tissue damage largely depends on heating due to power delivered by the electromagnetic field[1], given by the "specific absorption rate"(SAR) in watts per kilogram. Standards limit the power absorption to 80 mW/kg average SAR over the entire body, and 1.6 W/kg peak SAR to any 1 gram of tissue for 30 minutes or more. If a device radiates less than 0.74 W at the frequency of cellular phones, it is considered absolutely safe because it cannot deliver the limiting power levels outlined above.

This paper discusses computational modelling of the head in three dimensions, for the purpose of determining the local SAR levels throughout its volume when a cellular phone is in use. The emphasis is on the "finite-difference time-domain"(FDTD) method, although a variety of other techniques are also feasible[3,4]. We will review the basics of FDTD and how an FDTD model of a cellular phone and a head is constructed. Techniques for modelling the dispersive nature of biological tissue will be discussed, and then we will touch on some results that have been published that are pertinent to the assessment of cellular phone hazards.

The Finite-Difference Time-Domain Method

In Yee's finite-difference time-domain method[5], space is subdivided into cells of size Δx by Δy by Δz and time into steps of size Δt. The partial derivatives in Maxwell's curl equations are replaced by central-difference formulas involving the components of the electric field along the edges of the cells, and the components of the magnetic field normal to the faces of the cells. Initially all the fields are zero. The time function for the generator voltage is known and is used to obtain a known electric field applied at the base of the antenna. Time is advanced in steps of Δt, and

the permittivity and conductivity of each cell should be used[9,10]. This is included as a volume-averaged permittivity in Ref. [11], accounting for the fraction of a cell occupied by free-space compared to that composed of, for example, muscle.

Antenna Source Voltage Functions

The source voltage is applied as an electric field across the gap at the base of the antenna. The source time function must not contain any frequency components above the bandwidth for the FDTD cell space. If the source voltage time function is to be a sine wave, then it must turn on gradually, as an abrupt start would violate the grid's bandwidth restriction. Then the FDTD algorithm must be run for a sufficient number of time steps that the turn-on transients die away, and sinusoidal steady-state to be reached. For high-permittivity resonant structures, a great many time steps may be required[9], as very long time constants are involved. Under certain circumstances, resonance is encountered in electromagnetic models of human beings[12]. When steady-state is reached each field component in the grid will be sinusoidal, and the amplitude and phase can be determined from the time history for the last period of the input function.

To obtain the frequency response over a wide bandwidth, the FDTD code is often run with a sine wave input many times at individual frequencies. Alternately, we can take advantage of FDTD's solution of Maxwell's Equations in the time domain to obtain information over a wide bandwidth in a single run. The source voltage can be a Gaussian pulse or other time-limited function whose spectral content is restricted to bandwidth for which the FDTD grid is valid. Then the FDTD algorithm finds the time response of each field component in the cell space due to the source voltage pulse. Again, the FDTD algorithm must be run for a sufficient number of time steps to trace the transient response of each field component to zero value. The Fourier transform is used to find the response as a function of frequency. Yee's FDTD assumes that neither the conductivity nor the permittivity vary with frequency, and must be modified to model biological tissues over wide bandwidths, as discussed below.

Computing the Radiated Fields

The FDTD method obtains the time functions giving the value of the electric fields on each of the cell edges, and the corresponding magnetic fields at the centers of the cell faces, at each time step. These near field time functions are used to find the far fields or radiated fields of the cellular phone operating near the head, with a near-zone to far-zone transformation[13]. Thus at each time step, the far field in any direction can be found from the values of the near fields on a closed integration surface, usually taken to be a few cells inside the absorbing boundary of the cell space.

Electrical Parameters of Biological Materials

To construct an electromagnetic model of a human being, detailed anatomical information is required. Ref. [14] gives cross-sections of the head and body at approximately 2.5 cm spacing, obtained by dissection. By superimposing the grid of FDTD cells on each cross-section, it is possible to assign a tissue type to each cell. Ref. [15] constructed a cell model of a person in this way, assigning one of 14 different material types to each cell. For computation the cell size was 1.31 cm, with a total of about 145,000 cells in the model. At each frequency the relative permittivity of each of the tissue types are found from the literature[3,16-21] and are listed in Tables 1 and 2 for tissues relevant to modelling the head. Note that the permittivity of some types of tissue is quite high, and that both permittivity and conductivity change very significantly in the frequency range covered by the tables.

Table 1
The permittivity of biological materials at various frequencies.

Tissue	Ref	Frequency (MHz)									
		10	27.12	100	350	400	500	750	900	1000	1500
Brain,	3	163-352		57-90						37-55	
nerve	3		155	52	60						
	16							49			46
	17			63		50.3			41.2		
	20				74						
Bone,	3	37		23							
Fat	3		29	7.5	5.7						
	16							5.6			5.6
	17			12.2		9.2			7.3		
	20				5.7						
Muscle	3	162-204		64-90						57-59	
	3		106	74	53						
	16							52			49
	17			70.5		62.5			54.7		
	18			71-76			52-54			49-52	
	19			63		52.6	52.4		52		
	21								50.5		
	20				54						
Skin	3		106	25	17.6						
	16							52			49
	18			57			46.5			43-46	
	20					17.4					
Eye	3		155	85	80						
	16							80			80
Blood	3		102	74	65						
	18			69-81			67-70			60.5	
	20				65						

Modelling Dispersive Materials with FDTD

Tables 1 and 2 illustrate that tissue is quite "dispersive", that is, the permittivity and conductivity of tissue varies quite rapidly with frequency. But in Yee's FDTD the relative permittivity ε_r and conductivity σ cannot change with frequency. To obtain the fields inside a model of a head or body over a wide frequency band, the FDTD code must be run with a sine wave excitation at many individual frequencies, with the appropriate permittivity and conductivity at each frequency. But we lose the inherent advantage of a time domain method, in which the response to a pulse input function obtains wideband information in a single run. To regain this capability, the FDTD algorithm must be modified to directly incorporate the dispersive nature of biological materials.

Table 2
The conductivity of biological materials at various frequencies.

Tissue	Ref	Frequency (MHz)									
		10	27.12	100	350	400	500	750	900	1000	1500
Brain,	3	0.21-0.63		0.48-0.95						0.81-1.2	
nerve	3		0.45	0.53	0.65						
	16							1.2			1.4
	17			4.7		7.5			12.2		
	20				0.62						
Bone,	3	0.024		0.057							
Fat	3		0.04	0.07	0.072						
	16							0.09			0.12
	17			0.215		0.88			1.4		
	20				0.07						
Muscle	3	0.69-0.96		0.75-1.05						1.38-1.45	
	3		0.74	1.0	1.33						
	16							1.54			1.77
	17			6.8		9			13.8		
	19			0.62		0.68	0.72		0.92		
	21								1.2		
	20				1.3						
Skin	3		0.74	0.55	0.44						
	16							1.54			1.77
	17				0.42						
Eye	3		0.45	1.9	1.9						
	16							1.9			1.9
Blood	3		0.28	1.1	1.2						
	20				1.22						

The simplest model of materials with frequency-dependent permittivity and conductivity is given by the Debye equation[3]. The frequency dependence of the complex relative permittivity is described with a single relaxation time, according to

$$\varepsilon_r(\omega) = \varepsilon_{r\infty} + \frac{\varepsilon_{rs} - \varepsilon_{r\infty}}{1 + j\omega\tau}$$

where ω is the operating frequency in rad/sec, $\varepsilon_{r\infty}$ is the relative permittivity at high frequencies, ε_{rs} is the "static" relative permittivity at zero frequency, and τ is the relaxation time. Ref. [22] describes a frequency-dependent finite-difference time-domain or $(FD)^2TD$ method. The relation between the electric flux density, the frequency-dependent permittivity and the electric field in the frequency domain

$$D(\omega) = \varepsilon_r(\omega)\varepsilon_0 E(\omega)$$

becomes a convolution in the time domain. Ref. [22] modifies the Yee FDTD algorithm to compute the convolution as a running sum, which must be maintained for each location in the cell space. Water, which has a slowly-varying permittivity in the range 0 to 80 GHz, is modelled with $\varepsilon_{rs} = 81$, $\varepsilon_{r\infty} = 1.8$, and relaxation time $\tau = 9.4$ picoseconds with good agreement with the exact solution in a one-dimensional geometry.

Ref. [23] applies the $(FD)^2TD$ method to model muscle from 40 to 433 MHz. The relative permittivity of muscle varies with frequency much more rapidly than that of water. At 40.68 MHz, it is 97.3, declining to 53 at 433 MHz, while the conductivity rises from 0.693 S/m at 40.68 MHz to 1.43 at 433 MHz[24]. Ref. [23] choses $\varepsilon_{r\infty} = 15$, $\varepsilon_{rs} = 120$, $\sigma = 0.64$ S/m and relaxation time $\tau = 6.67$ nanoseconds to obtain a reasonable representation of the frequency dependence of the relative permittivity and conductivity of muscle from 40 to 400 MHz. The paper models a two-dimensional cylindrical structure with $(FD)^2TD$ and compares the result to the exact solution in the form of a Bessel function series evaluated at individual frequencies, with excellent agreement.

Ref. [25] extends the $(FD)^2TD$ method to handle multiple second-order Lorentz poles. The permittivity is represented as

$$\varepsilon_r = \varepsilon_{r\infty} + (\varepsilon_{rs} - \varepsilon_{r\infty}) \sum_{p=1}^{P} \frac{G_p \omega_p^2}{\omega_p^2 + 2j\omega\delta_p - \omega^2}$$

where $\sum_{p=1}^{P} G_p = 1$, P is the number of poles, and ω_p and δ_p are the resonant frequency and damping coefficient, respectively, of the p-th pole. The method is an extension of the convolution technique used in Ref. [22] for a simple Debye pole. Ref. [26] extends the method to include multiple simple poles of the Debye type as well as complex poles.

Ref. [11] offers an alternate formulation for $(FD)^2TD$ based on the solution of a differential equation relationship between the electric flux density D and the electric field E at each time step. The method is applied to model material properties in terms of two simple Debye poles, that is, using two relaxation times. Ref. [27] gives the permittivity of muscle in terms of five relaxation times, valid over a wide frequency range. In Ref. [26] the representation is simplified to use only two time constants, to obtain a reasonable representation of frequency variation of muscle's permittivity from 20 MHz to 20 GHz. The $(FD)^2TD$ method is applied to the parts of a whole-body model composed of muscle to calculate induced currents in the body at 40, 150 and 350 MHz.

Ref. [28] provides estimates of the parameters required to represent 12 types of biological tissue with the two relaxation time model, valid up to 3 GHz. Each tissue has its individual values of the two "static" permittivities, and the "high frequency" permittivity required for the dispersion model. But all the tissue types are modelled as having the same relaxation times τ_1 and τ_2. This permits the actual permittivity of each cell of the FDTD model to be chosen by volume averaging according to the fraction of the cell occupied by each type of tissue. This improves the resolution of models having a somewhat coarse cell size. Then a single run of the $(FD)^2TD$ code obtains the field strengths in each cell up to 915 MHz, which would require many runs of the Yee FDTD code with a single-frequency sine wave excitation.

SAR Studies using the FDTD Method

It is thought that the principal cause for concern for exposure to electromagnetic fields such as those radiated by cellular phones is due to the heating of tissue. The "specific absorption rate"(SAR) gives the rate at which energy is supplied to tissue, or the power supplied per unit mass, and is given for one cell of an FDTD model by

$$SAR = \frac{\sigma}{2\rho}(E_x^2 + E_y^2 + E_z^2)$$

where σ is the conductivity, E_x, E_y, and E_z are amplitudes of the x, y, and z components of the sinusoidally-varying electric fields, and ρ is the mass density of the tissue in the cell. Most studies seek to evaluate the SAR for comparison with safety standards.

Before computational methods that are able to handle dielectric materials became available, measurements were the only means to determine the radiation patterns of portable radios operated near a human head or body. Indeed measurements will continue to provide a quick and accurate means of determining whether cellular phone antenna provides adequate coverage. A typical measurement uses a "head phantom" filled with a material designed to simulate the average electrical properties of biological tissue[29]. Also, embedded field strength probes or temperature probes in a head phantom may provide a useful means of confirming the accuracy of field strength or SAR values obtained by computation. Ref. [30] used a whole-body phantom to measure the power absorbed by a person near a cellular phone antenna on a car. The car phone system is designed to radiate between 3 and 10 watts. The study showed that, for a child standing 15 cm from the antenna, which is very close, the antenna would have to radiate 35 watts to exceed the safety standard.

Ref. [29] considered the energy deposited in the head by a portable radio at 840 MHz, with a whip antenna and a sleeve dipole. The radio differs from a cellular phone in that it is normally held in front of the face with the antenna extending vertically near the operator's eyes and forehead. In Ref. [20] the temperature rise in a head phantom was measured. A "hot spot" was found near the antenna, but the associated temperature rise was so small that there is no potential for tissue damage.

Ref. [20] studied the energy absorbed by a human in the field of a distant antenna, represented by an incident plane wave. Ref. [20] used an FDTD model of the torso having 1.27 cm cells, derived from the cross-sectional anatomy of Ref. [14]. The material properties of each cell were assigned depending on the volume fraction of the cell occupied by each tissue type. The torso model had 16628 cells, and was centered in a space of 36 by 24 by 44 cells for a total of 38016 cells. A sinusoidal excitation was used at both 100 MHz and 433 MHz, with time stepping for three cycles to reach steady state. The SAR was determined for cross-sections of the torso. The study was extended in Ref. [15]. The torso model was extended to become a complete model of a "standard man" 175 cm tall, weighing 70 kg. At 100 MHz, 2.62 cm cells were used with an FDTD space size of 23x12x68 or 18768 cells. At 350 MHz, 1.31 cm cells were used for better resolution, and the overall space used 45x24x135 or 145800 cells. As before, a sinusoidal source was used, and time-stepping was carried out for three cycles to reach "steady state". It was found that at 100 MHz there is a considerable difference between the SAR in the body isolated in space compared to the body standing on a ground plane, but at 350 MHz, there is not much difference.

Ref. [21] studied the changes in the performance of a handheld telephone set at 900 MHz and 1900 MHz due to the presence of the operator's hand and head. The telephone set was modelled as a perfectly-conducting box with a quarter-wave monopole on top. The hand and the head were represented as pure muscle tissue. The head was modelled as a sphere of radius 9 cm; the hand was a block 10 cm wide and 2 cm thick wrapped around the lower part of the telephone set. The excitation was a Gaussian pulse modulated with a cosine wave, permitting the impedance and other parameters to be found over a small bandwidth around the cosine's frequency. The total number of cells in the model was 141,680; time stepping was carried out for 1500 steps. The input impedance of the antenna and the azimuth radiation pattern of the FDTD model were compared with the measured impedance and pattern of a real person holding the telephone set. The changes in the impedance and azimuth pattern of the telephone set due to the operator that were expected from the FDTD model were found in the measurement. However, the model was too simple to predict these quantities precisely.

FDTD is often used to study the problem of hyperthermia, in which an applicator is applied to the body to deliver electromagnetic energy to a tumor, which is then destroyed by electromagnetic heating. Ref. [31] studied the use of dipoles to apply energy to tumors at 70 and 95 MHz. In this application, CAT scans taken of an individual patient's body were used to construct an FDTD model with 34751 cells. The FDTD model predicts the internal SAR values when energy is applied with a standard array of dipoles, excited with a sinusoid at a single frequency. The objective is to design the excitation of the array to achieve high SAR in the tumor, but low absorption rates elsewhere to prevent damage to healthy tissue.

Ref. [28] used $(FD)^2TD$ to study the SARs in the whole body when exposed to a plane wave. As discussed above, the electrical parameters of each tissue type were described with a dispersion model using two relaxation times, valid to 3 GHz. The method was used to find the SAR averaged over layers of the body at frequencies from 20 to 915 MHz, due to plane wave exposure. $(FD)^2TD$ allows the computation of the fields in the body as a function of time due to a narrow pulse, which contains energy over a wide range of frequencies. Ref. [28] graphs the net current induced at various cross-sections of the body as a function of time, including the dispersive effects of the tissues.

Conclusion

Because of the concerns of the general public that cellular phone operation might have an associated health risk, there is tremendous interest and activity in predicting field strengths and specific absorption rates inside the head. But at present there is little published work dealing specifically with the SAR in the head at the frequency of cellular telephones. Existing studies of hazards associated with radio-frequency fields were used to develop the standard maximum field strengths and power levels[2] such that, to the best of available knowledge, cellular telephones pose no health risk. As discussed in this paper, the analytic and numerical tools for detailed accurate computation of field strength levels inside the head have greatly improved in the past five years. We can expect a landslide of information as these methods are applied to assess the SAR levels to be expected in the head when using a cellular phone.

Acknowledgement

Dr. M.A. Stuchly's assistance in supplying reference material is gratefully acknowledged.

References

1. M. Fischetti, "The Cellular Phone Scare", Special Report/Communications, IEEE Spectrum, pp. 43-47, June, 1993.
2. "IEEE Standard for Safety Levels with Respect to Human Exposure to Radio Frequency Electromagnetic Fields, 3 kHz to 3 GHz", IEEE C95.1-1991, IEEE, Piscataway, New Jersey.
3. O.P. Gandhi, Editor, "Biological Effects and Medical Applications of Electromagnetic Energy", Prentice-Hall, New Jersey, 1993.
4. N. Kuster and Q. Balzano, "Energy Absorption Mechanism by Biological Bodies in the Near Field of Dipole Antennas Above 300 MHz", IEEE Transactions on Vehicular Technologies, Vol. VT-41, No. 1, pp. 17-23, February, 1992.
5. K.S. Yee, "Numerical Solution of Initial Value Problems Involving Maxwell's Equations in Isotropic Media", IEEE Trans. on Antennas and Propagation, Vol. AP-14, No. 3, pp. 302-307, May, 1966.
6. G. Mur, "Absorbing Boundary Condition for the Finite-Difference Approximation of the Time-Domain Electromagnetic Field Equations", IEEE Trans. on Electromagnetic Compatibility, Vol. EMC-23, No. 4, November, 1981.
7. R. Luebbers, L. Chen, T. Uno, and S. Adachi, "FDTD Calculation of Radiation Patterns, Impedance, and Gain for a Monopole Antenna on a Conducting Box", IEEE Transactions on Antennas and Propagation, Vol. 40, No. 12, pp. 1577-1583, December, 1992.
8. K.R. Umashankar, A. Taflove and B. Beker, "Calculation and Experimental Validation of Induced Currents on Coupled Wires in an Arbitrary Shaped Cavity", IEEE Trans. on Antennas and Propagation, Vol. AP-35, No. 11, pp. 1248-1257, November, 1987.
9. C.W. Trueman, R.J. Luebbers, S.R. Mishra and C. Larose, "RCS of High Permittivity Cubes Computed by FDTD with Prony Extrapolation", Third International Conference on Electromagnetics in Aerospace Applications, Torino, Italy, September 14-17, 1993.
10. J.G. Maloney and G.S. Smith, "A Comparison of Methods for Modeling Electrically Thin Dielectric and Conducting Sheets in the Finite-Difference Time-Domain (FDTD) Method", IEEE Trans. on Antennas and Propagation, Vol. 41, May, 1993.
11. O.P. Gandhi, B-Q Gao and J-Y Chen, "A Frequency-Dependent Finite-Difference Time-Domain Formulation for General Dispersive Media", IEEE Trans. on Microwave Theory and Techniques, Vol. MTT-41, No. 4, pp. 658-665, April, 1993.
12. M.J. Hagmann, O.P. Gandhi, J.A. D'Andrea and I. Chatterjee, "Head Resonance: Numerical Solutions and Experimental Results", IEEE Trans. on Microwave Theory and Techniques, Vol. MTT-27, No. 9, pp 809-813, September, 1979.
13. R.J. Luebbers, K.S. Kunz, M. Schneider and F. Hunsberger, "A Finite-Difference Time-Domain Near Zone to Far Zone Transformation", IEEE Trans. on Antennas and Propagation, Vol. AP-39, No. 4, April, 1991.
14. A.C. Eycleshymer and D.M Schoemaker, "A Cross-Section Anatomy", D. Appleton and Co., New York, 1911.
15. D.M. Sullivan, O.P. Gandhi and A. Taflove, "Use of the Finite-Difference Time-Domain Method for Calculating EM Absorption in Man Models", IEEE Trans. on Biomedical Engineering, Vol. BME-35, No. 3, pp. 179-186, March, 1988.
16. A. Taflove and M. E. Brodwin, "Computation of the Electromagnetic Fields and Induced Temperatures within a Model of the Microwave-Irradiated Human Eye", IEEE Transactions on Microwave Theory and Techniques, Vol. MTT-23, No. 11, pp. 888-896, November, 1975.
17. G. Hartsgrove, A. Kraszewski, and A. Surowiec, "Simulated Biological Materials for Electromagnetic Radiation Absorption Studies", Bioelectromagnetics, Vol. 8, pp. 29-36, 1987.

18. M. A. Stuchly and S. S. Stuchly, "Dielectric Properties of Biological Substances - Tabulated", Microwave Power, 15(1), pp. 19-26, 1980.
19. W. T. Joines, Y. Zhang, C. Li, and R. L. Jirtle, "The Measured Electrical Properties of Normal and Malignant Human Tissues From 50 to 900 MHz", Medical Physics, Vol. 21, No. 4, pp. 547-550, April 1994.
20. D. M. Sullivan, D. T. Borup, and O. P. Gandhi, "Use of Finite-Difference Time-Domain Method in Calculating EM Absorption in Human Tissues", IEEE Transactions on Biomedical Engineering, Vol. BME-34, No. 2, pp. 148-157, February, April, 1987.
21. J. Toftgard, S.N. Hornsleth, and J. B. Andersen, "Effects on Portable Antennas of the Presence of a Person", IEEE Trans. on Antennas and Propagation, Vol. AP-41, No. 6, pp. 739-746, June, 1993.
22. R. Luebbers, F. P. Hunsberger, K. S. Kunz, R. B. Standler, and M. Schneider, "A Frequency-Dependent Finite-Difference Time-Domain Formulation for Dispersive Materials", IEEE Transactions on Electromagnetic Compatibility, Vol. 32, No. 3, pp. 222-227, August, 1990.
23. D.M. Sullivan, "A Frequency-Dependent FDTD Method for Biological Applications", IEEE Trans. on Microwave Theory and Techniques, Vol. MTT-40, No. 3, pp. 532-539, March, 1992.
24. C.C. Johnson and A.W. Guy, "Nonionizing Electromagnetic Wave Effects in Biological Materials and Systems", Proc. IEEE, Vol. 60, pp. 692-718, June, 1972.
25. R. Luebbers and F. Hunsberger, "FDTD for N-th Order Dispersive Media", IEEE Trans. on Antennas and Propagation, Vol. AP-40, No. 11, pp. 1297-1301, November, 1992.
26. R. Luebbers, D. Steich and K. Kunz, "FDTD Calculation of Scattering from Frequency-Dependent Materials", IEEE Trans. on Antennas and Propagation, Vol. AP-41, No. 9, pp. 1249-1257, September, 1993.
27. W.P. Hurt, "Multiterm Debye Dispersion Relations for Permittivity of Muscle", IEEE Trans. Biomed. Eng., Vol. BME-32, pp. 60-63, 1985.
28. C.M. Furse, J.-Y. Chen and O.P. Gandhi, "The Use of the Frequency-Dependent Finite-Difference Time-Domain Method for Induced Current and SAR Calculations for a Heterogeneous Model of the Human Body", IEEE Trans. on Electromagnetic Compatibility, Vol. EMC-36, No. 2, pp. 128-133, May, 1994.
29. Q. Balzano, O. Garay, and F. R. Steel, "Heating of Biological Tissue in the Induction Field of VHF Portable Radio Transmitters", IEEE Transactions on Vehicular Technology, Vol. VT-27, No. 2, pp. 51-56, May, 1978.
30. A.W. Guy and C-K Chou, "Specific Absorption Rates of Energy in Man Models Exposed to Cellular UHF Mobile-Antenna Fields", IEEE Trans. on Microwave Theory and Techniques, Vol. MTT-34, No. 6, pp. 671-680, June, 1986.
31. D. Sullivan, "Three Dimensional Computer Simulation in Deep Regional Hyperthermia Using the Finite-Difference Time-Domain Method", IEEE Transactions on Microwave Theory and Techniques, Vol. MTT-38, No. 2, pp. 204-211, February, 1990.

APPENDIX 2

Concordia University, ENGR 410 Report
by Mina Danesh
September 1994

ABSORPTION OF RF ENERGY BY THE HUMAN HEAD

A Report
Presented to
The Department of Electrical Engineering
Concordia University

In Fulfillment
of the Requirements
of Engineering 410

by
Mina Danesh
I. D. 3133060
Concordia University
September 1994

ABSTRACT

Absorption of RF Energy by the Human Head
by: Mina Danesh

Portable cellular telephones, operating between 800 and 900 MHz and emitting 0.6 W of power, were recently a matter of concern for people regarding health hazards. Although manufacturers follow the standards set by the exposure guidelines for electromagnetic radiation by choosing the accepted power for the device, research on possible biological effects is maintained. To approach this problem, the finite-difference time-domain (FDTD) method is applied to model the operator and the phone set with cells, and to obtain the corresponding electromagnetic fields for each cell. Since electrical properties of biological tissues vary with frequency, this dispersive material case is handled by extending the FDTD code. A three-dimensional head model has been built with twenty-seven tissues. Its FDTD representation and the phone set model are also described. Tissue damage is determined by the resultant power delivered by the electromagnetic fields, given by the specific absorption rate (SAR) levels. SAR results of previous papers using the FDTD method applied to the entire or part of the human body in the radio frequency range are presented for comparison with the safety limits.

Key Words: cellular telephones, health hazards, FDTD method, head model, cellular phone model, SAR levels, safety limits.

TABLE OF CONTENTS

LIST OF FIGURES AND TABLES

Chapter 1 - INTRODUCTION

Handheld portable cellular phones have been questioned by the media and the public on whether they cause a health threat [1][1]. The antenna lies right alongside a user's head, so the electromagnetic field strengths are high close to the head and may cause or exacerbate brain cancer, or damage body cells. North American cellular phones transmit signals between 824 and 850 MHz and receive signals between 870 and 890 MHz [2]. Even though skin reflects much of the energy and the body absorbs very little energy at 800 to 900 MHz, some safety limits for electromagnetic radiation, based on previous research results, have been published for applying exposure standards in the radio frequency range [3], [4]. Biological effects depend on the increase of temperature due to electromagnetic energy absorption, measured by the source absorption rate (SAR) in W per kg. The limit of 0.08 W/kg power absorbed has been set for averaged SAR over the whole body. Spatial peak SAR values should not exceed 1.6 W/kg, for 1 g of tissue, taken as a tissue volume in the shape of a cube, exposed for 30 minutes or more [3]. Since cellular phones radiate 0.6 W of power which is less than the standard power of 0.74 W at 850 MHz for which the maximum permissible exposure must be respected, therefore they are considered safe [3].

A way to approach this problem is to use the finite-difference time-domain (FDTD) method for modelling the tested objects and computing the resultant electromagnetic fields, such that the SAR levels can be found. Although other methods exist like the finite element/boundary element method [5], or the fast-Fourier-transform [6], these are seldom in use. In this report, the

---

[1] Numbers in brackets designate references at the end of the report.

FDTD method is described mathematically to obtain the electromagnetic fields for the general and the lossy material cases. To construct the head and the phone set models, the method consists of defining them within certain restrictions. A research project is under way at Concordia University [7], where only the head model has been built. Some previous papers dealt with SAR levels for the entire or part of the human body tested in the radio frequency range. These are presented for comparison with the safety limits.

Chapter 2 - THE FINITE-DIFFERENCE TIME-DOMAIN METHOD

2.1 - Yee Algorithm

2.1.1 - Formulation Steps

The FDTD method, first proposed by Yee [8], is directly derived from the time-dependent Maxwell curl equations

$$\nabla\times\bar{H}= \sigma E + \varepsilon\frac{\partial \bar{E}}{\partial t} \tag{1}$$

$$\nabla\times\bar{E}= -\mu\frac{\partial \bar{H}}{\partial t} \tag{2}$$

where $\bar{H}$ is the magnetic field, $\bar{E}$ the electric field, σ the electrical conductivity, ε the permittivity and μ the permeability. Equations (1) and (2) are then used in the following form for the FDTD purpose

$$\frac{\partial \bar{H}}{\partial t} = -\frac{1}{\mu}\left(\nabla\times\bar{E}\right) - \frac{\sigma^*}{\mu}\bar{H} \tag{3}$$

$$\frac{\partial \bar{E}}{\partial t} = -\frac{\sigma}{\varepsilon}\bar{E} + \frac{1}{\varepsilon}\left(\nabla\times\bar{H}\right) \tag{4}$$

where σ^* is the magnetic conductivity. The electromagnetic fields are composed of their respective incident and scattered fields

$$\bar{E}=\bar{E}^{\text{total}} =\bar{E}^{\text{incident}} +\bar{E}^{\text{scattered}} \tag{5}$$

$$\bar{H}=\bar{H}^{\text{total}} =\bar{H}^{\text{incident}} +\bar{H}^{\text{scattered}} \tag{6}$$

By replacing $\bar{E}$ as in equation (5) and $\bar{H}$ as in equation (6), and rearranging equations (3) and (4), general formulas are obtained

$$\frac{\partial \bar{H}^{\text{scat}}}{\partial t} = -\frac{\sigma^*}{\mu}\bar{H}^{\text{scat}} - \frac{\sigma^*}{\mu}\bar{H}^{\text{inc}} - \frac{(\mu-\mu_0)}{\mu}\frac{\partial \bar{H}^{\text{inc}}}{\partial t} - \frac{1}{\mu}\left(\nabla\times\bar{E}^{\text{scat}}\right) \tag{7}$$

$$\frac{\partial \bar{E}^{\text{scat}}}{\partial t} = -\frac{-\sigma}{\varepsilon}\bar{E}^{\text{scat}} - \frac{\sigma}{\varepsilon}\bar{E}^{\text{inc}} - \frac{(\varepsilon-\varepsilon_0)}{\varepsilon}\frac{\partial \bar{E}^{\text{inc}}}{\partial t} - \frac{1}{\varepsilon}\left(\nabla\times\bar{H}^{\text{scat}}\right) \tag{8}$$

The next step is to replace the derivatives with differences, by retaining the first order terms only (defined as a second order accuracy according to Yee), as described mathematically below for a function f

$$\frac{\partial f}{\partial t} \equiv \lim_{\Delta t \to 0} \frac{f(x, t_2) - f(x, t_1)}{\Delta t} \approx \frac{f(x, t_2) - f(x, t_1)}{\Delta t} \tag{9}$$

$$\frac{\partial f}{\partial x} \equiv \lim_{\Delta x \to 0} \frac{f(x_2, t) - f(x_1, t)}{\Delta x} \approx \frac{f(x_2, t) - f(x_1, t)}{\Delta x} \tag{10}$$

where Δt is the time step, and Δx the dimension of a cell side. As a matter of clarity, the case of a perfect conductor is taken to demonstrate the final results for the FDTD formulation. The scattered fields are in free space, thus $\sigma^* = \sigma = 0, \mu = \mu_0$, and $\varepsilon = \varepsilon_0$. For the perfect conductor, the conductivity is infinity. Taking the scalar parts of equations (7) and (8) for a perfect conductor, and in this example, only the E_x^{scat} and H_y^{scat}

$$\frac{\partial E_x^{scat}}{\partial t} = \frac{1}{\varepsilon_0}\left(\frac{\partial H_z^{scat}}{\partial y} - \frac{\partial H_y^{scat}}{\partial z}\right) \tag{11}$$

$$\frac{\partial H_y^{scat}}{\partial t} = \frac{1}{\mu_0}\left(\frac{\partial E_z^{scat}}{\partial x} - \frac{\partial E_x^{scat}}{\partial z}\right) \tag{12}$$

and replacing derivatives with differences, the final FDTD form is obtained

$$\frac{E_x^{scat,n} - E_x^{scat,n-1}}{\Delta t} = \frac{1}{\varepsilon_0}\left[\frac{\Delta H_z^{scat,n-\frac{1}{2}}}{\Delta y} - \frac{\Delta H_y^{scat,n-\frac{1}{2}}}{\Delta z}\right] \tag{13}$$

$$\frac{H_y^{scat,n+\frac{1}{2}} - H_y^{scat,n-\frac{1}{2}}}{\Delta t} = \frac{1}{\mu_0}\left[\frac{\Delta E_z^{scat,n}}{\Delta x} - \frac{\Delta E_x^{scat,n}}{\Delta z}\right] \tag{14}$$

As shown in Fig. 1, the components of the electric field are along the edges of the cells, and the components of the magnetic field are normal to the faces of the cells, thus perpendicular to the electric field components. As time is advanced in steps of Δt (determined by a stability condition described in the next section), at each time step, the value of each electric field component along the edges and then the value of each magnetic field component are found. Thus the electric and magnetic fields are interleaved spatially and temporally because of the central differencing, referred to as "leap frog in time" scheme. The electric field at time n is

updated from its prior value at n-1 and the adjacent magnetic field values at time n-$\frac{1}{2}$ as shown by the example equation (13). Then the magnetic field at time n+$\frac{1}{2}$ is updated from its previous value at n-$\frac{1}{2}$ and the adjacent electric field values at time n, as in equation (14). After each update of $\bar{E}$ and $\bar{H}$, the index n is increased by 1 and the process is repeated [9].

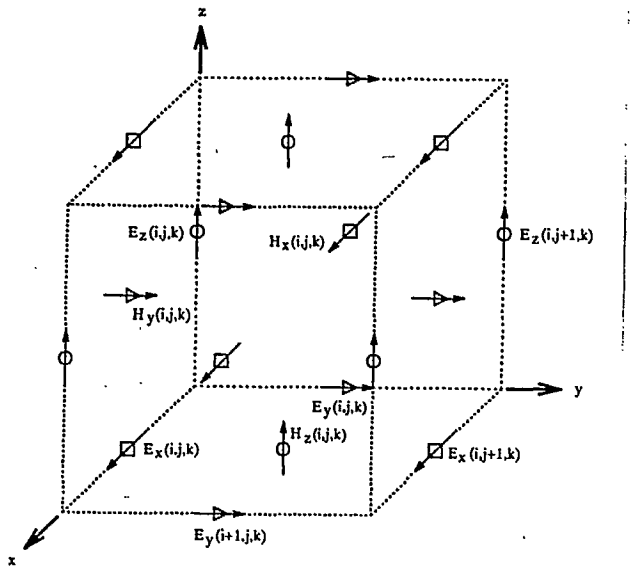

Fig. 1. Yee cell geometry [10].

2.1.2 - Requirements

As to apply the FDTD method, a problem space must be defined for the cell size, the required dimensions in terms of cells for the whole three-dimensional Cartesian (rectangular) coordinate system space, the time step, and the incident field. The space used for calculations is divided into cells, generally taken as cubical for the simplicity of formulations of equations and 3D representation of surrounding objects, as shown in Fig. 1: it is defined as the Yee cell geometry. Each side of the cell is defined as $\Delta x = \Delta y = \Delta z$ [9]. The cell size depends on the smallest wavelength of the incident field, which depends on the greatest permittivity of the

scattered object, for the case of dielectric materials, where $\lambda = \frac{c}{f\sqrt{\varepsilon_r}}$, and f is the frequency at which the device is operating [11]. For perfect conductors, the wavelength is inversely proportional to the frequency. The cell size must be equal or less than one-tenth of the wavelength [12]. But in some cases as for the human body representation, the cell size must be at the most one-quarter of the wavelength [11]. The entire space is defined as N_x, N_y, and N_z determined by the number of cells required for the scattered object and extra free space cells or "white spaces" that must separate the FDTD model from the outer boundary, such that interactions (of scattered fields) between the model and the boundary are reduced to insignificant levels. The time step is defined by the Courant stability condition

$$c\,\Delta t \leq \sqrt{(\Delta x)^2 + (\Delta y)^2 + (\Delta z)^2}$$

and for cubical cells, the formulation becomes

$$\Delta t \leq \frac{\Delta x}{c\sqrt{3}}$$

where c is the velocity of light since the space in which the scattered object is placed is free space [12]. The incident field must be analytically specified as one of the following parameters: multipath, planewave, continuous wave (CW) or pulse-modulated such as Gaussian pulses [3]; the source-object configuration: near- and far-field; its intensity, frequency, and polarization. For a far zone transformation, the direction of the far zone must also be specified. The fields and sources are set to zero at initial time, often taken as time zero. The next step is to build the required test object by specifying the type of materials other than free space for each cell locations: this is described in more details in the modelling chapter. The required response type could be a voltage, current, electric or magnetic field, power, etc. As shown in the previous section, the electromagnetic fields calculations advance one step at a time, for the indices i, j, and k which go from 1 to N_x, N_y, and N_z respectively [12]. On the outer surfaces of the cell space,

some of the neighboring fields components needed to evaluate the enclosing field components of the cells are outside the problem space or are not available, therefore an outer radiation boundary condition (ORBC) is defined, such that the surfaces of the cell space could absorb the scattered or radiated fields incident upon them; but since the condition is imperfect, reflection from the outer boundary can occur [13]. A known ORBC was developed by Mur: a first order condition goes back one step in time and into the space one cell location, for a second order condition, it looks back two steps in time and inward two cell locations (this is mostly used so as to go with Yee's second order accuracy) ; this method must be applied with certain restrictions considering the cell space [14]. The last step may involve transformation of the near zone FDTD fields to the far zone scattering calculations which consists in evaluating the electric and magnetic currents surrounding the object within a closed surface and then computing the scattered fields in the far zone. All these requirements must be translated into a program code: its flowchart is shown in Fig. 2. The use of the computer has some restrictions regarding CPU time and memory, thus limiting the number of cells used [12].

2.2 - Dispersive Material Case

The FDTD method , represented by the basic equations (7) and (8), includes also materials with constant permittivity and conductivity. But lossy ($\sigma \neq 0$) dielectrics like biological materials are described over a wide frequency range as illustrated by Tables 1 and 2: the relative permittivity or the conductivity changes values as the frequency varies. Therefore, these dispersive materials are frequency-dependent. For applying the FDTD code to these materials, the run must be performed at several frequency values, with the appropriate electrical

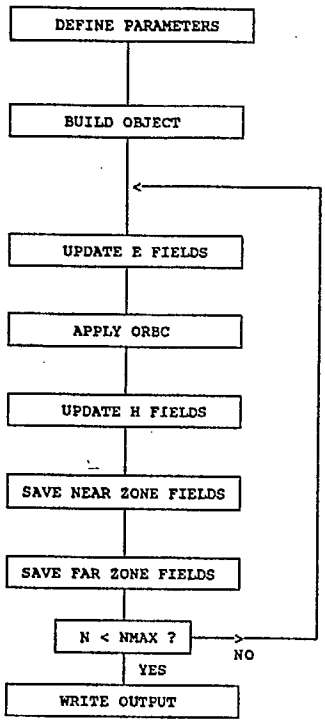

Fig. 2. FDTD flow chart [15].

properties, but the time-domain method is not respected, since transient results (of the incident wave) provides faulty approximation, like higher values of the electric field [16], [17]. To obtain accurate results, the Yee's method should be extended. Some methods were proposed by various papers, as described below.

Instead of having a constant real permittivity, dispersive materials are related to a constant complex permittivity ε^* with $\varepsilon^* = \varepsilon_0\left(\varepsilon_\infty + \frac{\varepsilon_s - \varepsilon_\infty}{1 + j\omega t_0} - j\frac{\sigma}{\omega\varepsilon_0}\right)$, defined as a Debye pole, where ε_∞ is the infinite frequency relative permittivity, $\varepsilon_\infty = \lim_{\omega\to\infty} \varepsilon_r$; ε_s the static relative permittivity, $\varepsilon_s = \lim_{\omega\to 0} \varepsilon_r$; t_0 the relaxation time and ω the angular velocity at which the device is operating [16].

Another method deals with a frequency-dependent FDTD code called $(FD)^2TD$. The formulation consists of relating the electric flux density with the electric field in the frequency domain by the complex frequency-dependent permittivity: $D(\omega) = \varepsilon_0 \varepsilon_r(\omega) E(\omega)$ which becomes a discrete time-domain convolution. A two-relaxation Debye equation defined as

$$\varepsilon_r(\omega) = \varepsilon_\infty + \frac{\varepsilon_{s1} - \varepsilon_\infty}{1 + j\omega\tau_1} + \frac{\varepsilon_{s2} - \varepsilon_\infty}{1 + j\omega\tau_2}$$

is also used, and real values are found for: $\varepsilon_r = \mathrm{Re}[\varepsilon_r(\omega)]$ and $\sigma = \omega \mathrm{Im}[\varepsilon_r(\omega)]$ [18], [19], [20].

The $(FD)^2TD$ could also include an N-th order dispersion Lorentz pole used in a medium with p poles, the relative permittivity is represented as follows:

$$\varepsilon_r(\omega) = \varepsilon_\infty + (\varepsilon_s - \varepsilon_\infty) \sum_{p=1}^{p} \frac{G_p \omega_p^2}{\omega_p^2 + 2j\omega\delta_p - \omega^2} \text{ with } \sum_{p=1}^{p} G_p = 1$$

where ω_p and δ_p are the p-th resonant frequency and damping coefficient, respectively. The convolution is run as a recursive sum for each location in the cell space [21]. Other variations of these methods also exist [17], [22]. The extension of the FDTD code requires more calculations, thus more CPU time and electrical constants data.

Chapter 3 - ELECTROMAGNETIC MODEL OF THE HEAD AND THE CELLULAR PHONE

The three-dimensional (3D) problem space consists of the head and the cellular phone models at the center surrounded by the white space.

3.1 - Cell Model of the Head

The first step was to make a head with cubical cells, each having its own tissue type: this is what has been done up to now in the research project. Then an FDTD model has to be created.

3.1.1 - Constructing the Head Model

A realistic model has been constructed based on a cross-sectional anatomy book [23] of a standard man (1.75 m of height and weighing 70 Kg [24]), containing transversal sections of the head tilted with certain angles as shown on the center lateral section of Fig. 3. Sections 1 to 10' are approximately equispaced by 0.25 inch or 6.35 mm and sections 11 to 18 are separated by half an inch. To implement the data of the given cross-sections within computer data, each cross-section had to be digitized, then put together to obtain the 3D head model.

The cell size chosen was 3.3 mm, but since the scale size from the original images of the book is 4/3, the size of the transparent grid used for the images was 2.5 mm. The center back of each section was taken as the reference point. Programs were written for the Fortran compiler for the PC and the DEC station, using available libraries for graphics and for the tablet digitizer

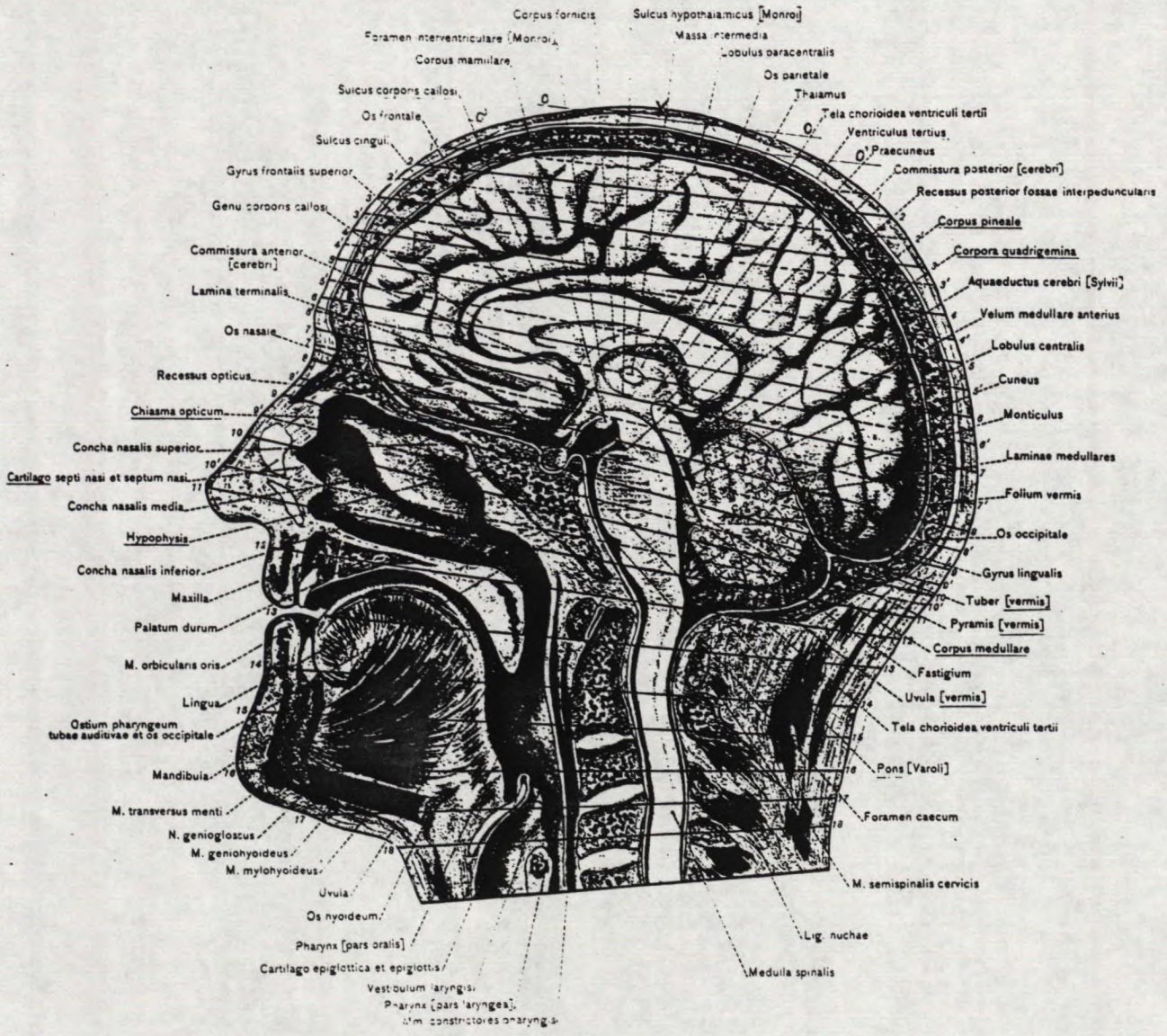

Fig. 3. Center lateral section of head [25].

(used only on the PC). By superimposing a transparent grid of 18x20 cm of 2.5 mm cell size on the section image, a tissue type represented by a number, from 2 to 30, was chosen for each cell, using the digitizer. For cells containing more than one material, the tissue which had the biggest surface for that cell was chosen arbitrarily. For each cross-section, the cells' data were stored in a file. Fig. 4 shows the section image of the book and Fig. 5 is the corresponding image with

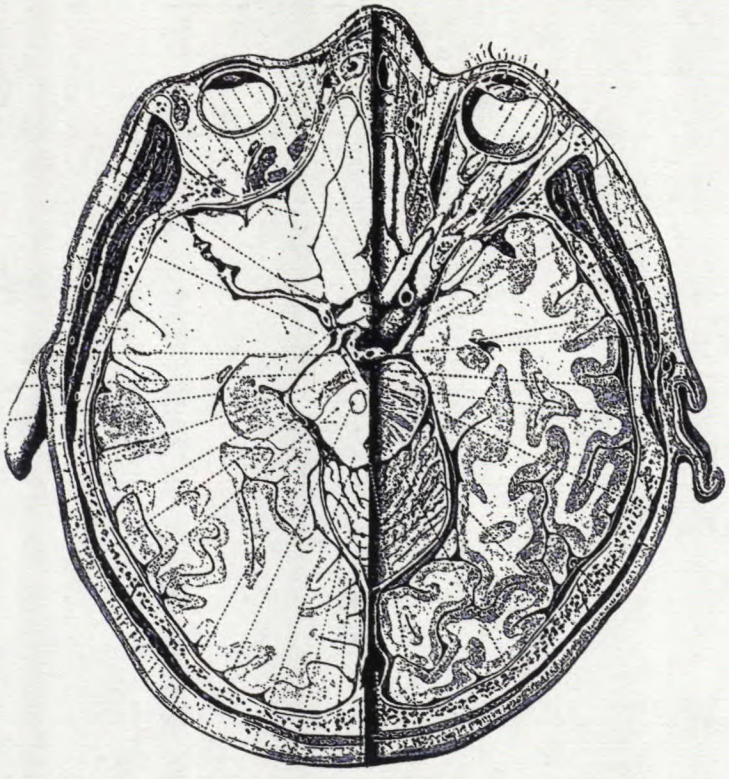

Fig. 4. Sagittal cross-section 8' on the right half [26].

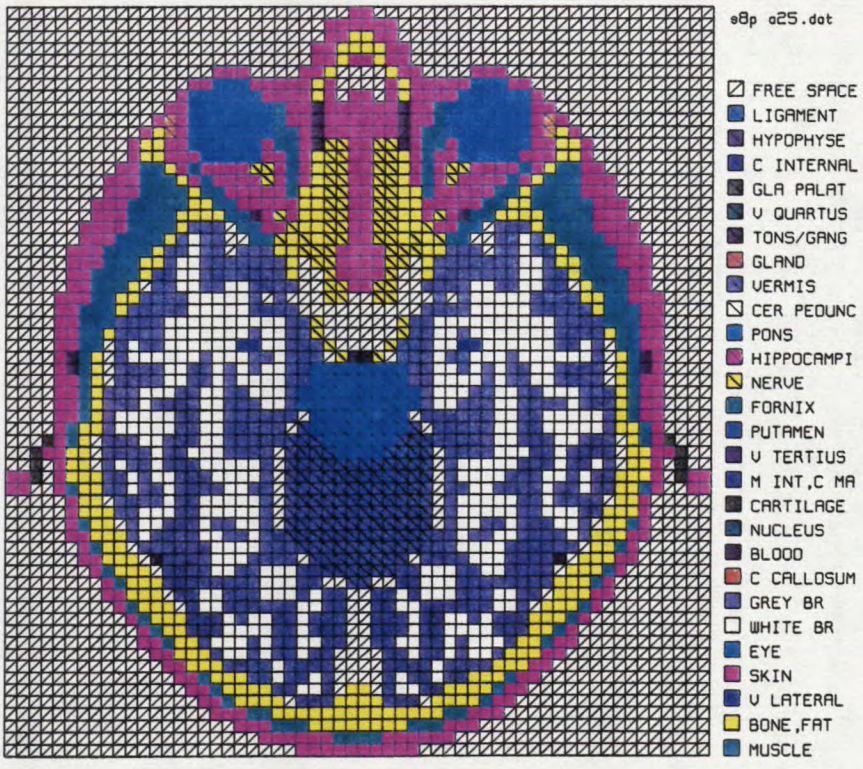

Fig. 5. Equivalent cross-section 8' obtained by digitization.

the different tissue types. The list of tissues was chosen arbitrarily, some of them for which dielectric properties were found and the properties of the others will be approximated. For constructing the head model, sections 0 and 0' have been added to define a more curved-shape top of head. A file was built to store the reference points: front and back of each cross-section and a top point as shown by a cross in Fig. 3, by using the coordinates of the tablet mouse to get more precision. A 16x18x19 cm space representation for the 3D model was made which results in a 64x72x76 cell space having 350208 cells. To obtain the complete head, an algorithm was developped: for each cell on the YZ plane, several computations had to be done. If a cell layed between two cross-sections, then the distances calculated from the center of the cell to each of the sections were compared; if, for example, the distance from the upper cross-section was the smallest, then the cell belonged to this section and got the number corresponding to the tissue type for each x from its data file. If a cell did not belong to any section, then it had the number 0 corresponding to free space. The case for which a cell layed between the top point and the first cross-section, the tissue type was assigned to be the one of the section. After 3 hours of CPU time on the DEC station, a rough model of the head was obtained. Since the cut of the cross-sections are tilted, the cells belonging to different sections on the layers may not have been totally matched together to obtain uniform shapes and consistency of tissues. A fourth program was written to view the model in the XY, or YZ, or XZ planes, and edit cells on layers to respect the uniformity of the head. Fig. 6 presents the final model on the YZ plane, where the red lines correspond to the cross-sections.

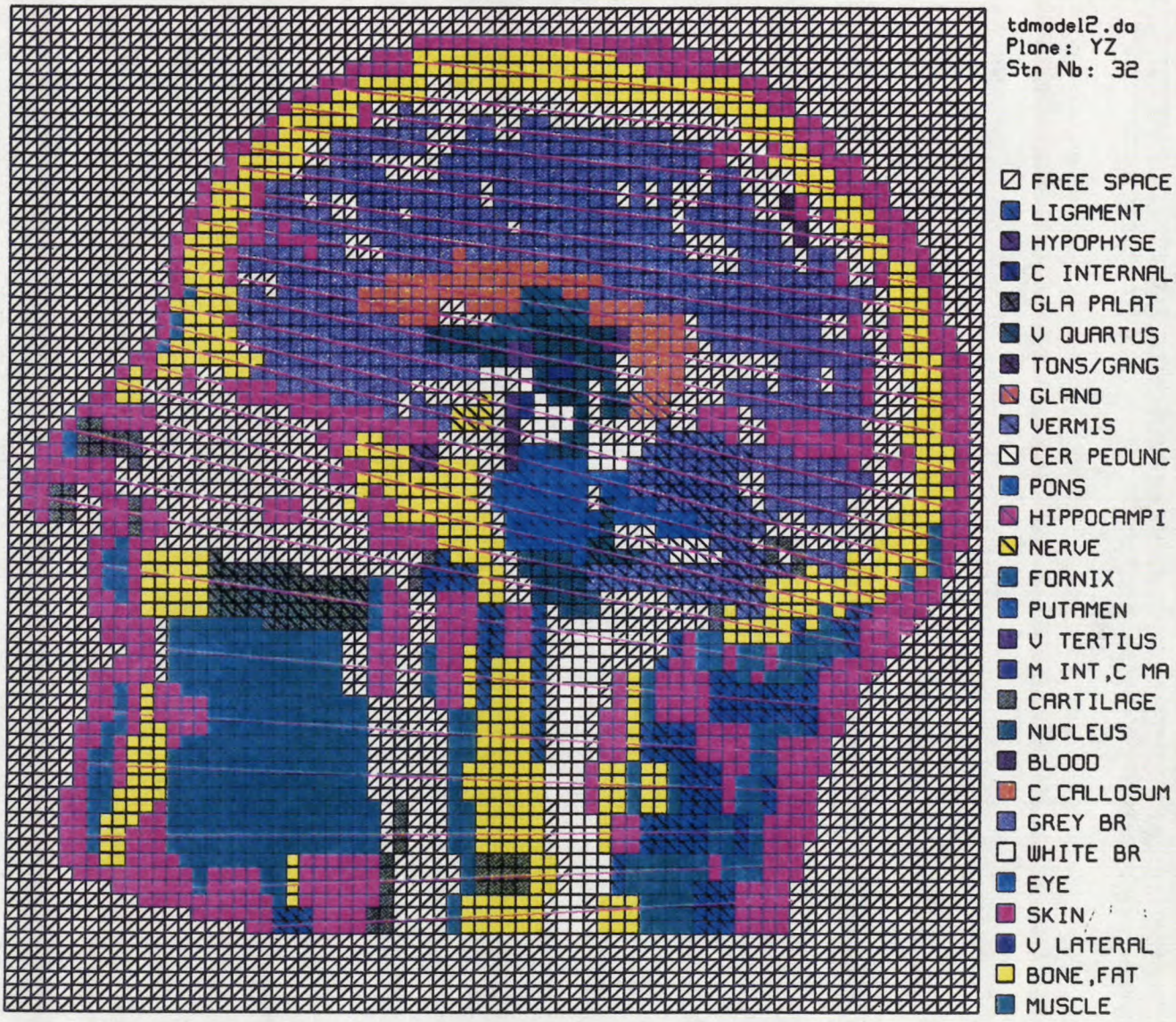

Fig. 6. Final head model: lateral section on plane YZ of the 3D space.

3.1.2 - FDTD Model

To apply the previous head model to the FDTD code, the relative permittivity and conductivity of the correspondent tissue type, listed in Fig. 6, are assigned to each cell. Some of the biological material electrical properties of the human head are listed in Tables 1 and 2, noting that both permittivity and conductivity do vary significantly with frequency: the permittivity decreases and conductivity increases as frequency increases. At 2.45 GHz the relative permittivity for grey and white matter of human brain is 46 and 32.6 respectively [35]. Although some tissues like putamen or hypophyse are not present in the tables, their dieletric properties could be approximated by other tissue properties, or taken from animal's data. Electrical properties were found from dog's white and grey matter, for example, at 850 MHz, $\varepsilon_r(\text{grey}) = 45$, $\varepsilon_r(\text{white}) = 30 - 35$ which correspond closely to the values found above, and $\sigma(\text{grey}) = 10, \sigma(\text{white}) = 7.5$ [36]. These properties are then used in calculating the electromagnetic fields as described in the previous chapter. But at the boundary, for updating the field components, volume averaged properties is used for all of the applicable cells: the permittivity and the conductivity are "weighted averaged", since at the boundary, a cell must take into account the amount of free space and that of the tissue [19].

3.2 - Model of the Cellular Phone

A portable cellular phone consists of a parallelepiped box and a quarter-wavelength monopole antenna as shown in Fig. 7 with $a = 60$ mm, $h = 50$ mm, $b = 10$ mm, $c = 50, 130,$ or

Table 1. Relative permittivity of biological materials at various frequencies.

Tissue	Ref	Frequency (MHz)									
		10	27.12	100	350	400	500	750	900	1000	1500
Brain,	27	163-352		57-90						37-55	
nerve	28		155	52	60						
	29							49			46
	30			63		50.3			41.2		
	31				74						
Bone,	27	37		23							
fat	28		29	7.5	5.7						
	29							5.6			5.6
	30			12.2		9.2			7.3		
	31				5.7						
Muscle	27	162-204		64-90						57-59	
	28		106	74	53						
	29							52			49
	30			70.5		62.5			54.7		
	32			71-76			52-54			49-52	
	33			63		52.6	52.4		52		
	34								50.5		
	31				54						
Skin	28		106	25	17.6						
	29							52			49
	32			57			46.5			43-46	
	31				17.4						
Eye	28		155	85	80						
	29							80			80
Blood	28		102	74	65						
	32			69-81			67-70			60.5	
	31				65						
Cartilage	24			7.5	5.7						

200 mm, w = 10 or 30 mm, and the radius of the antenna wire is 0.5 mm for typical models. The box is made of a 5 mm thick plastic case surrounding the metal chassis representing the circuit board and the internal elements. For the dielectric plastic case, it is taken as lossless and has relative permittivity of 2. There is a 2.5 mm air space gap between the metal chassis and the plastic shell, and a 2.5 mm radius hole through the dielectric layer through which the monopole

Table 2. Conductivity (S/m) of biological materials at various frequencies.

Tissue	Ref	Frequency (MHz)									
		10	27.12	100	350	400	500	750	900	1000	1500
Brain,	27	0.21-0.63		0.48-0.95						0.81-1.2	
nerve	28		0.45	0.53	0.65						
	29							1.2			1.4
	30			4.7		7.5			12.2		
	31				0.62						
Bone,	27	0.024		0.057							
fat	28		0.04	0.07	0.072						
	29							0.09			0.12
	30			0.215		0.88			1.4		
	31				0.07						
Muscle	27	0.69-0.96		0.75-1.05						1.38-1.45	
	28		0.74	1	1.33						
	29							1.54			1.77
	30			6.8		9			13.8		
	33			0.62		0.68	0.72		0.92		
	34								1.2		
	31				1.3						
Skin	28		0.74	0.55	0.44						
	29							1.54			1.77
	31				0.42						
Eye	28		0.45	1.9	1.9						
	29							1.9			1.9
Blood	28		0.28	1.1	1.2						
	31				1.22						
Cartilage	24			0.067	0.072						

passes. The wire monopole is modelled by setting a straight line where the electric field is zero along the wire axis except for the component at the base of the monopole: this gap is used as a voltage source which induces a current to flow, thus "exciting" the antenna. The source must be specified as a voltage time function. This method is used because the wire diameter is smaller than the FDTD cell size [37]. This thin wire approach is used to calculate the magnetic fields surrounding all of the electric fields along the wire axis [38].

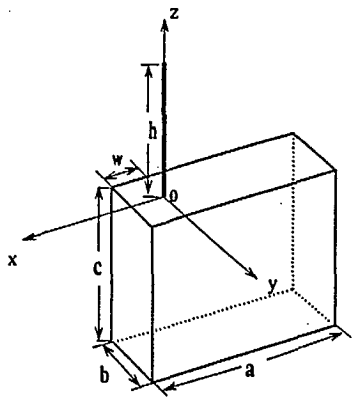

Fig. 7. Geometry of monopole antenna on a conducting box [37].

If the source voltage time function is a sine wave, it must be turned on gradually, as an abrupt start would violate the grid's bandwidth restriction. Then the FDTD calculations are continued until all transients are dissipated, and sinusoidal steady-state are reached [39], which could require a great many time steps (especially when the run is used with high-permittivity resonant structures such as human bodies specified as hot spots [4]). The Fourier-transform is used to find the response in the frequency domain [39]. To obtain the frequency response over a wide bandwidth, the FDTD code is often run with a sine wave input, many times at individual frequencies. But since the FDTD code uses Maxwell's equation in the time domain, information can be obtained over a wide bandwidth in a single run; taking the voltage source as a time-limited function such as a Gaussian pulse whose spectral content is restricted to bandwidth for which the FDTD grid is valid. Then the FDTD algorithm finds the time response of each field component in the space due to the source pulse. These near-field time functions obtained are used to find the far-fields of the cellular phone operating near the head, with a near- to far-field transformation [40]. At each time step, the far-field in any direction can be found from

the values of the near-fields on a closed integration surface, thus some cells must be taken inside the absorbing boundary. This also restricts the minimum number of cells which separate the head from the phone handset models, depending on the ORBC chosen.

Chapter 4 - SPECIFIC ABSORPTION RATE STUDIES

4.1 - Definition of the Specific Absorption Rate

The biological effects such as an increase in temperature due to electromagnetic fields exposure is measured by the power supplied per unit mass defined as the specific absorption rate (SAR) in W per kg. The SAR depends on electric field strength in tissues [4], and is given by

$$SAR_{ijk} = \frac{\sigma_{ijk}}{\rho_{ijk}} \left(\frac{|E_x|^2 + |E_y|^2 + |E_z|^2}{2} \right)_{ijk}$$

where for the ijk-th FDTD cell, σ is the conductivity, ρ the mass density of the tissues in the cell, E_x, E_y, and E_z are amplitudes of the x, y, and z components [41]. Some values of the mass density for different tissues are presented in Table 3. The mass density of water is 1000 kg/m^3, and since the human body contains approximately 90% of water, then an averaged value for the entire body will also be around 1000 kg/m^3.

Table 3. Mass density (kg/m^3) of certain biological tissues.

Tissues	Ref	Value
Skin	42	800
	11	1,100
Fat	42	940
Muscle	42	1,100
	11	1,040
Eye	11	1,034
Brain	11	1,030
Bone	11	1,850
Blood	11	1,060
Whole Body	26	1,000

4.2 - Previous Studies and Comparison with the Safety Limits

Some papers studied global SAR results with their own models. With the SAR values obtained, comparison is made with the safety standards.

A head model taken from the anatomical book [23] was built with a 3.2 mm cell size, with brain, bone/fat, muscle, skin, blood, eye humour, lens and sclera materials. The head contains 126000 cells. For the absorbing boundary, 10 cells from the nearest tissue in any direction were taken, resulting in a 550000 cells problem space. The incident field is a plane wave coming from the front and side of the head. The SAR histogram plot across the eye section shows that at 800 MHz, most of the energy is absorbed by the eye (where it reaches a maximum), brain, muscle and skin; the bone has the lowest absorption, noting that tissues with high conductivity tend to absorb more energy than the ones with low conductivity (conductivities are presented in Table 2 for the above tissues); and at 2.45 GHz, only superficial absorption is present in the skin and the eyes. From the cross-section passing through the nose, at 1.66 GHz, resonance (intensification of electromagnetic field strengths in a certain group of cells) occurs in the nose. A one-year old child head model was derived by taking the adult's head model and reducing it to 70% or changing the cell size to 2.22 mm. For the infant, absorption is more centralized: SAR values for the brain are higher. Eye resonance is also present: for the adult, it appears between 800 and 1200 MHz, for the child, between 1.2 and 1.8 GHz. SAR results in W/kg per V/m were tabulated and are in the order of 10^{-3} for 1 g of tissue. Thus for the electric field varying from 174 to 208 V/m, the maximum SAR is 0.0576 W/kg and the minimum is

0.0483 W/kg [11]: these values fall below the safety limit of 0.08 W/kg. For an incident plane wave, the radiation is considered safe.

Another research has been done using the same head models for the adult and the infant, but the problem space includes a half-wavelength dipole of wire radius 1 mm which represents a mobile communication transceiver. The dipole is excited by driving a voltage source of 1 V/m across the gap, and is placed in front of the left eye, spaced at 3.5 cm from its center. For the adult model: at 892 MHz, the dipole is made of 53 cells, and at 1.89 GHz, 25 cells; for the infant model, it is composed of 75 cells at 900 MHz, and of 35 cells at 1.93 GHz. The absorbing boundary was defined as 20 cells from the dipole or 10 cells from the nearest tissue in any direction, whichever was the biggest. The space consists of 950000 cells. For the infant, SAR histograms show that at 900 MHz, absorption is higher in the eyes (specially in the left one), brain, muscle and skin, and at 1.9 GHz, absorption is present only in the left eye. Tables for the eyes and the whole head indicate SAR values, for different head-dipole cell separation from 1 to 16, ranging from 30.4 to 2.47 W/kg at 892 MHz, and 62.3 to 2.69 W/kg at 1.89 GHz for the adult; from 28.6 to 3.3 W/kg at 900 MHz, and 89.8 to 4.93 W/kg at 1.9 GHz for the infant. These results are obviously incorrect because of the positionning of the transceiver in front of the head and the representation of the device as an ideal dipole. Average power were expected to be around 1 W/kg; however, some values could have exceeded the safety limit of 1.6 W/kg [43].

Ref. [41] has built an entire human body model with a cell size of 1.31 cm and fifteen tissues. The $(FD)^2TD$ method is used with a two-relaxation Debye equation. The incident source is a pulse. Total problem space consists of 404838 or 42x63x153 cells where 24x45x135 are for the body. Results of layer averaged SAR are plotted for frequencies of 20, 40, 150, 350, 500,

700, and 915 MHz. The highest values are located in the neck, knee, and ankle for all frequencies and the head from 700 MHz; they range from 0.25 to 0.7 W/kg for the neck, from 0.23 to 0.8 W/kg for the knee, from 0.3 to 1.8 W/kg for the ankle, and for the head, it is 0.2 W/kg. As the frequency increases, values decrease or stay the same. These results are below the safety limit of 1.6 W/kg, except for the ankle [3], thus there is no potential for tissue damage.

Ref. [24] proposes another model of a standard man with fourteen tissues. At 100 Mhz, the cell size is 2.62 cm resulting in a 23x12x68 space, and at 350 MHz, the size is 1.31 cm to obtain an FDTD space of 45x24x135 cells for more resolution. With an incident plane wave, SAR results are compared between the body isolated in space and the body standing on a ground plane: values are higher for brain, eyes, lung, heart, liver, and ankle for the grounded case varying from 0.018 to 0.47 W/kg. Whole body SAR corresponds to around 0.1 W/kg at 100 MHz and 0.056 at 350 MHz. The maximum SAR in the brain is 0.18 W/kg at 350 MHz. These results are below the safety limits, however for the whole body at 100 MHz, it does exceed the limit of 0.08 W/kg by 0.2 W/Kg, but again precision must be applied to the FDTD model to obtain more accurate results.

Chapter 5 - CONCLUSION

To ensure the general public that cellular phones may or may not cause health risks, researches are under way. The usefulness of the FDTD method is that it can handle biological materials represented as lossy dielectrics as well as having an excited source field inside the problem space (near-zone) instead of sending an incident field from outside the space (far-zone). Therefore, the head and the phone set can be modelled using this technique without any problems. Special care has to be taken for the absorbing boundaries to ensure getting the proper field strengths results when running the FDTD code. The way proposed by the exposure safety guidelines of analyzing the biological effects is to calculate the absorption of the electromagnetic fields obtained for each tissue cell, or SAR. Although some papers discuss about SAR levels, uncertainty is still maintained as whether the values are accurate, because of unproper modelling. Exact results concerning application to cellular telephones were not yet published.

Therefore, with the research going on at Concordia University, the head model obtained must be represented as an FDTD cell model by weighting-averaging the cells with tissues' dielectric constants. With the phone set model and the conditions for the absorbing boundaries, the FDTD problem space will be defined. The antenna could be excited with different sources such as pulses or continuous waves. The final SAR values will be analyzed and conclusions could be drawn. Other interesting results could also be obtained for different sizes of heads and phone sets, a female head, different ages of the operator, a hand wrapped around the phone; a whole body model will be useful to see all the possible effects, as well.

REFERENCES

1. M. Fischetti, "The Cellular Phone Scare", Special Report/Communications, IEEE Spectrum, June 1993, pp. 43-47.

2. C.Y. Lee, Mobile Cellular Telecommunications Systems, New York: McGraw-Hill, 1989, p.72, WEB TK 6570 M6L35 1989.

3. "IEEE Standard for Safety Levels with Respect to Human Exposure to Radio Frequency Electromagnetic Fields, 3 kHz to 3 GHz", IEEE C95.1-1991, Piscataway, New Jersey: IEEE.

4. International Non-Ionizing Radiation Committee of the International Radiation Protection Association, "Guidelines on Limits of Exposure to Radiofrequency Electromagnetic Fields in the Frequency Range from 100 kHz to 300 GHz", Health Physics, Vol. 54, No. 1, January 1988, pp. 115-123.

5. F. J. C. Meyer and D. B. Davidson, "A 2D Finite Element/Boundary Element Method for Solving Electromagnetic Fields in and Around a Human Cross-Section Near a Line Source", IEEE/SAIEE AP/MTTS-93 Proceedings, August 5 1993, pp. 12-1 12-10.

6. D. T. Borup and O. P. Gandhi, "Fast-Fourier-Transform Method for Calculation of SAR Distributions in Finely Discretized Inhomogeneous Models of Biological Bodies", IEEE Transactions on Microwave Theory and Techniques, Vol. 32, No. 4, April 1984, pp. 355-360.

7. S. J. Kubina, C. W. Trueman, W. Lauber, and S. R. Mishra, "Cellular Phones and Humans - A Neophyte Outlook", Conference Proceedings of the Symposium in Antenna Technology and Applied Electromagnetics (ANTEM), Ottawa, Canada, August 3-5 1994, pp. 87-96.

8. K. S. Yee, "Numerical Solution of Initial Value Problems Involving Maxwell's Equations in Isotropic Media", IEEE Transactions on Antennas and Propagation, Vol. AP-14, No. 3, May 1966, pp. 302-307.

9. R. J. Luebbers and K. S. Kunz, The Finite Difference Time Domain Method for Electromagnetics, Boca Raton, Florida: CRC Press, 1993, pp. 11-20, WEB QC 665 E4K82 1993.

10. Luebbers and Kunz, p. 37.

11. P. J. Dimbylow and O. P. Gandhi, "Finite-Difference Time-Domain Calculations of SAR in a Realistic Heterogeneous Model of the Head for Plane-Wave Exposure from 600 MHz to 3 GHz", Phys. Med. Biol., Vol. 36, No. 8, 1991, pp. 1075-1089.

12. Luebbers and Kunz, pp. 24-32.

13. Luebbers and Kunz, pp. 43-44.

14. G. Mur, "Absorbing Boundary Condition for the Finite-Difference Approximation of the Time-Domain Electromagnetic Field Equations", IEEE Transactions on Electromagnetic Compatibility, Vol. EMC-23, No. 4, November 1981, pp. 377-382.

15. Luebbers and Kunz, p. 27.

16. R. Luebbers, "Lossy Dielectrics in FDTD", IEEE Transactions on Antennas and Propagation, Vol. 41, No. 11, November 1993, pp. 1586-1588.

17. R. Luebbers, D. Steich, and K. Kunz, "FDTD Calculation of Scattering from Frequency-Dependent Materials", IEEE Transactions on Antennas and Propagation, Vol. 41, No. 9, September 1993, pp. 1249-1257.

18. R. Luebbers, F. P. Hunsberger, K. S. Kunz, R. B. Standler, and M. Schneider, " A Frequency-Dependent Finite-Difference Time-Domain Formulation for Dispersive Materials", IEEE Transactions on Electromagnetic Compatibility, Vol. 32, No. 3, August 1990, pp. 222-227.

19. O. P. Gandhi, B-Q. Gao, and J-Y. Chen, "A Frequency-Dependent Finite-Difference Time-Domain Formulation for General Dispersive Media", IEEE Transactions on Microwave Theory and Techniques, Vol. 41, No. 4, April 1993, pp. 658-665.

20. O. P. Gandhi, J-Y. Chen, and C. M. Furse, "A Frequency-Dependent FDTD Method for Induced-Current Calculations for a Heterogeneous Model of the Human Body", IEEE MTT-S International Microwave Symposium Digest, Albuquerque, New Mexico, Vol. III, June 1-5 1992, pp. 1283-1286.

21. R. J. Luebbers, and F. Hunsberger, "FDTD for Nth-Order Dispersive Media", IEEE Transactions on Antennas and Propagation, Vol. 40, No. 11, November 1992, pp. 1297-1301.

22. W. D. Hurt, "Multiterm Debye Dispersion Relations for Permittivity of Muscle", IEEE Transactions on Biomedical Engineering, Vol. BME-32, No. 1, January 1985, pp. 60-63.

23. A. C. Eycleshymer and D. M. Schoemaker, A Cross-Section Anatomy, Second Edition, New York: D. Appleton and Co., 1970, pp. 3-43, McG QS 4E97 1970 O/S.

24. D. M. Sullivan, O. P. Gandhi, and A. Taflove, "Use of the Finite-Difference Time-Domain Method for Calculating EM Absorption in Man Models", IEEE Transactions on Biomedical Engineering, Vol. 35, No. 3, March 1988, pp. 179-185.

25. Eycleshymer, p. 7.

26. Eycleshymer, p. 21.

27. O. P. Gandhi, Biological Effects and Medical Applications of Electromagnetic Energy, New Jersey: Prentice Hall, 1993, pp. 88-89.

28. Gandhi, p. 121.

29. A. Taflove and M. E. Brodwin, "Computation of the Electromagnetic Fields and Induced Temperatures within a Model of the Microwave-Irradiated Human Eye", IEEE Transactions on Microwave Theory and Techniques, Vol. MTT-23, No. 11, November 1975, pp. 888-896.

30. G. Hartsgrove, A. Kraszewski, and A. Surowiec, "Simulated Biological Materials for Electromagnetic Radiation Absorption Studies", Bioelectromagnetics, Vol. 8, 1987, pp. 29-36.

31. D. M. Sullivan, D. T. Borup, and O. P. Gandhi, "Use of Finite-Difference Time-Domain Method in Calculating EM Absorption in Human Tissues", IEEE Transactions on Biomedical Engineering, Vol. BME-34, No. 2, February 1987, pp. 148-157.

32. M. A. Stuchly and S. S. Stuchly, "Dielectric Properties of Biological Substances - Tabulated", Microwave Power, Vol. 15, No. 1, 1980, pp. 19-26.

33. W. T. Joines, Y. Zhang, C. Li, and R. L. Jirtle, "The Measured Electrical Properties of Normal and Malignant Human Tissues From 50 to 900 MHz", Medical Physics, Vol. 21, No. 4, April 1994, pp. 547-550.

34. J. Tofgard, S. N. Hornsleth, and J. B. Andersen, "Effects on Portable Antennas of the Presence of a Person", IEEE Transactions on Antennas and Propagation, Vol. AP-41, No. 6, June 1993, pp. 739-746.

35. L. Jofre, M. S. Hawley, A. Broquetas, E. Reyes, M. Ferrando, and A. R. Elias-Fuste, "Medical Imaging with a Microwave Tomographic Scanner", IEEE Transactions on Biomedical Engineering, Vol. 37, No. 3, March 1990, pp. 303-312.

36. K. R. Foster, J. L. Schepps, R. D. Stoy, and H. P. Schwan, "Dieletric Properties of Brain Tissue between 0.01 and 10 GHz", Phys. Med. Biol., Vol. 24, No. 6, 1979, pp. 1177-1187.

37. R. Luebbers, L. Chen, T. Uno, and S. Adachi, "FDTD Calculation of Radiation Patterns, Impedance, and Gain for a Monopole Antenna on a Conducting Box", IEEE Transactions on Antennas and Propagation, Vol. 40, No. 12, December 1992, pp. 1577-1583.

38. K. R. Umashankar, A. Taflove, and B. Becker, " Calculation and Experimental Validation of Induced Currents on Coupled Wires in an Arbitrary Shaped Cavity", IEEE Transactions on Antennas and Propagation, Vol. AP-35, No. 11, November 1987, pp. 1248-1257.

39. R. J. Luebbers and J. Beggs, "FDTD Calculation of Wide-Band Antenna Gain and Efficiency", IEEE Transactions on Antennas and Propagation, Vol. 40, No. 11, November 1992, pp. 1403-1407.

40. R. J. Luebbers, K. S. Kunz, M. Schneider, and F. Hunsberger, "A Finite-Difference Time-Domain Near Zone to Far Zone Transformation", IEEE Transactions on Antennas and Propagation, Vol. 39, No. 4, April 1991, pp. 429-433.

41. C. M. Furse, J-Y. Chen, and O. P. Gandhi, "The Use of the Frequency-Dependent Finite-Difference Time-Domain Method for Induced Current and SAR Calculations for a Heterogeneous Model of the Human Body", IEEE Transactions on Electromagnetic Compatibility, Vol. 36, No. 2, May 1994, pp. 128-133.

42. R. M. W. Lau, R. J. Sheppard, G. Howard, and N .M. Bleehen, "The Modelling of Biological Systems in Three Dimensions using the Time Domain Finite-Difference Method: II. The Application and Experimental Evaluation of the Method in Hyperthermia Applicator Design", Phys. Med. Biol., Vol. 31, No. 11, 1986, pp. 1257-1266.

43. P. J. Dimbylow, "FDTD Calculations of the SAR for a Dipole Closely Coupled to the Head at 900 MHz and 1.9 GHz", Phys. Med. Biol., Vol. 38, No. 3, 1993, pp. 361-368.